# Evaluating the Thermal Properties of Soils Based on Measured Ground Temperatures

By

Gabriel Jacob Pavon

A Thesis Submitted to the Faculty of Graduate Studies of

The University of Manitoba

in Partial Fulfillment of the Requirement for the Degree of

MASTER OF SCIENCE

Department of Civil Engineering

University of Manitoba

Winnipeg, Manitoba

# Abstract

Almost one quarter of the earth's surface is underlain by permafrost where more than 5% is located in mountain areas. Investigations have determined deterioration and warming of the permafrost zones as the zero isotherm moves towards the north affecting the life cycle performance of civil infrastructure. Proper understanding of the thermal interaction between the permafrost and civil infrastructure is critical in engineering design.

The thermal properties of soils are fundamental parameters to determine the rate of freezing and thawing of the ground. The changes in the thickness of the active layer are dependent on these thermal properties. These changes can contribute to thaw settlement and frost heave of the ground.

The thesis evaluates the thermal properties of permafrost in five selected sites. Measured data were simulated through numerical models using TEMP/W computer program. Measured and simulated data were compared using statistical analysis. Sensitivity analysis was employed to investigate the importance of the thermal conductivity and volumetric heat capacity in the geothermal models. The thesis shows the similarities or differences of the thermal properties between the lowland and the mountain permafrost.

## Acknowledgments

I would like to express my gratitude to my academic advisors Dr. Marolo Alfaro and Dr. Lukas Arenson for their supervision, teaching and support that were fundamental for the development of this thesis. Their sharing of knowledge in and out of the classroom was always constant.

I appreciate the feedback and insightful ideas provided by my committee research member Dr. Hartmut Holländer. Definitely, his guidance and advice made this research possible.

I would like to thank Mr. Kerry Lynch whose assistance and efforts were critical for the monitoring of Provincial Road 391 and ensuing collection of data.

I would like to thank my colleagues and friends from Winnipeg and abroad that always provided encouragement and new ideas.

Finally, I express my deepest gratitude to my parents and brothers that always stayed at my side where I needed it the most. Their support and love have no limits. Overall, I recognize the support of my beautiful wife Vanessa who has been a counselor and guidance in all my endeavors.

Gabriel Jacob Pavon
February 2018

# Table of Contents

## Chapter 3: Site Descriptions and Collection of Data



## Chapter 4: Geothermal Numerical Modelling

## Chapter 5: Results

## Chapter 6: Discussions

# List of Tables

## Chapter 4



## Chapter 5



## Chapter 6

## List of Figures

### Chapter 2

## Chapter 3

## Chapter 4



## Chapter 5

# List of Copyrighted Figures with Permission

## Chapter 2



## Chapter 3

# List of Notations

$A$ area

$C$ volumetric heat capacity

$c_f$ frozen volumetric heat capacity

$C_i$ specific heat capacity of ice

$C_s$ specific heat capacity of soil

$c_u$ unfrozen volumetric heat capacity

$C_w$ specific heat capacity of water

$I_{af}$ air freezing index

$I_{at}$ air thawing index

$I_{sf}$ surface freezing index

$I_{st}$ surface thawing index

$k$ thermal conductivity

$k_f$ frozen thermal conductivity

$k_u$ unfrozen thermal conductivity

$L$ soil volumetric latent heat of fusion

$L'$ latent heat of water

$m$ applied boundary flux

$n_f$ freezing N-factor

$n_t$ thawing N-factor

$Q$ quantity of heat

$q$ heat flux across a surface

$R$ resistance

$S$ slope of the change in temperature

$T_1$ initial temperature

$T_2$ final temperature

$t_1$ initial time

$t_2$ final time

$x$ length of the element

$W_f$ frozen water content

$W_u$ unfrozen water content

$w_u$ total unfrozen volumetric water content

$\gamma_d$ dry density

$\lambda$ capacity of heat storage

# CHAPTER 1: Introduction

## 1.1 Background

The behaviour of the soil in cold regions is influenced by climate-affected surface conditions and the heat flowing from the earth's interior. Understanding the interaction of thermal conditions with the frozen ground, improves the proper design of engineering structures. The problems associated with frost action are critical and part of scientific concern in engineering analysis (Williams and Smith, 1989). For instance, the development of ice lenses between soil particles, which takes place during freezing, produces frost heave that lifts up the surface layers of the soil. Furthermore, softening of the soil as a result of water saturation during thawing creates frost boils, which affect the bearing capacity of soils (Jumikis, 1966).

Ground temperature can be analyzed through heat conduction theory, which stipulates that for a given element of soil, heat flows from regions of higher temperature to regions of lower temperature. Proper analysis of the thermal conditions of the ground involves correct understanding of the thermal properties of the soil, which are affected by temperature, organic content, mineralogy, density and moisture content. Seasonal freezing and thawing cycles affect the thermal properties of the soil as a consequence of the phase change in the moisture content (Farouki, 1981; Williams and Smith, 1989).

The rate of heat transfer is determined by the thermal conductivity. The change in temperature depends on the volumetric heat capacity. Furthermore,

the latent heat of fusion dominates transient problems that experience any gradual phase change as a function of the unfrozen water content.

Permafrost monitoring has been analyzed to investigate ground temperatures in plain and mountain regions in Canada (Canadian Cryospheric Information Network Website, 2016) and Europe through Permafrost and Climate in Europe (PACE) (Harris et al. 2009). Geothermal models utilize in-situ soil properties to find feasible alternative solutions to compare and determine the temperature of permafrost. The input thermal conductivity of these models can be determined through different laboratory testing methods such as the Steel Needle Probe Method (ASTM D5334-14, 2014) and the Guarded Hot Plate Method (ASTM C177-13, 2013).

The thesis evaluates the thermal conductivity and volumetric heat capacity based on measured ground temperatures.

### 1.2 Research Hypothesis

The principal hypothesis of this thesis is that thermal properties of coarse and fine-grained soils can be evaluated based on ground temperatures with depth and time in and below the active layer.

### 1.3 Research Objectives

The research objectives are as follows:

1. To evaluate the thermal conductivity and volumetric heat capacity of soils in frozen and unfrozen states based on field measured data. This was done: a) using calibration of geothermal models, and b) following laboratory-testing procedure.

2. To carry out sensitivity analysis to investigate the more important thermal properties on the thermal performance of the ground.
3. To investigate the similarity or difference in the thermal analysis between lowland and mountain permafrost.

### 1.4 Research Scope

This thesis evaluates the thermal properties of soils involved in the freezing and thawing behavior of frost-affected ground. The author continued the work of Batenipour (2012), Kurz (2014) and Flynn (2015) in Manitoba, Canada, regarding the prediction of ground temperatures at PR391 utilizing the geothermal model created by Flynn (2015).

Four more geothermal models were prepared to compare measured data obtained in the Northwest Territories (De Guzman et al. 2017; Stirling et al. 2015), Swiss Alps (Arenson, 2002; Harris et al. 2009) and the Chilean Andes (unpublished data).

Climate data were obtained from agencies available in those locations. The thermal conductivity and volumetric heat capacity for the frozen and unfrozen states were calibrated with the constructed models by utilizing data from the literature and the measured spatial and temporal temperatures.

### 1.5 Organization of Thesis

Chapter 1 presents an introduction of the topic describing a background of the heat transfer problems and methods to determine the thermal properties of soils. It describes a research hypothesis, a research scope and the organization of thesis.

Chapter 2 provides a background of the soil thermal properties, focusing on the thermal conductivity, the volumetric heat capacity and the latent heat of soils. This chapter describes the permafrost conditions in Canada and the ground temperature regime, the problems associated with thawing permafrost, defines the concept of mountain permafrost, examines the measurement of temperature in the subsurface, highlights the importance of the thermal numerical modelling, and states the importance of the actual research.

Chapter 3 presents a description of each research site and analysis of collected data.

Chapter 4 breaks down the concept of the thermal numerical modelling, stating the theory and governing equations. The chapter describes the geothermal modeling in each research site: defining problem domain, material properties, boundary conditions, thermal properties from the literature, performance criteria and sensitivity analysis. It describes an alternate procedure to determine thermal conductivity based on the slope of temperatures variations with time.

Chapter 5 shows results of performance criteria, sensitive analysis, and alternate procedure. Geothermal models show simulated and measured data.

Chapter 6 presents a discussion of the performance criteria, sensitivity analysis, and calibrated thermal properties in lowland and mountain permafrost.

Chapter 7 provides a summary of the results, conclusions and recommendations.

# CHAPTER 2: Literature Review

## 2.1 Introduction

The chapter provides a review of the soil thermal properties and freezing and thawing characteristics of permafrost; a general review of the permafrost in Canada, the Swiss Alps and the Chilean Andes; instrumentation and numerical modelling to represent in-situ temperature conditions and methods to determine the thermal properties of soils.

## 2.2 Soil Thermal Properties

It is important to understand the scope of the soil heat transfer as a medium to design and mitigate infrastructural problems related to permafrost. Special attention must be taken when it comes to studying the impact of the temperature regime (as a result of freezing and thawing) in soils supporting infrastructure. Freezing temperatures decrease the hydraulic conductivity of soils. Thawing of the ice lenses in frozen soils increases the water flow caused by the hydraulic gradient (Hermansson et al. 2008). In order to determine the rate and penetration of freezing and thawing of soils, it is necessary to understand the behavior of the thermal properties.

### 2.2.1 Thermal Conductivity

Understanding of the thermal conductivity is essential to determine the effect of frost in soils utilized as foundation material for roads, airfields, pipelines and buildings. Most of the analytical and numerical methods that study the behavior of the ground temperature regime use the heat conduction theory as a principal

mechanism. The theory of heat conduction in solids states that when different parts of a solid body are at different temperatures, the heat flows from hotter to colder zones by a process of electronic and atomic energy transfer known as conduction. This can be expressed as follows:

$$Equation\ 2.1 \qquad Q = k\ \frac{T_2 - T_1}{x}\ At$$

where $Q$ is the quantity of heat (kJ) , $t$ is the time to conduct the heat (seconds), $A$ is the cross sectional area through which the heat flows ($m^2$), $x$ is the length of the element (m) , $T_2 - T_1$ is the change in temperature between different zones of the element (K) and $k$ is the coefficient of the thermal conductivity of the material (W/m.K).

According to Farouki (1981), the thermal conductivity of soils can be expressed as the amount of heat that flows normally across a surface of unit area of soil in unit of time under a unit of the temperature gradient of the soil surface. Figure 2.1 shows the behaviour of a prismatic element of soil, where the heat flows from a hotter to a colder zone by conduction.

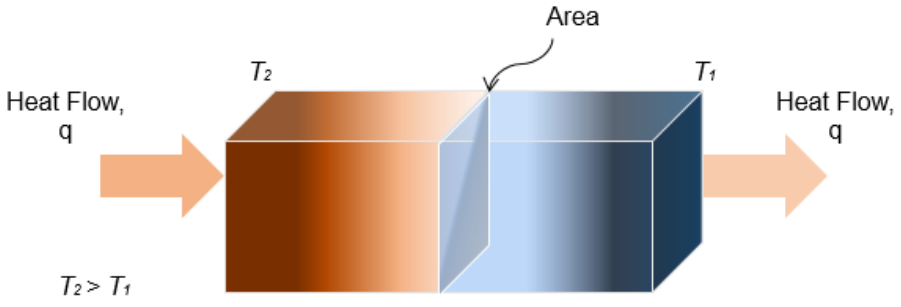


**Fig. 2.1. Heat flow through a prismatic element of soil**

There is an intrinsic relation between thermal conductivity and the mineral content, porosity, degree of water saturation and temperature as shown in Figure 2.2 (Terzaghi, 1952).

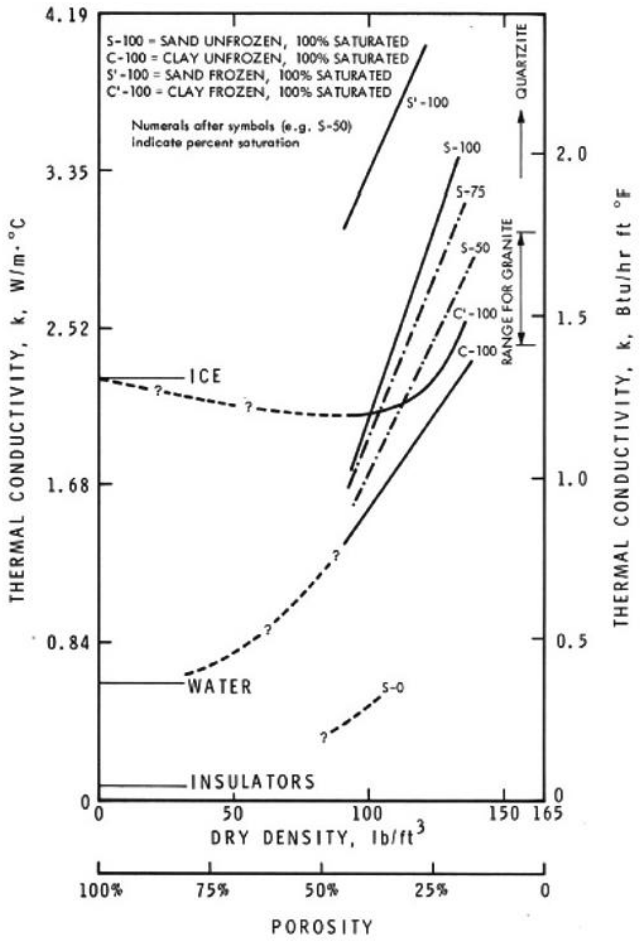


**Figure 2.2 Relationship between thermal conductivity and mineral content, porosity, and density for frozen and unfrozen sand and clay at various degrees of saturation (Terzaghi 1952) (Used with permission).**

### 2.2.1.1 Soils Composition

Some factors to take into account for the thermal analysis of the soils structure are the arrangement of the particles, the number and nature of contacts

between the soil particles, the effect that other components (e.g., water) have on the contacts. The arrangement of the soil structure affects the orientation of the heat flow. The points of contact between the soils particles represent the areas through which the heat is transferred. In general, soils are composed by parent minerals such as: quartz, calcite, feldspar and mica (Donahue et al. 1977). Generally, coarse-grained soils (granular contacting skeleton structure) are formed by quartz, which have a high thermal conductivity. On the other hand, fine-grained soils contain micaceous minerals, including clay, which has a lower thermal conductivity (Johnston et al. 1981).

The thermal conductivity of soils improves with increasing degree of water saturation. Retained films of water between the soil crystals improve the heat transfer in the contact areas (Birch et al. 1940). This water acts as a binding or cementing material, creating a bridge that enhances the thermal conduction between the soil particles. Normally, fine-grained soils contain high porosity and low quartz content, showing lower thermal conductivity. However, they used to store a higher content of water and, thus, in some cases, clays and silts present thermal conductivities close to ranges of the coarse-grained soils (Hermansson et al. 2008). Figure 2.3 represents functions of different soils and water content (GEO-SLOPE International Ltd, 2008). As can be seen, the increment of conductivity is related to the increment of water content and the soil that can retain such a volume of water.

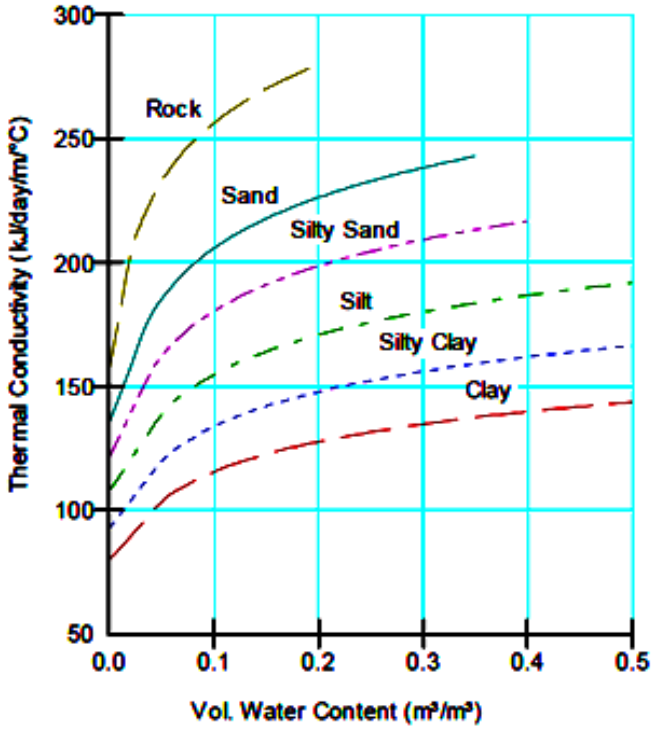


**Figure 2.3. Thermal conductivity vs water content functions (GEO-SLOPE International Ltd, 2008) (Used with permission).**

The thermal conductivity of soils increases with dry density for factors such as: more solid matter per unit soil volume, less air or water porosity per unit soil volume and improved heat conduction across the areas of contact between the soils particles (Farouki, 1981). For this reason, the thermal conductivity with depth shows increasing values as the compressive stress creates more zones of heat transfer.

### 2.2.1.2 Ice Content in Soils

Water in soils may be present as vapor in the pore, as water in the liquid phase above 0℃, as ice below 0℃ or as unfrozen water below 0℃. When water

freezes, ice cementation occurs and bonding forces increase their magnitude, leading to a better heat conduction in frozen soils (Farouki, 1981).

The thermal conductivity of ice is up to four times higher than unfrozen water. As a result, the thermal conductivity in well-saturated soils provides substantial increments at or below freezing temperatures (Farouki, 1981).

Hermansson et al. (2008) reported that the unfrozen water retained in frozen soils improves the thermal interaction between the soil particles and ice. Fine-grained soils retain a larger amount of unfrozen water at temperatures below 0℃, and then, their thermal conductivity tends to increase when temperatures keep decreasing. On the other hand, as coarse soils show low levels of saturation, their thermal conductivity is slightly affected at freezing temperatures.

Figures 2.4 to 2.5 represent relations between ice content and soils temperature and their corresponding thermal conductivities (Hansson et al. 2004*;* GEO-SLOPE International Ltd, 2008). It is shown that increments in thermal conductivity are directly proportional to increments in volumetric ice content. As stated above, fine soils that hold unfrozen water at or below 0℃ show more changes in thermal conductivity with decreasing temperatures compared to granular soils.

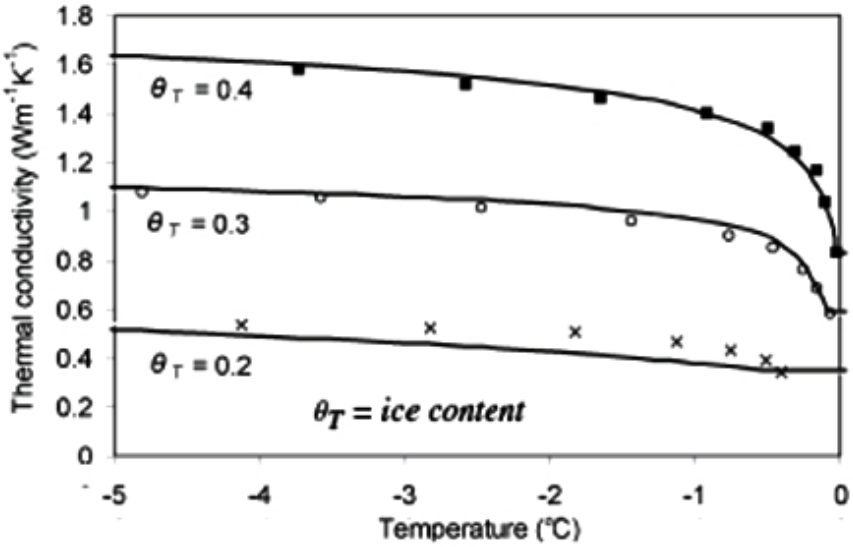


**Figure 2.4. Relationship between thermal conductivity and ice content. (Hansson et al. 2004) (Used with permission).**

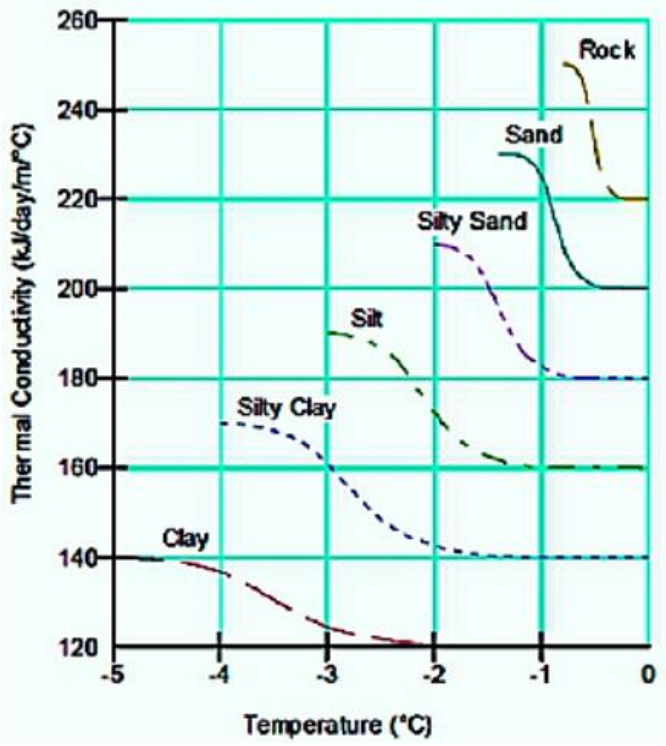


**Figure 2.5. Thermal conductivity vs temperature functions (GEO-SLOPE International Ltd, 2008) (Used with permission).**

#### 2.2.1.3 Soils Thawing

During thawing, the soils structure remain stable until an external force is applied. In general, thawed soils preserve the cracks and cavities created during the freezing process. Further wetting and drying in cohesive soils causes swelling and shrinkage with notable loss of material. As a result, the soil hydraulic conductivity is increased with the consequent reduction of dry unit weight. This disturbance in the natural bonding of the soils structure reduces their thermal conductivity (Farouki, 1981).

Water from thawing permafrost results in thaw settlement. Thaw settlement depends on the distribution of ice in the frozen soil and the swelling properties of the thawed soil. The viability to use thawed permafrost as a foundation material depends on the degree of deformation and strength during thawing. (Johnston et al. 1981). Thaw settlement was studied in situations related to embankments (e.g. Batenipour, 2012), building foundations (e.g. Hanna et al. 1990), design of buried pipelines, gas, oil and water supply wells and retaining structures (e.g. Johnston et al. 1981).

### 2.2.2 Volumetric Heat Capacity

The volumetric heat capacity of soils is the amount of heat required to change the temperature of a unit volume of soil by one degree. Due to the heat capacity of a substance is equivalent to the sum of the heat capacity of its components, the volumetric heat capacity of a soil can be obtained by adding the heat capacity of its different constituent parts. Then, the volumetric heat capacity

of a frozen soil (kJ/m$^3$. ℃) can be described as follows (GEO-SLOPE International Ltd, 2008):

$$Equation\ 2.2 \qquad C = \gamma_d\,(C_S + C_W\,W_u + C_i\,W_f)$$

Where $\gamma_d$ is the dry density of the soil, $C_S$ is the specific heat capacity of the soils particles, $C_W$ is the specific heat capacity of water, $C_i$ is the specific heat capacity of ice, $W_u$ is the unfrozen water content and $W_f$ is the frozen water content. Then, the volumetric heat capacity of a soil depends on its water content, temperature (whether the soil is frozen or unfrozen) and its unit weight.

For unfrozen soils, the volumetric heat capacity continues to increase when the water content is increased as shown in Figure 2.6. Fine-grained soils show heat capacities higher than coarse-grained soils as they retain larger moisture content (GEO-SLOPE International Ltd, 2008).

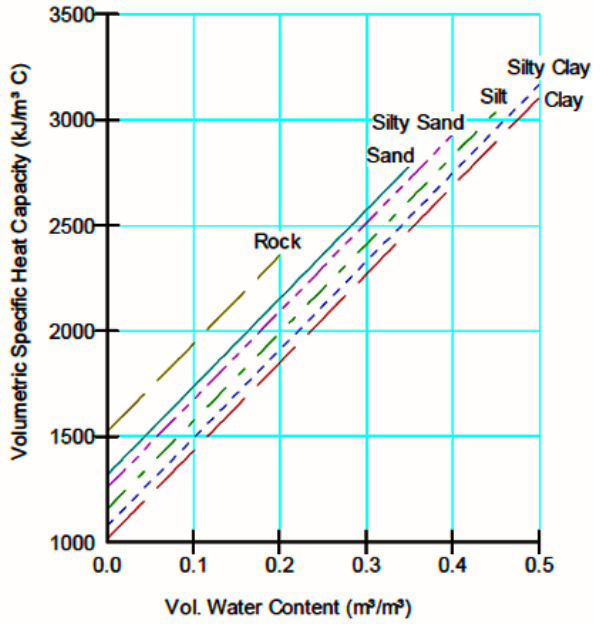


**Figure 2.6. Volumetric heat capacity vs volumetric water content functions (GEO-SLOPE International Ltd, 2008) (Used with permission).**

### 2.2.3 Latent Heat of Fusion

The latent heat of fusion, $L$, is another property utilized in thawing and frost penetration analysis of soils. Its study is extended to the treatment of icing problems on pavements and the heating/firing of soils (Jumikis, 1966). The latent heat of fusion is defined as the amount of heat energy absorbed when a unit mass of ice is converted into liquid with no change in temperature (isothermal process). The same amount of heat is released in order to convert water into ice with no change in temperature. Thus, before ice melts, a latent heat of 333.7 kJ/kg first has to be absorbed and the same amount of heat first has to be dissipated by the water to be transformed into ice (Andersland and Ladanyi, 2004).

The latent heat of fusion of a given soil can be expressed as (Andersland and Ladanyi, 2004):

$Equation\ 2.3$ $$L = \gamma_d L' \frac{w - W_u}{100}$$

where $L$ is the soil volumetric latent heat of fusion( kJ/m$^3$ ), $L'$ is the mass latent heat of water (333.7 kJ/kg), $\gamma_d$ is the dry soil density, $w$ is the total water content and $W_u$ is the unfrozen water content of the frozen soil. For coarse-grained soils with low content of unfrozen water below 0 ℃, $W_u$ will tend to be very small, assuming a value of zero for practical calculations (Andersland and Ladanyi, 2004)

## 2.3. Permafrost in Canada

Permafrost is the thermal condition in soils or rocks maintaining temperatures below 32℉ (0℃) over at least two consecutive winters and the intervening summer (Brown and Kupsch, 1974). This is defined only on the basis of temperature and time; frozen water may or may not be present.

According to Brown et al. (1997), 20-25% of the world land surface is underlain by permafrost. Permafrost in the Northern Hemisphere extends up to 25% of the land area (International Permafrost Association, 2016). Figure 2.7 shows the distribution of permafrost in Canada. In general, the Canadian permafrost is divided into four spatial extents or zones based on the percentage of land area underlain by permafrost : the Continuous Permafrost Area (≥90 to 100%), the Discontinuous Permafrost Area (≥50 to < 90%), the Sporadic Permafrost area (≥10 to <50%), and the Isolated Patches Permafrost Area (≥0 to <10%) (Brown et al. 1997). The presence of permafrost in these zones is controlled by climate (e.g. the mean annual air temperature), terrain conditions and civil works.

Terrain factors such as vegetation, slope, aspect, hydrology, snow cover and soil/rock type, have substantial effect on the permafrost conditions. For instance, vegetation helps preserving the permafrost thickness and depth of the active layer (top layer that freezes and thaws annually) penetration during summer (Brown, 1966a).

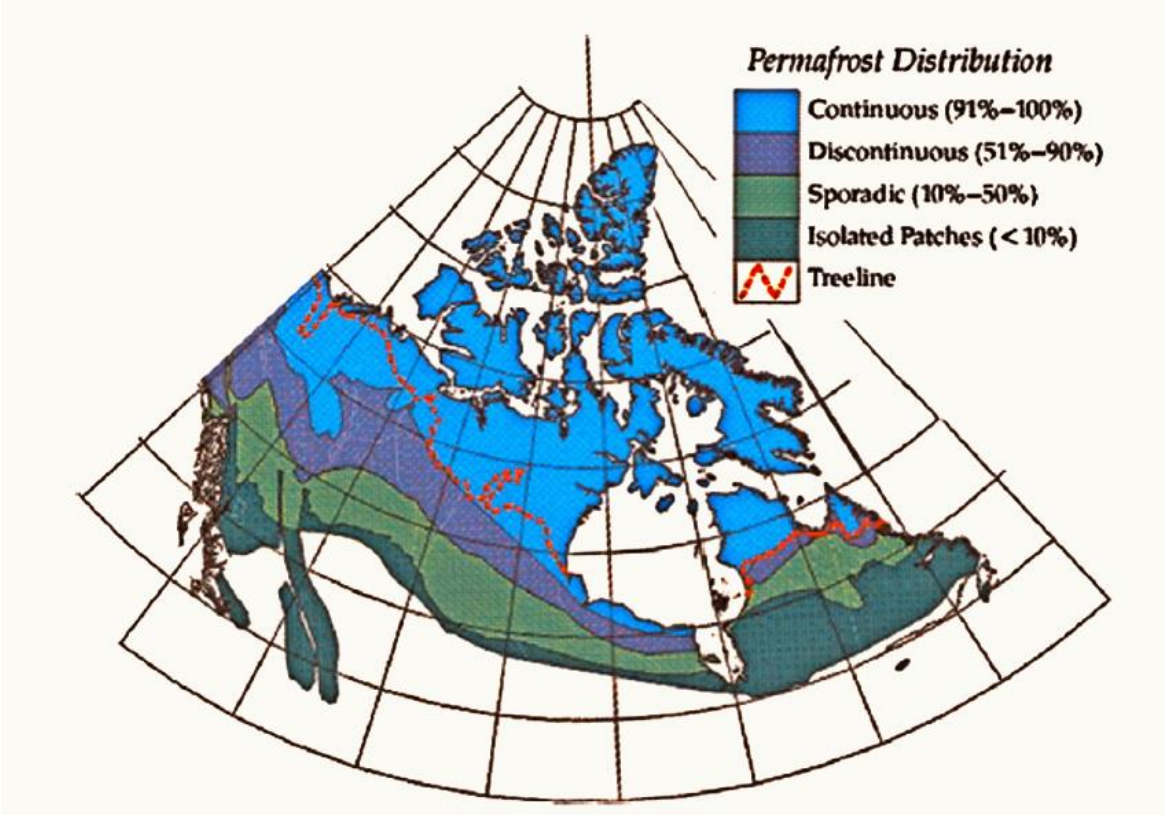


**Figure 2.7. Distribution of permafrost in Canada (Brown et al. 1997) (Used with permission).**

### 2.3.1 Ground Temperature Regime

Ground temperature variations depend mainly on the annual air temperature changes. However, the magnitude and extension are affected at the same time by the vegetation, surface and ground water, snow surface cover and thermal properties of soil. Figure 2.8 shows the typical ground temperature regime (temperature vs. depth) in permafrost. This regime is affected by past and present climate and terrain conditions. Discontinuous permafrost zones may show regimes with temperatures in the range of 0℃ to about -5℃, and mean annual air temperatures of -1℃ to about -8℃. Meanwhile, continuous zones may

register ground temperatures of -5℃ to -15℃ and mean annual air temperatures of -8℃ to about -19℃ (Brown, 1966b; Johnston et al. 1981).

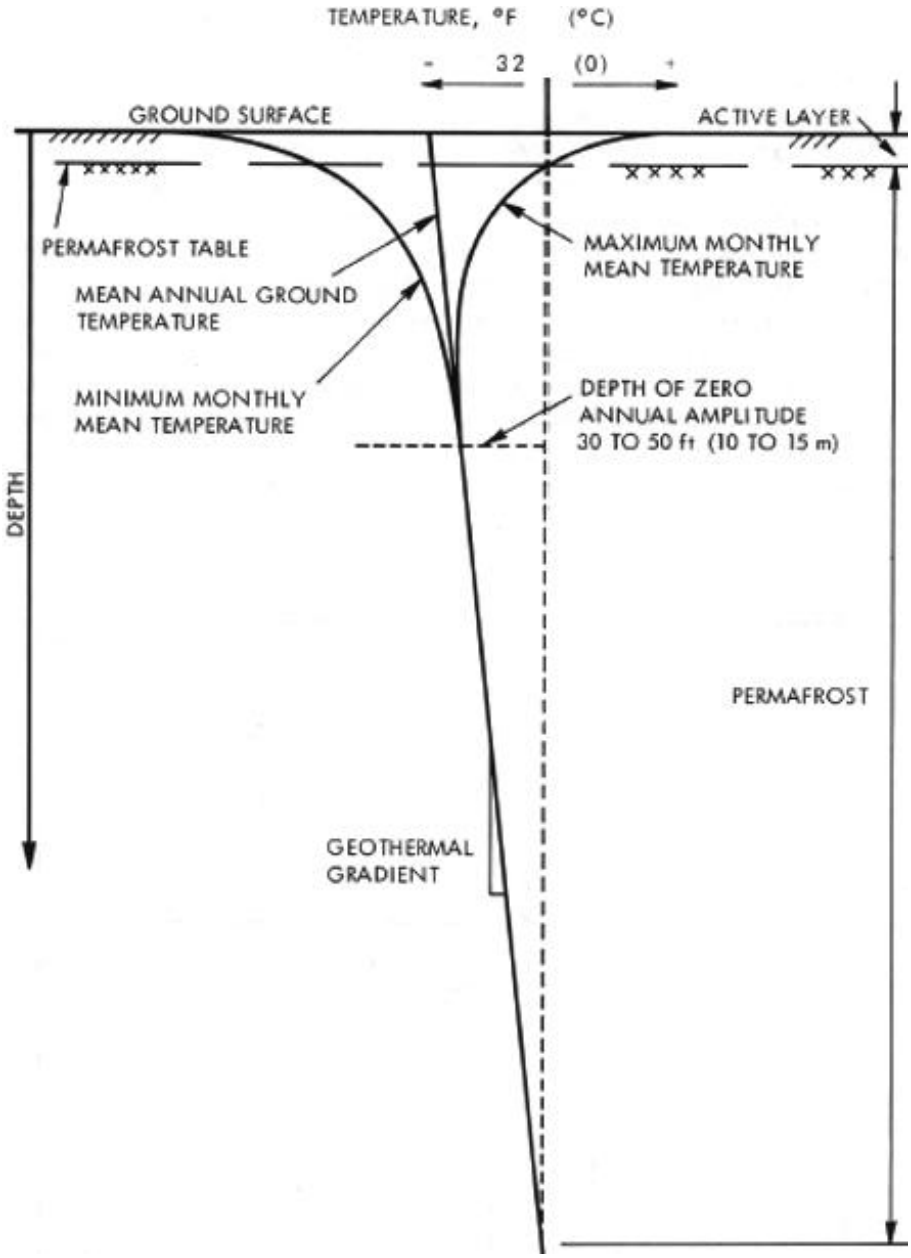


**Figure 2.8. Typical ground temperature regime in permafrost (Brown et al. 1981) (Used with permission).**

## 2.4 Mountain Permafrost

Rock glaciers are ice-rock mixtures moving downslope exposing notorious viscous flow composition. They may be described as the principal geomorphological definition of mountain permafrost (Barsch 1996, Berthling 2011). Mountain permafrost is defined as permafrost in mountain areas located at low and high latitudes and in the Artic or Antarctic (Gruber and Haeberli, 2009) presenting conditions affected by the mountain topography. Around 6-7% of the total permafrost is composed by mountain permafrost, with 80.4% being in the Asian mountains, 0.2% in the European Alps (Stearns 1966; Arenson, 2002) and 19.4% in the American mountains (Fujii and Higuchi, 1972; Arenson, 2002). Gruber and Haeberli (2009) explained that the main indicative of this type of permafrost is its spatial variability, providing examples as follows:

a. Elevation and other related geometric characteristics such as slope, aspect, curvature, or roughness.
b. Surface micro-climatology, dominated by changes in elevation.
c. Subsurface material thickness and composition, dominated by different mechanisms of erosion, deposition and grain-size fractionation.
d. Water disposition, affected by surface shape, contributing area and subsurface material.
e. Snow cover, which is affected by precipitation, wind drift, avalanches and surface micro-climate.

Mountain permafrost contains particular geographic characteristics such as ice faces, rock glaciers, hanging glaciers and push-moraines, which are related

to its evolution and development. This landscape evolution affects the long-term mechanisms of transfer of sediments. (Gruber and Haeberli, 2009). As Figure 2.9 shows (Gruber and Haeberli, 2009), this transfer of sediments produces variable regimes of natural hazards such as debris flows and rock/soil avalanches.

**Figure 2.9. Steep bedrock containing permafrost beneath the top station of the Corvatsch cable car, Switzerland. The observed debris are the result of rock fall activity produced by permafrost degradation (Courtesy of Dr. Stephan Gruber, 2006).**

Warming and thawing of mountain permafrost increase the risk of unexpected events in areas historically safe. Construction of infrastructures in mountain permafrost requires adequate techniques that may control ground movement and thermal disturbance, especially in zones where water is perched.

Normally, two types of formations identify the mountain permafrost: rock glaciers and creep formations produced by the slow deterioration of cohesive sediments with high ice content (Haeberli et. al. 2006). However, the lack of these phenomena do not suggest the absence of permafrost.

### 2.4.1 Swiss Alps

It is estimated that 4-6 % of the Swiss land surface is covered by permafrost. This means that 15% of the Swiss Alpine area is covered by mountain permafrost, which is normally found at 2300 masl (Matasci, 2012).

Permafrost and Climate in Europe (PACE) boreholes registered continuous warming during all the seasons, having their peaks in spring and summer (Harris et al. 2009). The Murtèl–Corvatsch rock glacier (Switzerland) was included in the PACE monitoring and is part of the measured data analyzed in this thesis. In general, the Murtèl–Corvatsch borehole drilled in creeping ice-rich rock debris presents a warming trend with high-amplitude inter-annual variations (Harris et al. 2003).

#### 2.4.1.1 Thawing of Alpine Permafrost

Since alpine permafrost controls the stability and hydraulic behavior of rocks and debris slopes, its thawing represents a significant threat for potential natural hazards by facilitating mass movements and slope instability failures (Stötter, 1994). Permafrost-related hazards include permafrost creep and transportation of material into debris flow zones, thaw settlement and frost heave, debris flow from permafrost due to increment of active layer, destabilization of frozen debris slopes, rock fall and rock avalanches (Krainer et. al. 2007).

As the melting permafrost destabilizes the soil structure, mountain permafrost in Switzerland has become a concern in terms of infrastructure due to elements

such as ski-lifts and avalanche control systems are attached to the frozen soil. (Noetzli and Von der Mühll, 2010; Matasci, 2012).

### 2.4.2 Chilean Andes

The Chilean and Argentinean rock glaciers represent examples of orogens of mid-latitude where they are present in abundantly concentration and dimension. (Trombotto et al. 1999; Brenning, 2005; Angillieri 2009; Azocar and Brenning, 2010)**.**

Current understanding of the impact and distribution of the Andean permafrost is limited compared with other regions of the world such as the Europen Alps. However, mining activities, for instance, have encourage further research of zones representing a source of freshwater reservoir. New investigations and discussions analyzed the hydrological and geomorphological scope of these rock glaciers. (Arenson and Jakob, 2010; Brenning, 2010)

## 2.5 Measurement of Soil Temperature through Thermistor-Based Systems

Thermistors are ceramic semiconductors whose resistance fluctuates with temperature. As their sensitivity is relatively high, measured temperatures show an accuracy in the range of 3 to 6% per degree Celsius. Thermistors utilized to measure soils temperature are negative temperature coefficient resistance (NTC). This means that their resistance decreases with the increment of temperature. Normally, thermistors are designed according to their nominal resistance at 25℃ (Ochsner, 2008).

In order to determine the soil temperature, it is necessary to measure the thermistor resistance and, thus converting that resistance (R) into a temperature estimate using the Steinhart-Hart equation as follows:

$Equation\ 2.4 \qquad T = [A + Bln(R) + Cln(R)^{3}]^{-1}$

where *T* is temperature (K) and *A, B, and C* are calibration constants for the specified thermistor. Constant current or voltage excitation from a data logger is required. Then, when the current or voltage is flowing through the thermistor at a low rate, the effect of self-heating is reduced. In most of the cases, thermistors have more accurate performance than other sensors (e.g. thermocouples) (Ochsner, 2008).

According to the International Permafrost Association (2008) for the case of permafrost monitoring, thermistors are inserted in and below the active layers (permafrost) in a vertical arrangement where they collect the temperature to be transferred to data loggers. Thermistors can be installed individually or in series deposited in an acrylic cylinder where the separation of nodes depends on local conditions. However, in most cases, they are placed every 0.5 m, where data can be recorded in a two-hour interval.

Thermistors register temperature variations whose downward propagation take considerable time based on several conditions (vegetation, surface bodies of water or perturbations, snow cover, ground water, thermal properties of the subsurface, etc.). The amplitude of temperature variations is gradually attenuated with depth until 15-20 m (depth of mean zero annual amplitude), but may extend

deeper depending on the surface conditions (International Permafrost Association, 2008).

## 2.6 Numerical Modelling

A numerical model is defined as a mathematical concept of a phenomenon representing a system. Process-based permafrost models determine the thermal state of the ground utilizing the heat transfer analysis (Riseborough et al. 2008). Permafrost modelling may define equilibrium conditions (steady state) or evolving conditions (transient state). Statistical and empirical relations in transfer functions between the atmosphere and the ground may predict the existence of permafrost and the active layer thickness (Riseborough et al. 2008).

Finite element models may show annual term changes of a deep ground temperature regime (transient method). Equations using parameters such as freezing and thawing indices and data from atmospheric conditions, define the relation between surface energy exchange and subsurface conditions (Riseborough et al. 2008). Numerical models permit the adaptation of materials, geometries and boundary conditions in terms of depth and time. (Riseborough et al. 2008).

## 2.7 Methods to Determine Thermal Properties of Soils

Different laboratory test methods have emerged in order to determine the thermal conductivity and volumetric heat capacity of frozen and unfrozen soils. These methods can be divided into two categories: steady-state methods and transient heat transfer methods. Steady-state methods require longer time to

obtain results as the sample needs to remain in a steady-state to show the measurements until equilibrium is achieved. On the other hand, transient methods are recognized for their time saving condition, adaptability and simple performance (Różański and Sobótka, 2013). Within the transient method, a well-known procedure is the steel needle probe method that was standardized for soils and soft rocks (ASTM D5334-14). The thermal needle probe is inserted in the specimen and applies a constant current where the change in temperature for heating phases is recorded. The rate of increase in temperature of the probe depends on the thermal conductivity of the surrounding medium. (Różański and Sobótka, 2013; ASTM D5334-14).

This thesis will evaluate the thermal conductivity and volumetric heat capacity of soils in frozen and unfrozen states. Figure 2.10 represents the methodology used for the evaluation of the thermal properties. In order to perform the analysis, measured data were obtained at different sites. Each analysis was performed through a geothermal modelling utilizing TEMP/W 2007 (GEO-SLOPE International ltd, Calgary, AB) geocomputer software. Initial thermal properties are obtained from the literature and introduced to the geothermal model. These properties are calibrated until the best fit of the measured and simulated temperatures is achieved. Two performance criteria are applied on the calibration results: root mean square error (RMSE) and coefficient of determination ($R^2$). Sensitivity analysis was carried out to find the most sensitive thermal properties in each geothermal model. The temperature variations of soils with time and depth (thermal regime) will be an indicative of the changes in heat conduction and heat capacity. The calibrated thermal properties will be shown in a table

indicating the frozen and unfrozen thermal conductivity as well as the frozen and unfrozen volumetric heat capacity. Furthermore, an alternative solution using the slope of the temperature variation with time will provide an estimate of the thermal conductivity in frozen and unfrozen states.

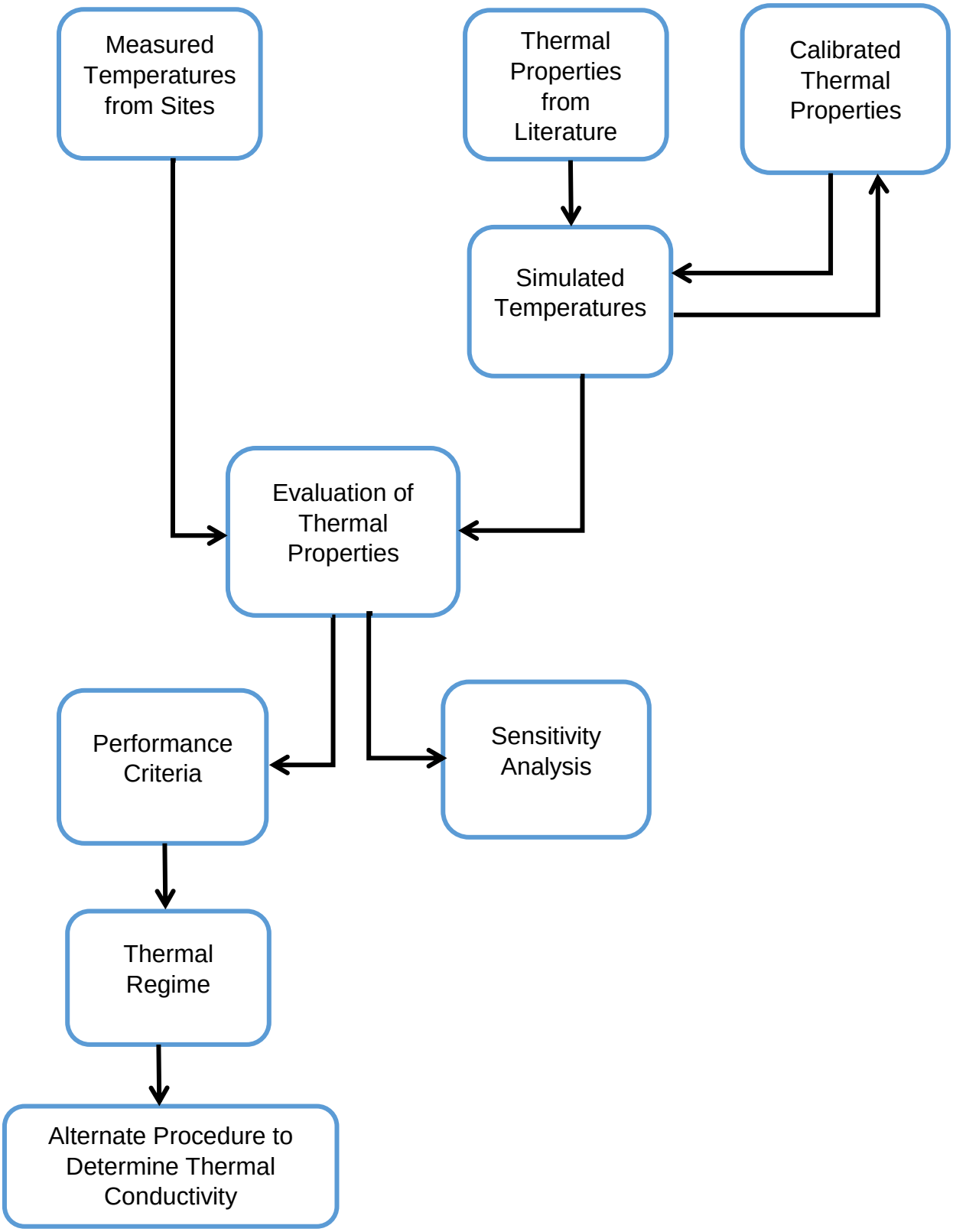


**Figure 2.10. Flowchart representing the methodology used for the evaluation of the thermal properties of soils.**

# CHAPTER 3: Site Descriptions and Collection of Data

## 3.1 Introduction

This chapter describes the site conditions and measured data from 1) Provincial Road PR391, Thompson, Manitoba, 2) Inuvik-Tuktoyaktuk Highway, Northwest Territories, 3) Highway 3, Behchoko-Yellowknife, Northwest Territories, 4) Murtèl-Corvatsch Rock Glacier, Engadin Region, Switzerland, and 5) Chilean Andes Rock Glacier, Chile.

Each site is located in areas of continuous permafrost or mountain permafrost, with the exception of Provincial Road PR 391 and Highway 3, Behchoko-Yellowknife, which are found in discontinuous permafrost zones. All data related to the projects are included in the Appendix.

## 3.2 Provincial Road PR391, Thompson, Manitoba

This project is located 18 km northwest of Thompson, Manitoba on Provincial Road 391 approximately at 55°50’ N / 98°01’ W as shown in Figure 3.1 (Flynn, 2015). PR 391 was initially constructed in the mid-1960’s as a compacted-earth road, converted into a gravel road in the 1970’s and upgraded with a bituminous pavement surface in the early 1980’s. This is now, an all-season road located in an area of discontinuous permafrost, and is the only route that provides access to Northern mining areas, hydroelectric generating stations and First Nations Communities in Northwestern Manitoba (Batenipour, 2012).

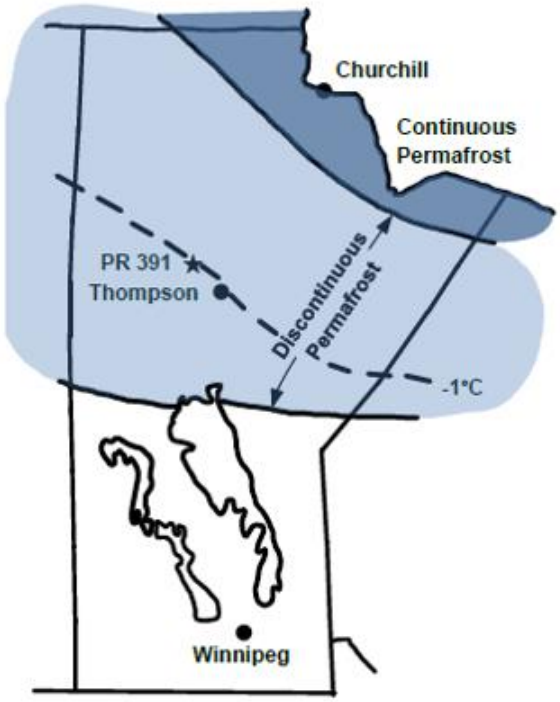


**Figure 3.1. Location of PR391 research site (Flynn, 2015) (Used with permission).**

The embankment consists of 5-6 m of gravel from the original construction and subsequent re-grading underlain by silty clay. Clayey silt with some organics is encountered at the toe of the embankment.

All measured data from this project was collected from Flynn (2015) and additional monitoring (2014-2017) carried out by the author of this thesis via satellite connected to a data acquisition system installed at the site for recording of temperature readings.

The thermistor strings installed at the mid slope and toe of the embankment in 2008 and at the shoulder and centreline in 2012 provided constant temperature data. Figure 3.2 shows a sketch of the thermistor strings arrangement.

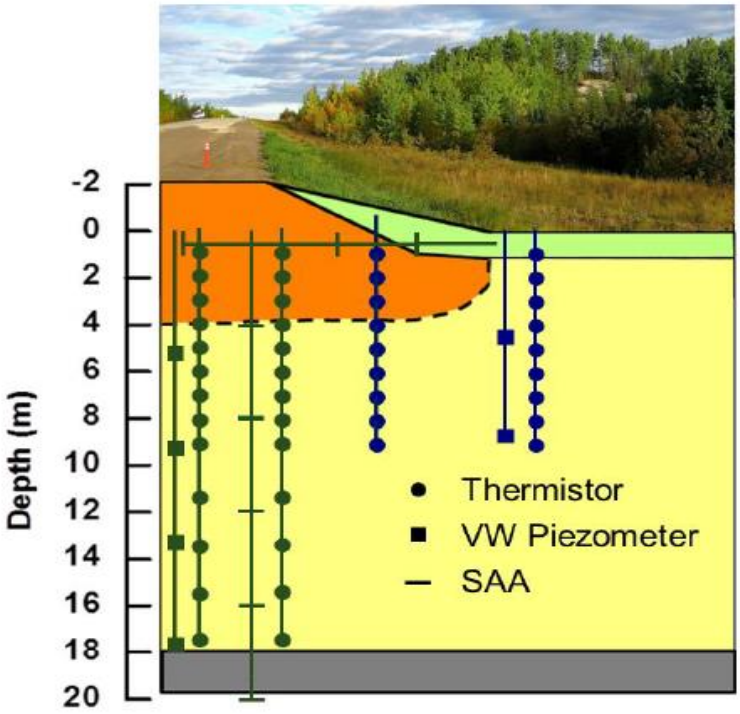


**Figure 3.2. Approximated cross section and installed instrumentation of the research site (Flynn, 2015) (Used with permission).**

Figures 3.3 through 3.6 show the annual maximum, minimum and average temperatures with depth in PR391 between October and April in 2014-2015, 2015-2016 and 2016-2017 at the toe, mid-slope, shoulder and centreline of the embankment respectively. The lack of data observed at the toe and shoulder of the embankment is the result of communication interruption with the data acquisition system.

The temperatures with depth at the toe and mid-slope (Figure 3.3 and 3.4) show average warm temperatures, reflecting higher values under the toe compared to the mid-slope. Freezing temperatures are seen below the shoulder and centreline of the embankment (Figure 3.5 and 3.6). Kurz (2014) and Flynn

(2015) reported that degrading permafrost (frost bulb) located below the embankment influenced this variation.

According to readings obtained by Batenipour (2012) and Flynn (2015), the depth of mean zero annual amplitude, the depth at which seasonal changes are reduced to a 0.1°C range, is reached at about 8-9 m below the surface level (from the toe level). This has also been observed from the monitored data between 2014 and 2017.

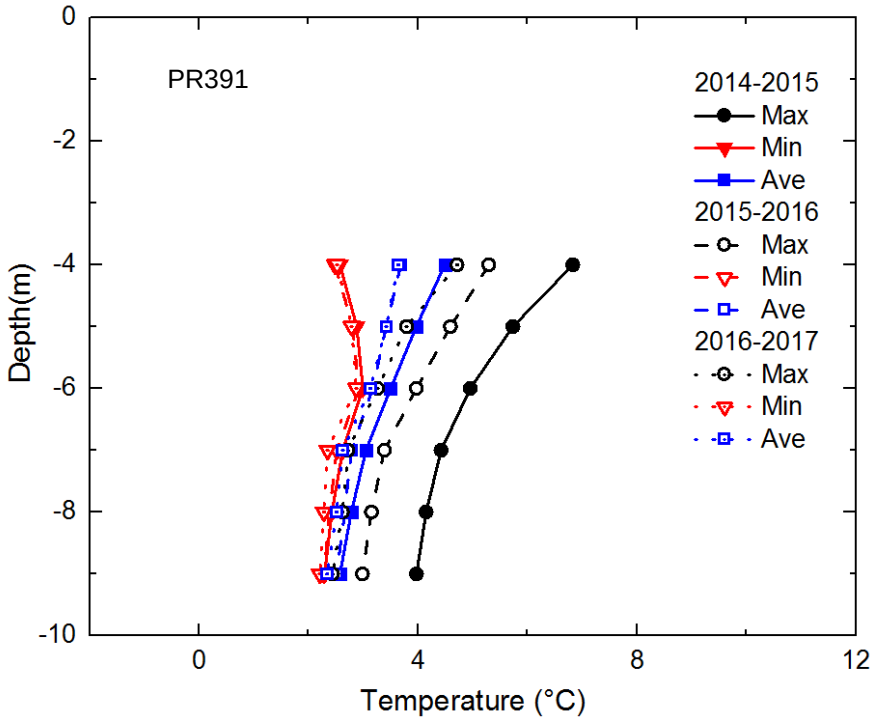


**Figure 3.3. Temperatures with depth between October 2014 and April 2017 at the toe of the embankment.**

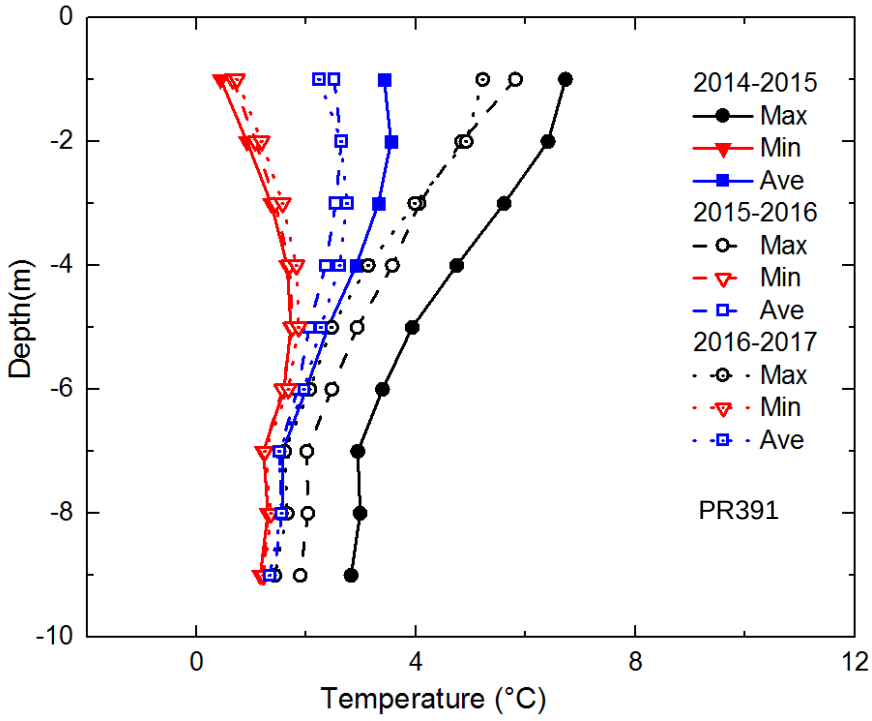


**Figure 3.4. Temperatures with depth between October 2014 and April 2017 at the mid-slope of the embankment.**

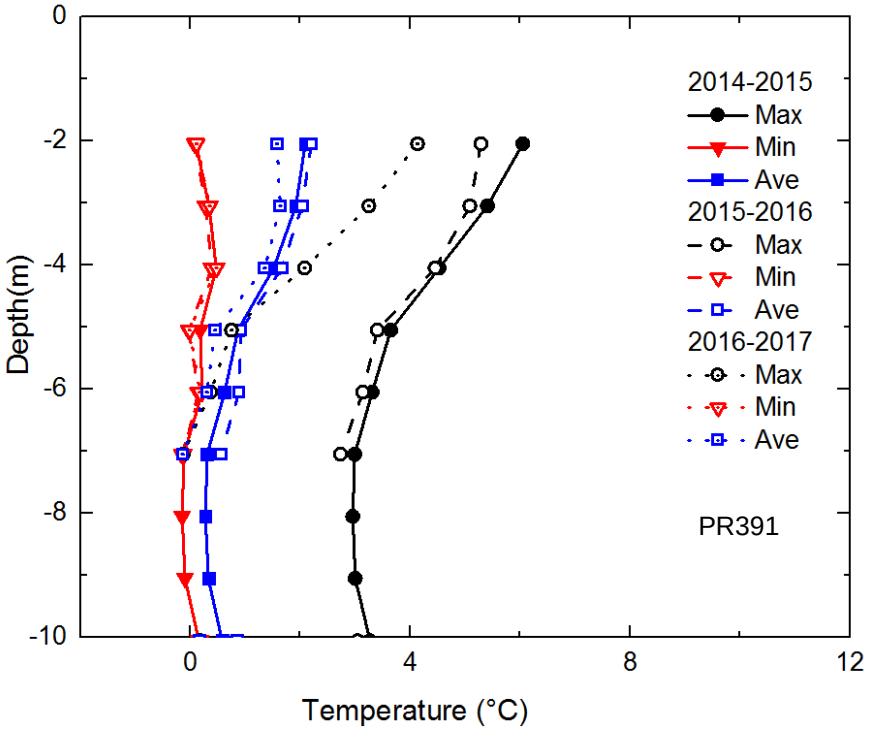


**Figure 3.5. Temperatures with depth between October 2014 and April 2017 at the shoulder of the embankment.**

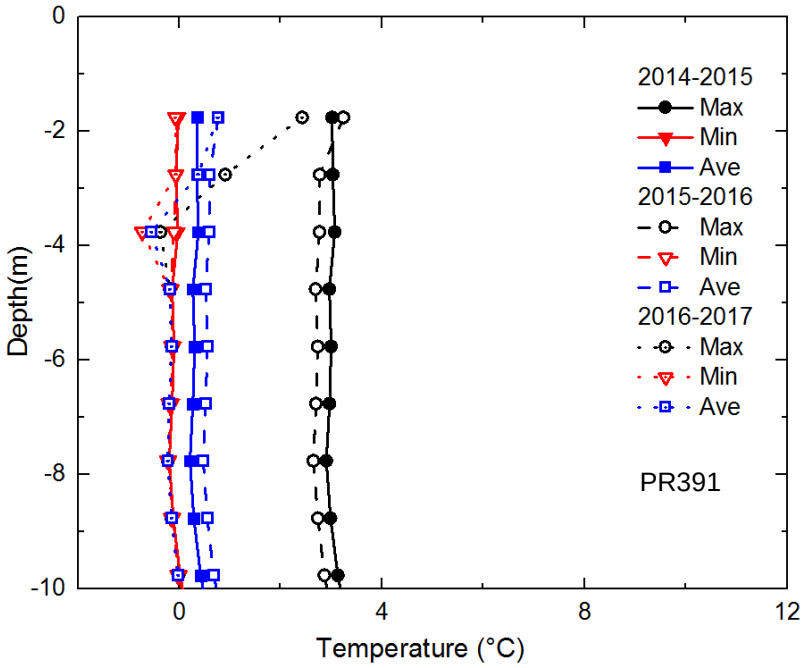


**Figure 3.6. Temperatures with depth between October 2014 and April 2017 at the centreline of the embankment.**

Figures 3.7 to 3.10 show variations of measured data at the toe, mid-slope, shoulder and centreline. As air temperatures have lower effect on the thermal regime due to the insulation of the embankment material, less variation with depth are noticed at the shoulder (Figure 3.9) and centreline (Figure 3.10) compared to the values at the toe (Figure 3.7) and the mid-slope (Figure 3.8) of the embankment.

Figures 3.9 and 3.10 show that the frost bulb region below the shoulder and centreline (at 8 and 9 m below the toe surface) experienced warm temperatures during certain days between 2014 and 2016 compared to the constant freezing temperatures measured by Flynn (2015). Temperatures below the shoulder (Figure 3.9) at 8 and 9 m, show warming temperatures after July 2015. After April 2016, no data is available at these depths below the shoulder. At the centreline

(Figure 3.10) at 8 and 9 m below the toe surface, temperatures return to a constant trend at 0 °C after April 2016.

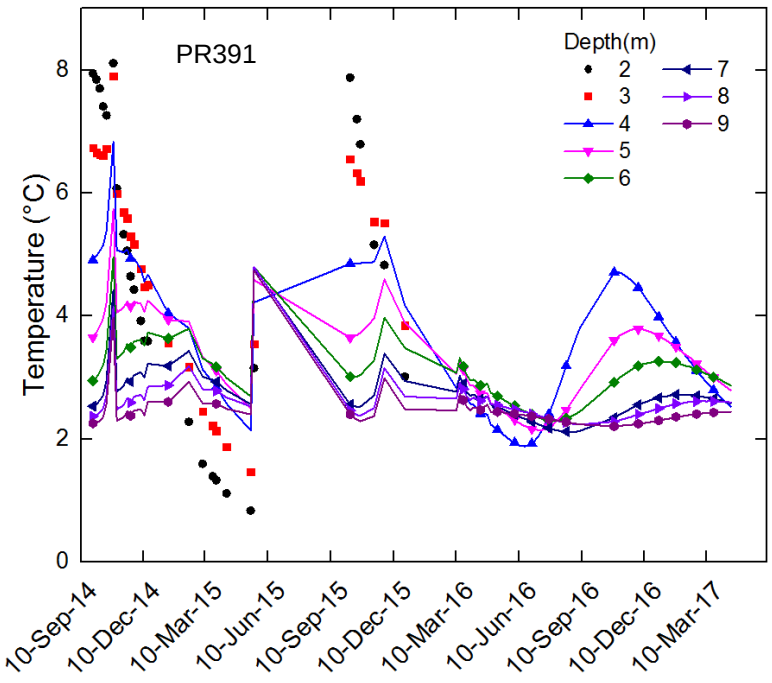


**Figure 3.7. Measured temperatures with time at the toe of the embankment.**

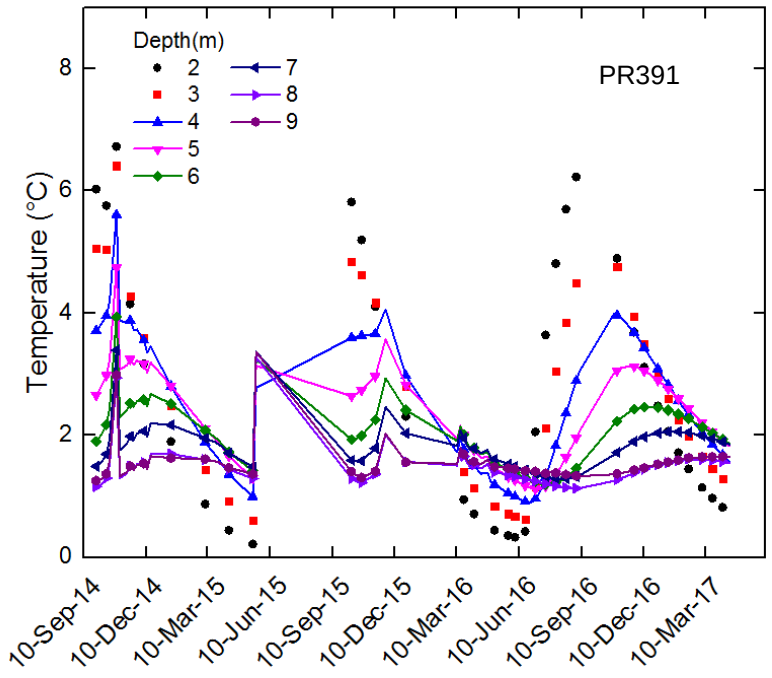


**Figure 3.8. Measured temperatures with time at the mid-slope of the embankment.**

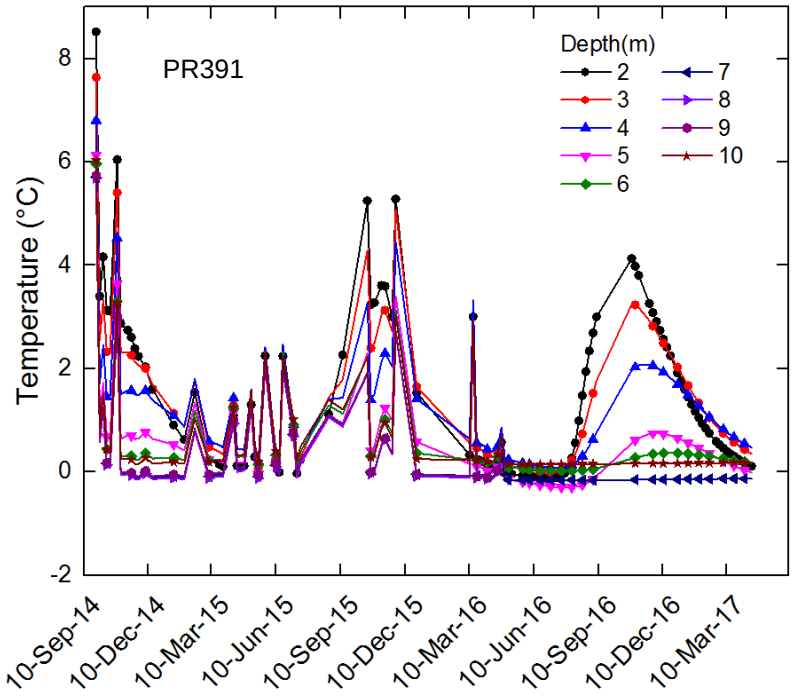


**Figure 3.9. Measured temperatures with time at the shoulder of the embankment.**

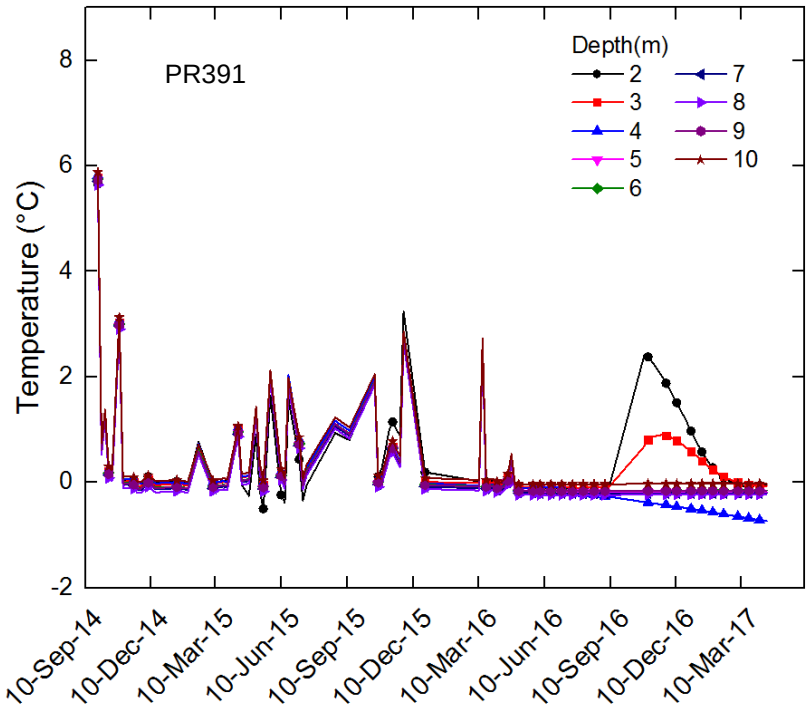


**Figure 3.10. Measured temperatures with time at the centreline of the embankment.**

### 3.3 Inuvik-Tuktoyaktuk Highway, Northwest Territories

Ongoing monitoring of instrumented test sections along the Inuvik-Tuktoyaktuk Highway is performed to study the behavior of reinforced and unreinforced embankments affected by natural thawing and settlements (De Guzman et al. 2015).

The test sections are located at 69°00 'N / 133°18 ‘W (Figure 3.11). Most of its fill materials are from glacial soil consisting of silty sand with high moisture content with some organic matter. The foundation is mainly composed of frozen peat or clay. Figure 3.12 shows the location of horizontally-laid thermistors strings installed at the top and base of embankment. The figure also shows the location of vertically-laid thermistors strings at the centreline and toe of the embankment (De Guzman et al. 2015).


**Figure 3.11. Map of the Inuvik-Tuktoyaktuk highway and the research section monitored by the University of Manitoba.**

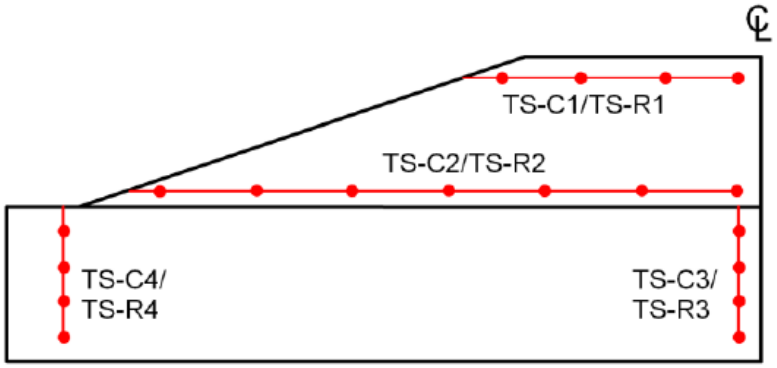


**Figure 3.12. Cross section representing the thermistor strings installed within the embankment and foundation. (De Guzman et al. 2015) (Used with permission)**.

Measured data from this site is obtained from De Guzman et al. (2017) between April 2015 and August 2016. Figures 3.13 to 3.16 show maximum, minimum and average temperature profiles at the top of the embankment, at the base of the embankment, at the centreline below the embankment (foundation) and at the toe of the embankment, respectively.

Figure 3.13 shows average freezing temperatures at the top of the embankment that varies between -3 °C and -4 °C. Figure 3.14 shows an average warming temperature near the surface of the slope that decreases towards the centreline of the embankment. Figure 3.15 shows temperatures underneath the foundation surface at the centreline of the embankment that reported values ranging from -10 °C to -4 °C. Figure 3.16 shows a thin active layer at the toe of the embankment with temperatures ranging from -9 °C to 6 °C.

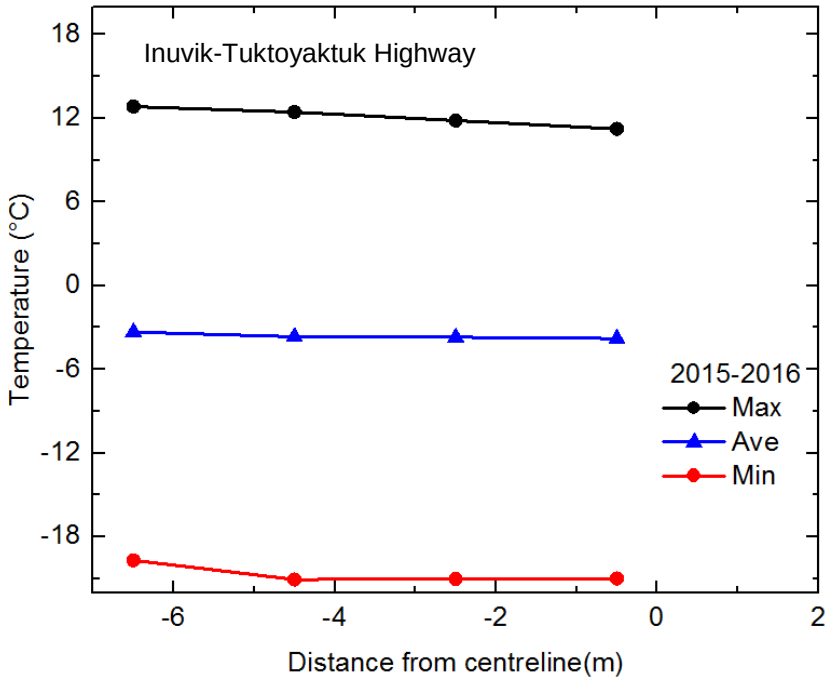


**Figure 3.13. Measured horizontal temperatures between Abril 2015 and August 2016 at the top of the embankment at a depth of 0.5 m.**

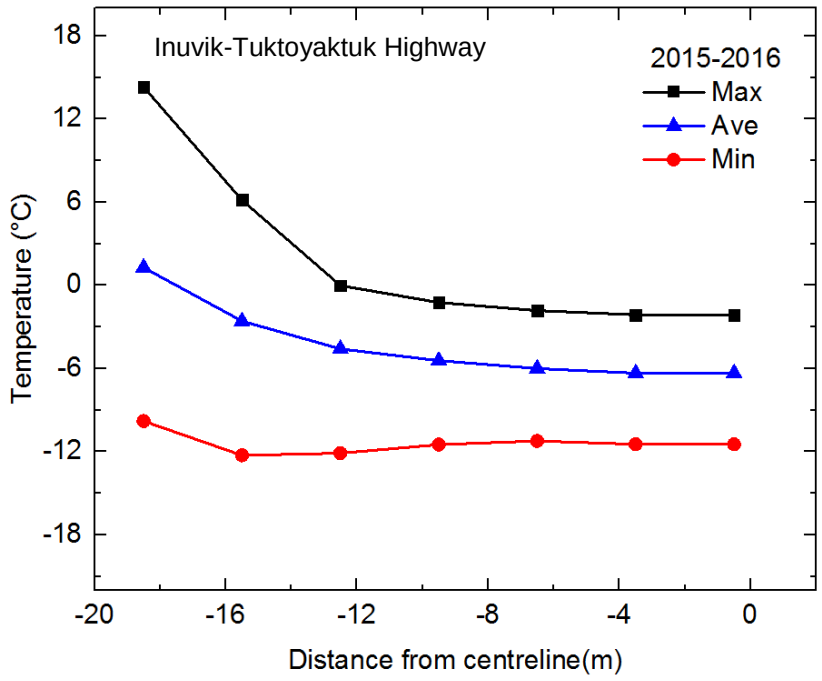


**Figure 3.14. Measured horizontal temperatures between Abril 2015 and August 2016 at the base of the embankment at 0.6 m from the foundation surface.**

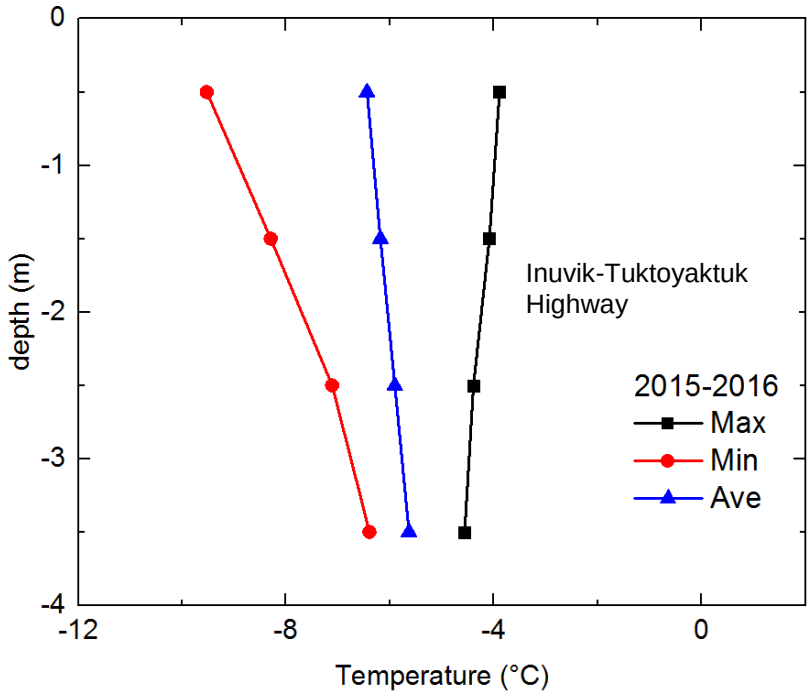


**Figure 3.15. Temperatures with depth between Abril 2015 and August 2016 at the centreline of the embankment below the foundation surface.**

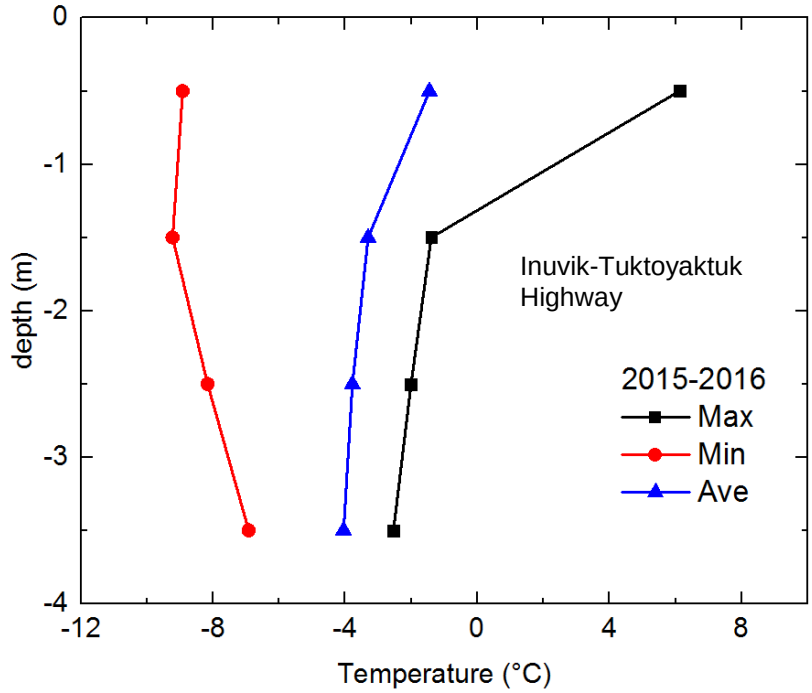


**Figure 3.16. Temperatures with depth between Abril 2015 and August 2016 at the toe of the embankment.**

Figures 3.17 to 3.18 show temperature variations of measured data at different distances from the centreline at the top and base of the embankment, respectively. Both figures show more variation of temperature near the slope surface. Figures 3.19 and 3.20 show temperature variations of measured data at different depths at the centreline of the embankment below the foundation surface and the toe of the embankment, respectively. Figure 3.19 shows low variations with depth compared to the measures at the toe of the embankment (Figure 3.20) where some warming temperatures are noticed near the surface. This is consistent with Alfaro et al. (2009) that future thawing and degradation of permafrost will start at the toe and will continue progressing towards the centreline below the embankment.

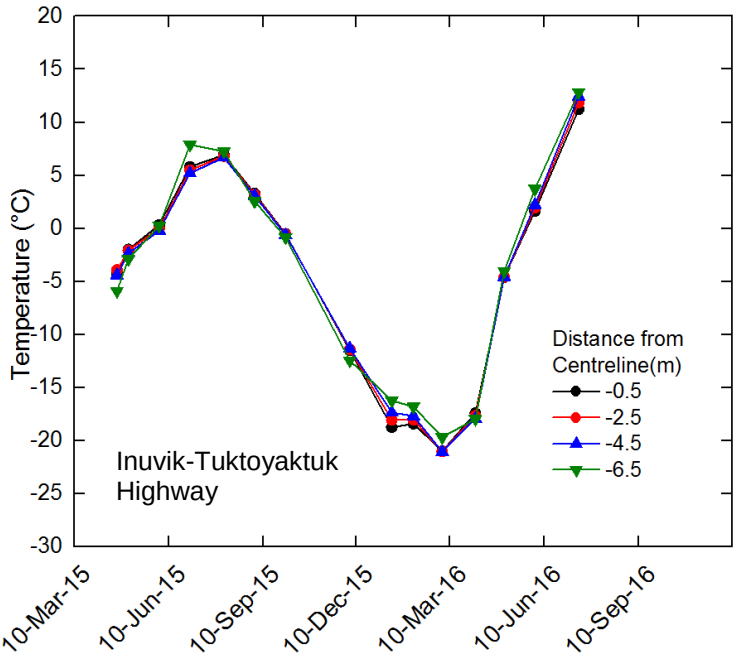


**Figure 3.17. Measured temperatures with time at the top of the embankment.**

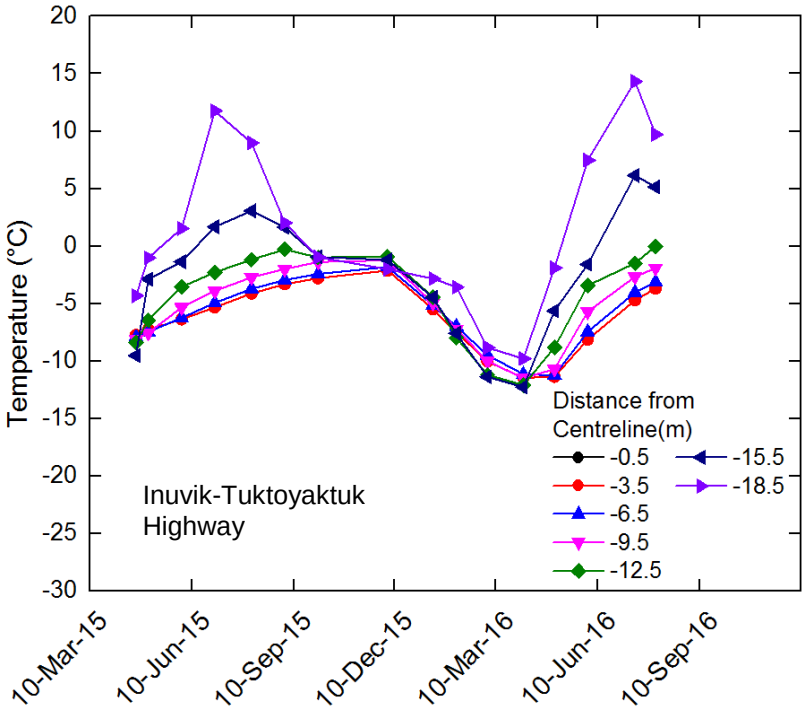


**Figure 3.18. Measured temperatures with time at the base of the embankment.**

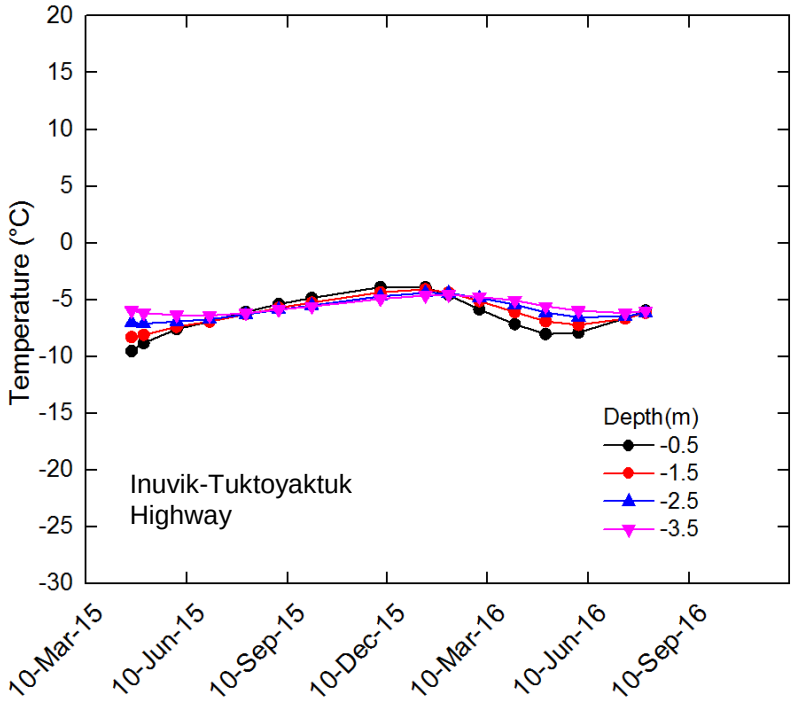


**Figure 3.19. Measured temperatures with time at the centreline of the embankment below the foundation surface.**

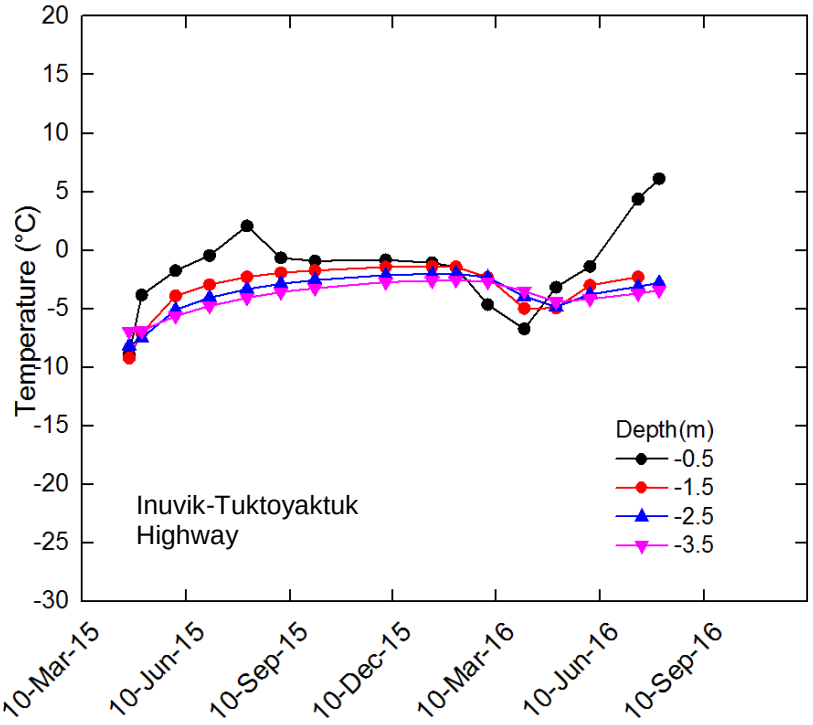


**Figure 3.20. Measured temperatures with time at the toe of the embankment.**

### 3.4 Highway 3, Behchoko-Yellowknife, Northwest Territories.

This project represents another case study aimed at investigating the degradation of permafrost on highways. The Government of the Northwest Territories in association with Engineers Canada, selected a section of 100 km of Highway 3, located between Behchoko(Rae-Edzo) and Yellowknife (Figure 3.21), to carry out a climate change vulnerability assessment of the road affected by warm and discontinuous permafrost (BGC Engineering Inc., 2011). The highway was originally constructed in 1968 as a clay embankment with gravel surface. Between 1999 and 2006, this section was re-aligned and re-built with chip-seal coating.

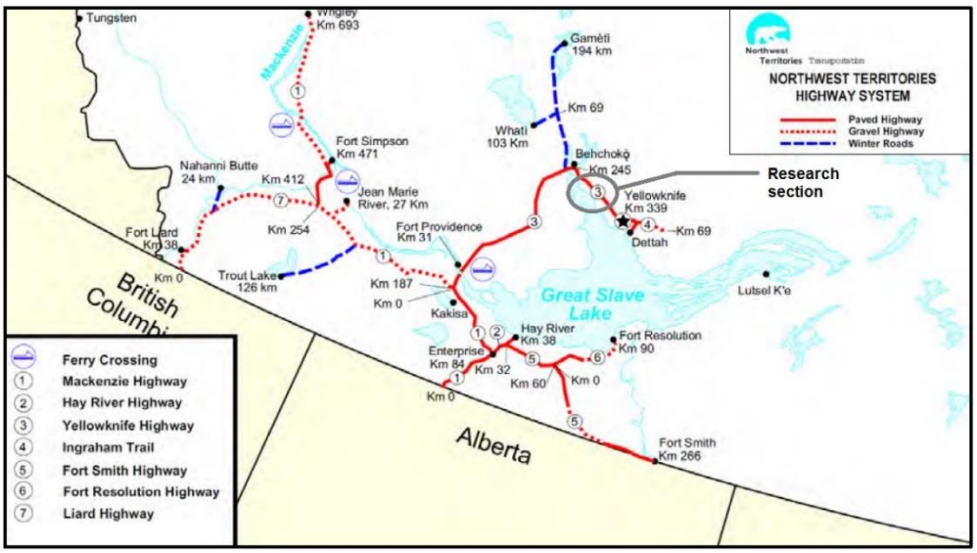


**Figure 3.21. Southern highway system of the Northwest Territories (GNWT- DOT).**

Cracking and settlements are attributed to permafrost degradation in the foundation in zones of elevated ice content. Continuous regrading and sealing of the embankment is utilized to maintain safe driving and proper conditions (Stirling et al. 2015; BGC Engineering Inc. 2011).

The project was divided into four test sections located at about 62°27'N / 114°21'W, 30 to 40 km west of Yellowknife, NWT. Measured data was collected between December 2012 and December 2014 from thermistors installed at 30 m off the road on the south of test section 3. Figure 3.22 shows the maximum, minimum and average temperatures with depth at the site. It can be seen a slight warming of average temperatures in 2012-2013 compared to average freezing temperatures reported in 2013-2014. These profiles reflect an active layer that extend to 3 m of depth underlain by warm permafrost. Below this depth, ground temperatures vary from -0.21 °C to -0.03 °C.

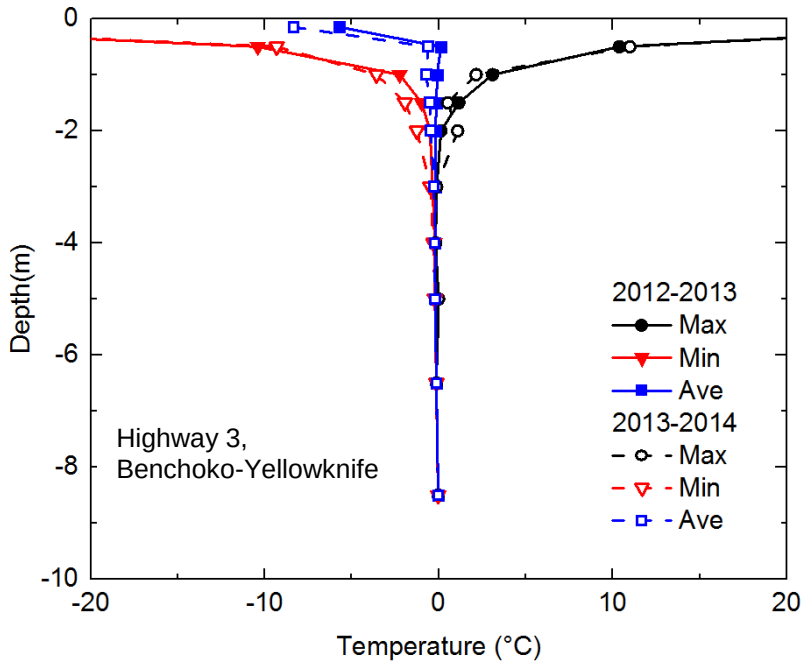


**Figure 3.22. Temperatures with depth between December 2012 and December 2014.**

Figure 3.23 represents temperature variations of measured data at different depths. It shows variations with slight changes below 3 m from the surface where temperatures are almost constant at 0°C. Furthermore, through mapping of the surrounding area, it can be seen large bodies of water, which can accelerate the deterioration of this permafrost during summer season.

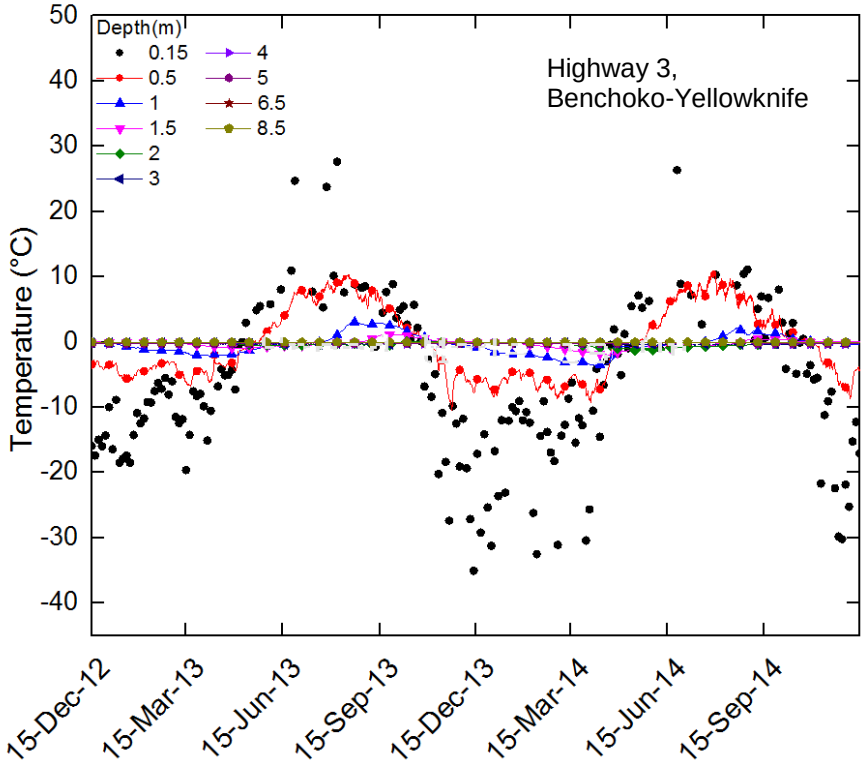


**Figure 3.23. Measured temperatures with time.**

### 3.5 Murtèl-Corvatsch Rock Glacier, Engadin Region, Switzerland

Mountain permafrost can be found under colder temperate conditions at high altitudes (Arenson, 2002). The present case study was part of the borehole monitoring program developed by Permafrost and Climate in Europe (PACE) (Figure 3.24). This rock glacier is likely the most investigated location in the European Alps, in terms of morphology, temperature, internal structure, hydrology and climate change of the mountain permafrost (Arenson, 2002).

This thesis used measured data from one of the two boreholes drilled in 2000, which has a depth of 63.2 m (Arenson, 2002). The extracted samples could be divided into 4 main layers as follows: top layer with large boulders, ice-rich layer, frozen gravel and unfrozen blocky layer. The upper layer showed

boulders of variable dimensions that can reach more than 1 m in diameter. Underneath the boulders, it is encountered a thick ice layer of about 20 m. This layer included low content of sand and silt. Further down, a layer of frozen gravel with some inclusions of sand and silt is located (ice volumetric content starts to decrease from 100% to 50-70%). The lowest layer showed large boulders containing large air voids and unfrozen water content (Arenson, 2002).

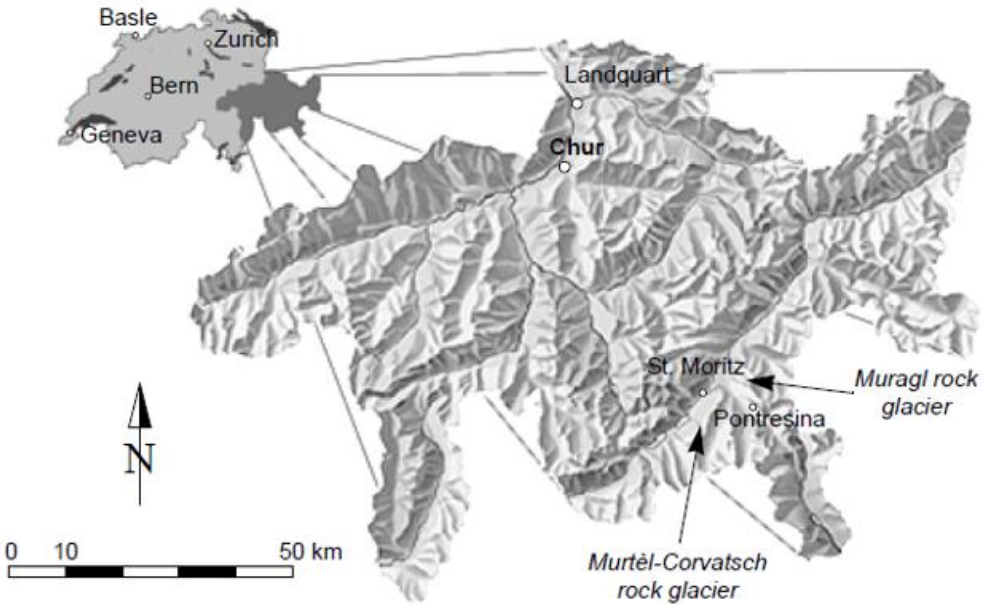


**Figure 3.24. Location of the Muragl and Murtèl-Corvatsch rock glaciers (Arenson, 2002) (Used with permission).**

Measured data were collected between September 2005 and September 2007. Figure 3.25 shows the maximum, minimum and average temperature with depth at the site. Figure 3.25 shows a regime with an active layer of about 2 m below the surface with average temperatures between -2°C and -3°C. A depth of zero annual amplitude is encountered at about 25 m. Below this depth,

temperatures are constant until 45m below the surface where variations are regulated by the earth's interior showing some warming temperatures.

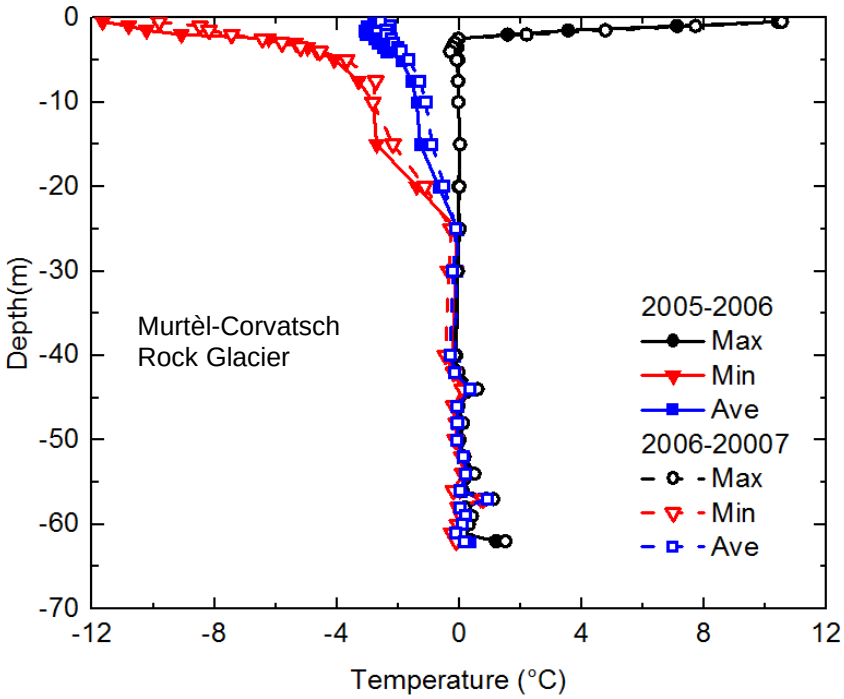


**Figure 3.25. Temperatures with depth between September 2005 and September 2007.**

Figure 3.26 shows temperature variations of measured data at different depths. It can be seen a high temperature variation between 0.5 and 2 m of depth. Below this level, in the ice-rich layer, temperatures are slightly constant below 0°C in winter and then, rise to be constant at 0°C in the following summer. Below 25 m of depth, temperatures stay at or above 0°C.

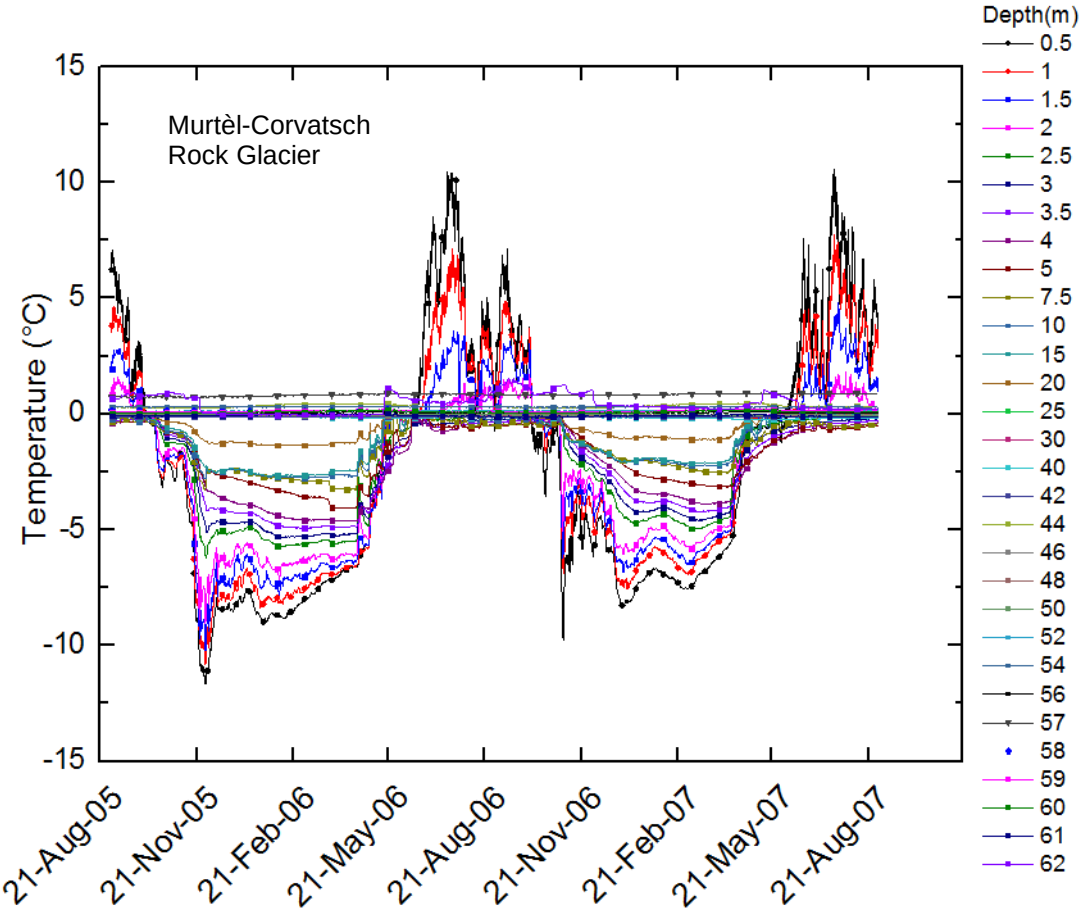


**Figure 3.26. Measured temperatures with time.**

### 3.6 Chilean Andes Rock Glacier, Chile

The exact location of this project is unpublished. Publications such as Monnier and Kinnard (2015), Azocar et al. (2016) and Arenson et al. (2010) were referred to study the characteristics of this mountain permafrost.

A clear understanding of this type of mountain permafrost becomes difficult due to the reduced number of deep borehole and limited development of models utilizing geophysical data and variable composition (Hausmann et al. 2007). However, methods such as GIS and generalized additive models for the permafrost mapping and distribution considering topographic, aerial and satellite

observations (Arenson and Jackob, 2010; Azocar et al. 2016), and ground-penetrating radar procedures to investigate the internal structure and composition have been recently developed to identify the extension and behavior in the Chilean rock glacier (Figure 3.27).

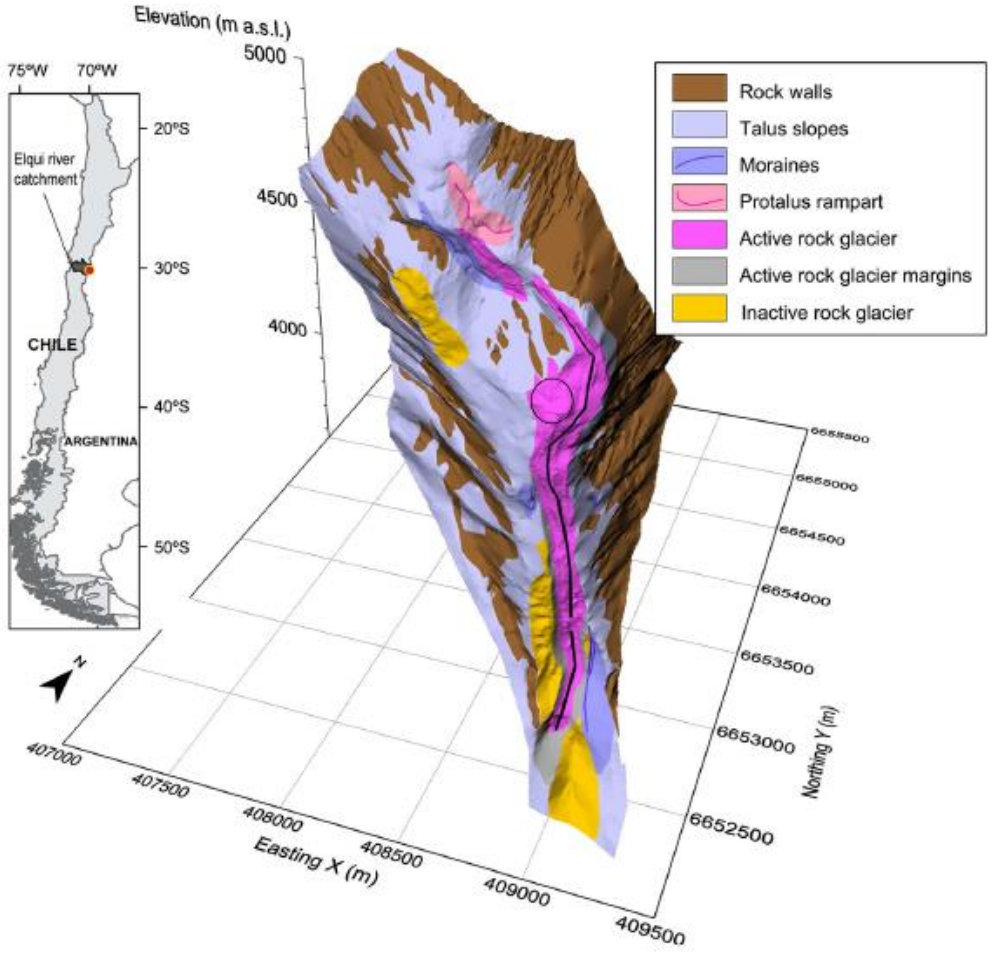


**Figure 3.27. Location map and 3-D geomorphological sketch of the Las Liebres rock glacier in the Chilean Andes (Monnier and Kinnard, 2015) (Used with permission).**

Measured data was collected between December 2009 and December 2011. Figure 3.28 shows the maximum, minimum and average temperature with depth at the site. The active layer thickness penetrates to about 1.7 m of depth. The average temperature in the active layer ranges between -1°C and -2°C. The

depth of zero annual amplitude is encountered at about 12 m of depth. Further down, sub-zero temperatures are relatively constant reaching an average of -1.5 °C at the bottom.

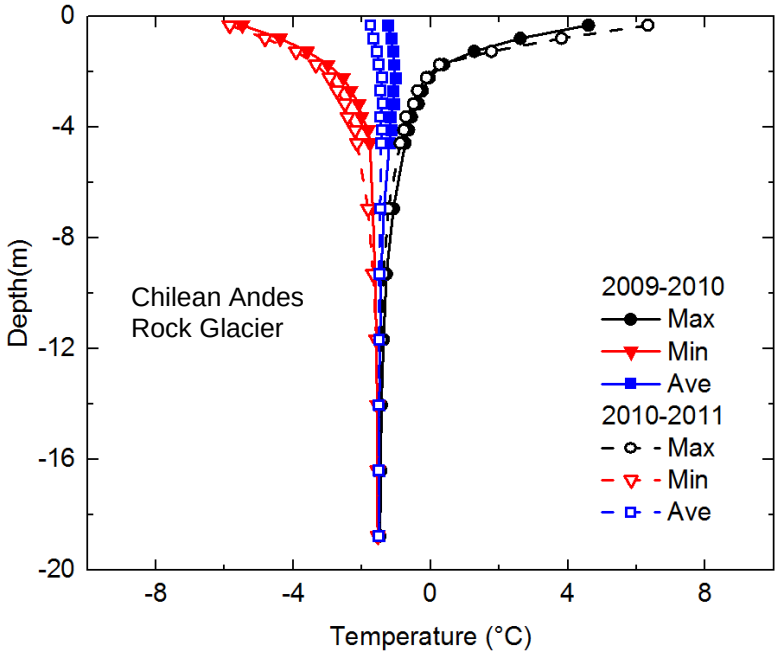


**Figure 3.28. Temperatures with depth between December 2009 and December 2011.**

Figure 3.29 shows temperature variations of measured data at different depths and times. Below the active layer, a delay of the peak in summer and the bottom in winter can be noticed. This is due to the fact that at greater depth measured ground temperatures take longer time to show seasonal variations. Temperatures are constant at about -1.5°C below 11.7 m where seasonal changes have no effect.

Investigations of similar rock glaciers encountered massive ice content, cobbles and gravels with some fines inclusions. In some cases water accumulated at the top of the permafrost table provided an insulation effect that reduced the penetration of the active layer (Arenson et al. 2010).

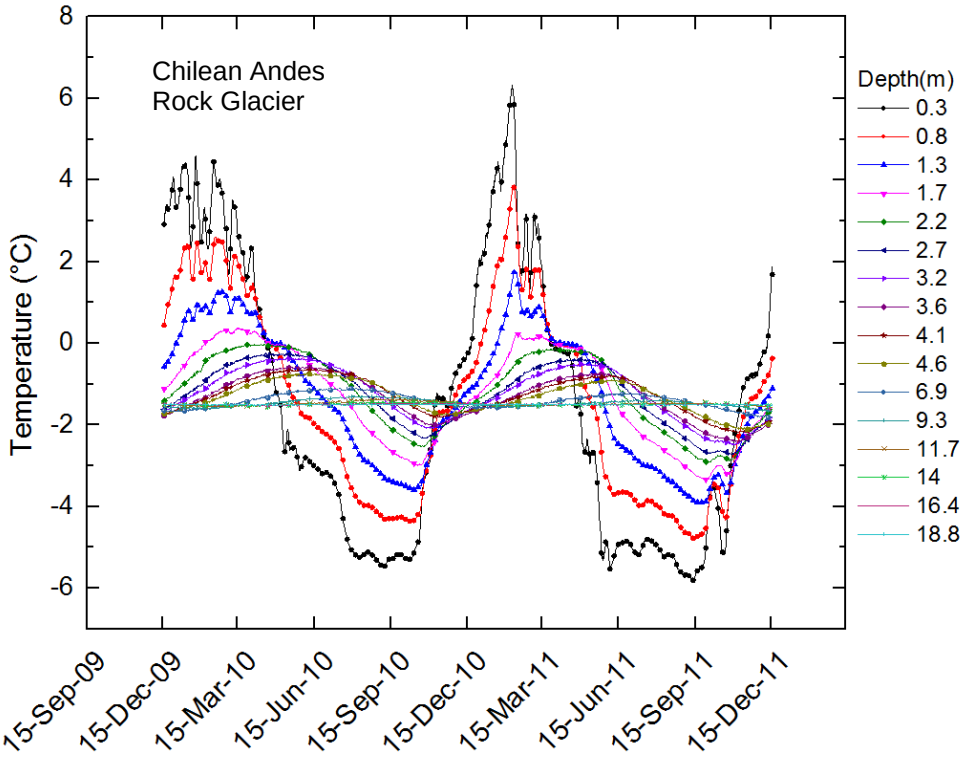


**Figure 3.29. Measured temperatures with time.**

# CHAPTER 4: Geothermal Numerical Modelling

## 4.1 Introduction

As stated in chapter 2, a numerical model is a mathematical representation of a real life system. Rykiel (1996) states that the accuracy of the model representation or validation depends on the evaluation of theory, implementation and data available. More data are required when the complexity of the model is increased (Riseborough et al. 2008).

Five geothermal models were prepared based on the sites presented in Chapter 3. The models represented in-situ conditions whose initially assumed thermal properties were obtained from literature. The models were adjusted and compared to the measured temperatures with depth and temperature variations with time. Thus, the thermal properties were calibrated for those specific sites and conditions. A sensitivity analysis was carried out to further evaluate the thermal properties. An alternate procedure to determine the thermal conductivity of soils based on the variation of temperature with time is also used. All models, parameters, and results are included in the Appendix.

## 4.2 Geothermal Modelling

The geothermal models were created using TEMP/W, an application computer program of GEO-SLOPE International Ltd, a software developer for geo-engineering and earth sciences research (GEO-SLOPE International Ltd., 2008). TEMP/W is a finite element software used to analyze thermal changes in the ground as a result of environmental factors and construction of civil structures. Its formulation can solve thermal problems affected by freezing and

thawing of soil applying the theory of forced convection, conduction and phase change. Its use has expanded to research institutions that investigate the permafrost degradation due to climate change, the effect of civil engineering structures on the thermal regime, and the groundwater flow systems affected by freezing temperatures. (GEO-SLOPE International Ltd, 2008)

### 4.2.1 Theory

The geothermal modelling can be solved through steady-state or transient analysis. The geometry of the system is defined by sketching the problem domain. Finite element numerical methods like TEMP/W consist of a domain subdivided into elements. These small pieces show individual characteristics that when interconnected, they represent the behavior of the entire system. The partition process of the sketch into small elements is called meshing or discretization.

After defining the geometry of the domain, it is required to assign the material properties. This thesis used the Full Thermal Model as a defining material model. The Full Thermal Model requires specified functions for the thermal conductivity and unfrozen volumetric water content. These functions depend on the temperature of the ground and the water/ice content of the analysis. The model requires the introduction of the frozen and unfrozen volumetric heat capacity of the soils.

In TEMP/W, boundary conditions are applied over the domain. These can be grouped into two main categories: thermal boundary conditions and climate boundary conditions. The thermal boundary conditions comprises constant

temperature, heat flux and thermal function. Constant temperature or heat flux can be applied at the bottom of the models to represent the average of temperature obtained by the thermistor at that point during the reported period. A thermal function (sine function model) can be applied at the surface of the geothermal model in sites where enough climate data from stations were unavailable. This thermal function varies with mean air temperature as a function of time, which is modified at the same time by a modifier function (N-factors vs temperature) in response to the surface temperature. The N-factors will be explained in section 4.2.3.

The climate boundary conditions (climate model) are represented by climate data obtained from climatological stations. The required climate measurements during a period of analysis are maximum and minimum air temperature, maximum and minimum relative humidity, wind speed and precipitation. The latitude of the site is introduced to determine the time of the date the sun rises and sets. Furthermore, an estimated built-in net solar radiation is included based on climate data, time of the year, latitude and ground surface albedo (ratio between reflected and incoming short wave solar radiation). The climate boundary conditions can be applied at the top of a surface layer. This layer is defined in response to rapid climatic changes and simulation of vegetation, snow or any disturbance.

The geothermal modelling presents some limitations while considering specific conditions. For instance, the geothermal modelling does not consider

chemical changes, volume changes and pore-water pressure changes associated to the heat flow (GEO-SLOPE International Ltd., 2008).

### 4.2.2 Governing Equations

Heat flux by conduction is represented on TEMP/W using equation 4.1, which is a modified version of equation 2.1:

$Equation\ 4.1$ $$q = -k\ \frac{\partial T}{\partial x}$$

where $q$ is the heat flux across the surface, $\frac{\partial T}{\partial x}$ is the temperature gradient and $k$ is the thermal conductivity. The negative sign indicates that heat is transferred from a point of high temperature to a point of low temperature. TEMP/W will merge this equation into a leading differential equation used for the formulation as follows:

$Equation\ 4.2$ $$\frac{\partial}{\partial x}\left(k_x\ \frac{\partial T}{\partial x}\right) + \frac{\partial}{\partial y}\left(k_y\ \frac{\partial T}{\partial y}\right) + m = \lambda\ \frac{\partial T}{\partial t}$$

where $k_x$ and $k_y$ are the thermal conductivities in the x and y directions, respectively, $m$ is the applied boundary flux and $\lambda$ is the capacity of heat storage. This equation affirms that the heat flux entering and leaving a volume of soil at a specified time is proportional to the change in the stored heat energy.

This capacity to store heat can be represented in the following formula:

$Equation\ 4.3$ $$\lambda = C + L\ \frac{\partial w_u}{\partial T}$$

Where $w_u$ is the total unfrozen volumetric water content, $T$ is the temperature, $C$ is the volumetric heat capacity of the soil and $L$ is the latent heat of water. $w_u$ can be expressed in terms of the unfrozen water content (0-100%) and volumetric water content of the soil. Equation 4.3 is divided into the volumetric heat capacity (frozen or unfrozen) representing the slope of the energy curve in the frozen or unfrozen regions and $L\ \frac{\partial wu}{\partial T}$ representing the rate of change of the latent heat associated with the phase change.

When substituting $\lambda$ in equation 4.2:

$$Equation\ 4.4 \qquad \frac{\partial}{\partial x}\left(k_x \frac{\partial T}{\partial x}\right) + \frac{\partial}{\partial y}\left(k_y \frac{\partial T}{\partial y}\right) + m = \left(C + L \frac{\partial w_u}{\partial T}\right) \frac{\partial T}{\partial t}$$

which is a representation of the complete differential equation utilized by TEMP/W.

### 4.2.3 Surface N-factors

As stated in chapter 2, local variations in air temperature, wind speed, precipitation, vegetation, snow cover, thermal properties and solar radiation affect the ground temperature. These factors regulate the air freezing and thawing indices that may be implemented for seasonal changes problems. The air freezing index ($I_{af}$) represents the number of negative degree-days (mean daily temperature times the number of days) between its maximum in autumn and its minimum in the following spring. The air thawing index ($I_{at}$) represents the number of positive degree-days between its minimum in the spring and its

maximum in the following autumn. Surface indices ($I_S$) are generally determined by an empirically defined N-factor, which can be represented as the ratio of the ground surface index to the air index as follows:

$Equation$ 4.5 $$n_t = \frac{I_{st}}{I_{at}}$$

$Equation$ 4.6 $$n_f = \frac{I_{sf}}{I_{af}}$$

where $I_{st}$ and $I_{sf}$ are the seasonal ground surface thawing and freezing indices, respectively. N-factors account for a complex form of atmosphere-soil system and therefore, their values will vary for a specific location (Riseborough et al. 2008). For instance, the thawing N-factor for two types of pavement (Portland cement concrete and bituminous) will show different values based on the surface short-wave absorptivity, thermal properties and external conditions (vegetation and climate). TEMP/W utilizes these N-factors to simulate the boundary conditions at the ground surface as a combination of a seasonal air temperature function and a modifier function. The modifier function represents the variations of the N-factor as a function of the ground temperature at the surface (GEO-SLOPE International Ltd, 2008).

### 4.2.4 Range of Values of Thermal Properties

Initial thermal properties used for the simulation of the measured temperatures were obtained from the literature. The sources were Flynn (2015), Andersland and Ladanyi (2004), Arenson et al. (2015), GEO-SLOPE International Ltd.(2008), Eppelbaum et al. (2014) and Robertson (1988). Table 4.1 shows the ranges for frozen and unfrozen thermal conductivities and

volumetric heat capacities used for the calibration of the geothermal models. The ranges for frozen and unfrozen thermal conductivity and frozen volumetric heat capacity are highly dependent on the density of the material. The ranges of unfrozen volumetric heat capacity are dependent on the volumetric water content. The thermal conductivity of boulders represent rocks with high quartz content as mentioned by Von der Mühll and Haeberli (1990) in Murthel-Corvatsch rock glacier and Monnier et al. (2009) in the French Alps. The thermal conductivities of gravel and sand represent the thermal conductivities of coarse-grained soils. The thermal conductivities of silt and clay represent the thermal conductivities of fine-grained soils. The frozen volumetric heat capacities depend on the dry density of the frozen soil. Generally, clays show higher range of unfrozen volumetric heat capacity due to water content retention.

The geothermal models do not consider the variation of thermal properties based on porosity and organic matter. Furthermore, the total moisture content is assumed to be fixed during the analysis. These are additional limitations in the modelling that may impact the results. No attempt was made to evaluate the effect of these limitations.

**Table 4.1. Range of thermal properties from the literature.**

| Material | Thermal Conductivity (kJ/days/m/°C) | | Vol. Heat Capacity (kJ/m³/°C) | |
|---|---|---|---|---|
| | Range of Values | | | |
| | $k_f$ | $k_u$ | $c_f$ | $c_u$ |
| Boulder | 1.5 - 6.3 | 1.2 - 5.9 | 560 - 3120 | 1500 - 2340 |
| Gravel | 0.5 - 4 | 0.25 - 3 | 560 - 3120 | 1500 - 2340 |
| Sand | 0.5 - 4 | 0.25 - 3 | 560 - 3120 | 1310 - 2780 |
| Silt | 0.1 - 2.2 | 0.1 - 1.8 | 560 - 3120 | 1160 - 3030 |
| Clay | 0.1 - 2.2 | 0.1 - 1.8 | 560 - 3120 | 1000 - 3100 |
| Ice | 2.1 - 2.76 | 0.56 - 0.58 | 1567 - 1887.3 | 4192.2 - 4217.7 |

### 4.2.5 Model Performance Criteria

Model calibrations are carried out to minimize the difference between measured and simulated temperatures. The performance criteria applied in the calibration results are the root mean square error (RMSE) and the coefficient of determination ($R^2$) criteria.

The root mean square error (RMSE) is used as a statistical criterion to measure the model performance by representing the sample standard deviation between measured and simulated data (Chai and Draxler, 2014).The RMSE is calculated using the individual difference (residuals) between measured and simulated values.

RMSE can be represented in equation 4.7 as follows:

$$Equation\ 4.7 \qquad RMSE = \sqrt{\sum_{i=1}^{n} \frac{(T_{mea} - T_{sim})^2}{n}}$$

Where $T_{mea}$ is the measured temperature from the thermistors, $T_{sim}$ is the simulated temperature from the geothermal models and $n$ is the number of observations. RMSE shows the same units of temperature (°C) of the measured and simulated data. RMSE values close to 0 represents a model that simulates temperatures similar or relatively close to measured temperatures.

The coefficient of determination ($R^2$) is a statistical measure of the proportion of the variance in observed values that is predictable from the simulated values. In linear regression, the coefficient of determination represents the square of the correlation between measured and simulated data. It measures how well the regression line approximates the observed or measured data. $R^2$ varies from 0 to 1. The higher the $R^2$ the better the regression model fits the measured data. An $R^2$ of 1 indicates that the regression line perfectly fits the data.

### 4.2.6 Sensitivity Analysis

A sensitivity analysis can be defined as the study of how the uncertainty in the output of a model can be associated to the different sources of uncertainty of the input parameters (Saltelli et al. 2008). The sensitivity analysis determines sensitive parameters that show more relevance for calibration (Holländer et al. 2016). In this study, the sensitivity analysis was carried out to quantify how variations of the calibrated thermal conductivities and volumetric heat capacities affect the performance of the model.

The sensitivity analysis was limited to the sine function models of temperature vs. time in the active layer. This is due to the sine function model shows values closer to the measured data, with the active layer showing higher

variation with time. The calibrated thermal conductivities and volumetric heat capacities were varied by ± 5%, ± 10% and ± 50%. These changes in thermal properties show new temperature variations of higher or lower amplitude than the base line temperature variation of the calibrated thermal properties. Finally, these new temperature variations will be compared with the base line temperature variation to measure the sensitivity of the parameters for a specific soil.

## 4.3 Provincial Road PR391, Thompson, Manitoba

### 4.3.1 Geometry

The geometry of the model is based on previous studies by Flynn (2015), Kurz (2014) and Batenipour (2012). The instrumented section is shown in Figure 4.1. The model has a lateral extent of 30 m and a depth of 12 m below the ground surface. At greater depths, seasonal changes produce minimal variations in the ground temperatures (Flynn, 2015).

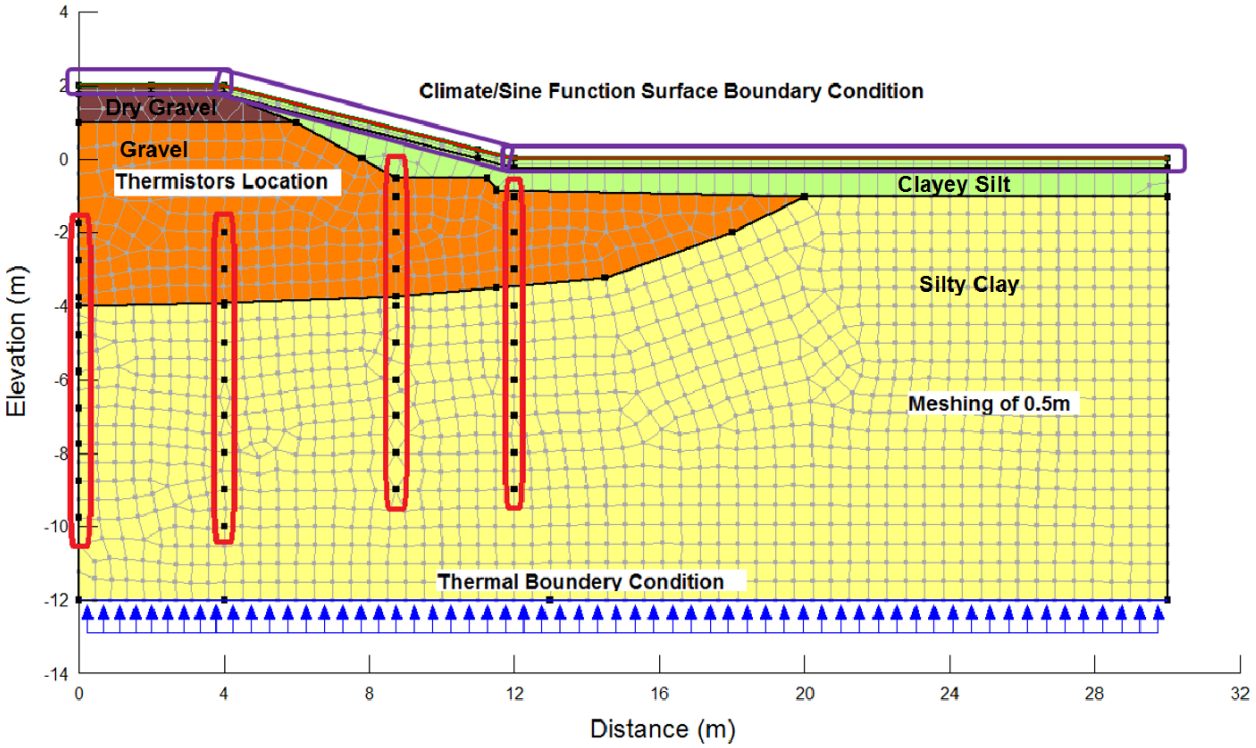


**Figure 4.1. Geothermal model cross section for PR391 showing boundary conditions, meshing and thermistors location.**

The ground profile consists of four main regions: silty clay, clayey silt, saturated gravel and dry gravel, where most of the foundation material is comprised by silty clay. The meshing is set at 0.5 m by 0.5 m. Finer mesh was also used, but the results were similar to the ones using the afore-mentioned mesh size.

### 4.3.2 Soil Properties

The model was analyzed as Full Thermal model. All the thermal properties in frozen and unfrozen states used for the calibration of the model were obtained from Table 4.1. The final calibrated values of the thermal properties using TEMP/W are shown in Table 4.2.

**Table. 4. 2. TEMP/W thermal material properties (PR391).**

| Material | Thermal Conductivity (W/m.K) | | Vol. Heat Capacity (kJ/m³/°C) | | In-situ VWC (m³/m³) |
|---|---|---|---|---|---|
| | $k_f$ | $k_u$ | $C_f$ | $C_u$ | |
| Silty Clay | 1.736 | 1.157 | 2050 | 2850 | 0.45 |
| Clayey Silt w/Organics | 1.968 | 1.273 | 1950 | 2700 | 0.45 |
| Saturated Gravel | 3.588 | 2.315 | 1850 | 2400 | 0.28 |
| Dry Gravel | 2.431 | 1.273 | 1500 | 1650 | 0.06 |

The unfrozen volumetric water content of the material represents the amount of water that remains unfrozen when temperatures change from zero to negative values. This ranges from 0 to 1 (1 means that 100% of the water in the soil is unfrozen) and is represented by a built-in function on TEMP/W based on the type of material. Furthermore, TEMP/W requires the in-situ volumetric water content, which is the volume of water per unit bulk volume of the material. For clayey silt and silty clay, these values were calculated by Kurz (2014) based on the gravimetric water content, the density of dry soil and water. The gravel was assumed to be completely saturated, with the exception of the upper layer that is replaced every year due to of maintenance operations (Flynn, 2015).

### 4.3.3 Boundary Conditions

The model was analyzed under transient conditions. A spatial function (Krigged function) was introduced to establish initial temperatures in the ground based on the measured data collected on September 25, 2010. This date was selected (two years before the data were collected) in order to equilibrate the initial conditions (Kurz, 2014). Parameters for a climate boundary condition were obtained from Environment Canada Data from the climate station at the

Thompson's airport located at 55.80° N / 97.86° W. The climate parameters included maximum and minimum daily temperature, maximum and minimum relative humidity, average wind speed and precipitation and a built-in estimated net solar radiation.

A second surface boundary condition was applied as a sine function boundary condition. This smoothed sine function is the fitted result of the mean annual air temperature. As mentioned in Section 4.2.1 and 4.2.3, an N-factor function modifies the sine function so the temperature of the ground can vary based on the type of soil and air temperature. The N-factors are shown in Table 4.3. The N-factors used by Flynn (2015) were calculated by trial and error. Due to differences in surface relief, solar radiation, vegetation and snow accumulation, they are lower than the ones utilized in the literature, mainly under freezing conditions (Flynn, 2015).

**Table 4.3. TEMP/W thermal modifiers factors (PR391) (after Flynn 2015).**

| Material | Freezing, $n_f$ | Thawing, $n_t$ |
|---|---|---|
| Road surface | 0.3 | 0.3 |
| Mid Slope | 0.1 | 0.6 |
| Toe | 0.01 | 0.73 |

A constant thermal boundary condition representing a unit flux of 3 kJ/days/m was established at the bottom of the model as shown in Figure 4.1. This value was based on the statement that geothermal gradients vary from 0.9 to 3.3°C per 100m (Brown, 1963) and the unfrozen thermal conductivity of silty clay (Flynn, 2015).

## 4.4 Inuvik-Tuktoyaktuk Highway, Northwest Territories

### 4.4.1 Geometry

The geometry is based on the diagram presented by De Guzman et al. (2015) and De Guzman et al. (2017), where only the instrumented section of the research site was considered (Figure 4.2). The model shows a foundation of 4 m by 29 m and an embankment of 5 m in height. The model shows a thick surface layer at the toe of the embankment in order to represent the slight temperature changes due to snow cover at the surface level. The meshing of the model is 0.5 m by 0.5 m.

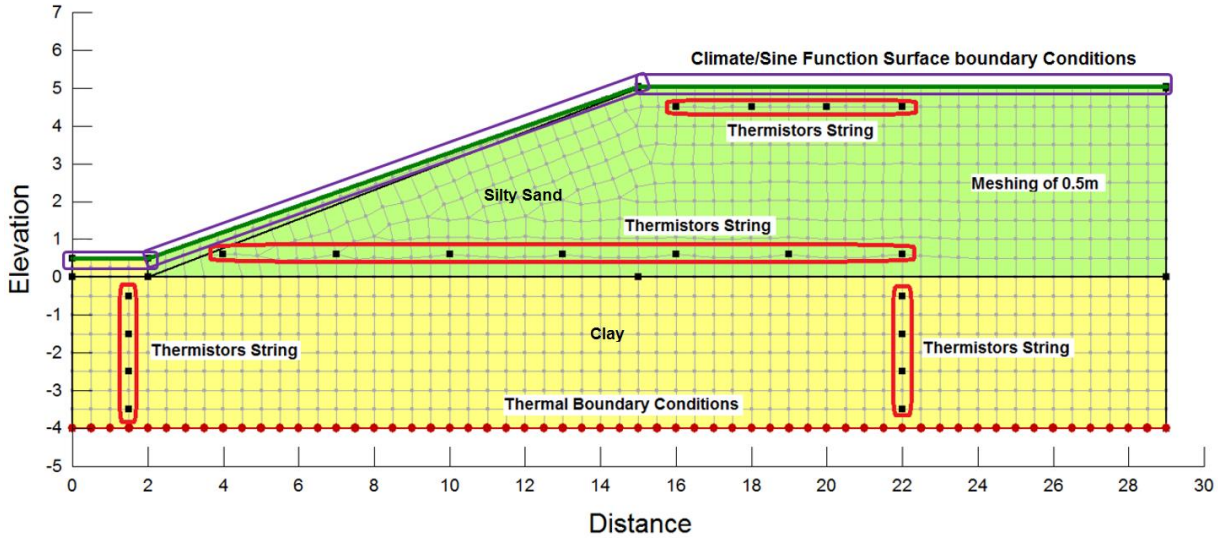


**Figure 4.2. Geothermal model Cross section for Inuvik-Tuktoyaktuk Highway showing boundary conditions, meshing and thermistors location.**

### 4.4.2 Soil Properties

The material model was analyzed as Full Thermal model. The embankment consists of silty sand and the foundation consists of clay. The thermal

conductivity and volumetric heat capacity of the silty sand and clay in frozen and unfrozen states were selected from Table 4.1. The in-situ volumetric water content of the embankment was estimated from the gravimetric water of the soil from the site. The final calibrated values of the thermal properties using TEMP/W are shown in Table 4.4.

**Table. 4.4. TEMP/W thermal material properties (Inuvik-Tuktoyaktuk Highway)**

| Material | Thermal Conductivity (W/m.K) | | Vol. Heat Capacity (kJ/m³/°C) | | In-situ VWC (m³/m³) |
|---|---|---|---|---|---|
| | $k_f$ | $k_u$ | $C_f$ | $C_u$ | |
| Silty Sand | 4.005 | 2.894 | 1950 | 2430 | 0.25 |
| Clay | 2.315 | 1.424 | 2000 | 2800 | 0.41 |

### 4.4.3 Boundary Conditions

The model was analyzed under transient conditions. Average initial temperatures were introduced for clay and silty sand. The climate boundary conditions were obtained from Environment Canada Data from the climate station located in Tuktoyaktuk, Northwest Territories at 69°26' N / 133°01' W. A sine function condition was established as a second surface boundary condition using N-factors obtained from Andersland and Ladanyi (2004) and shown in Table 4.5.

A constant thermal boundary condition of -5°C was set at the bottom of the model to represent the average temperature registered at that depth (Figure 4.2).

**Table. 4.5. TEMP/W thermal modifiers factors (Inuvik-Tuktoyaktuk Highway).**

| Material | Freezing, $n_f$ | Thawing, $n_t$ |
|---|---|---|
| Road Surface | 0.65 | 1.1 |
| Toe | 0.5 | 0.85 |

## 4.5 Highway 3, Behchoko-Yellowknife, Northwest Territories

### 4.5.1 Geometry

The height of the model extends to a depth of 8.5 m. The size of the mesh was 0.5 m by 0.5 m. A surface layer thickness of 0.3 m was considered to reasonably represent the effect of weather changes. (Figure 4.3).

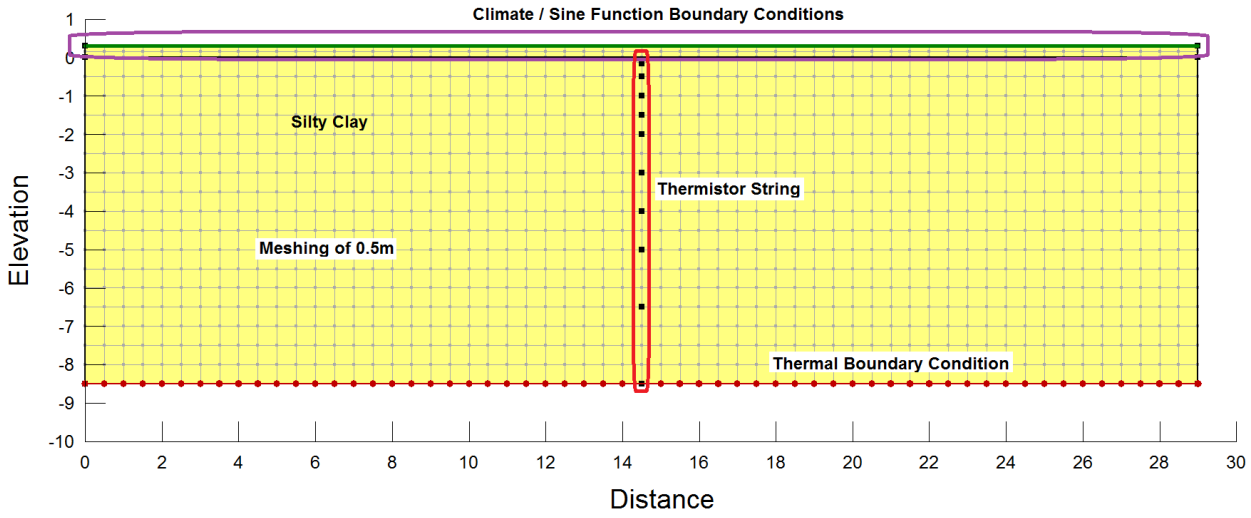


**Figure 4.3. Geothermal model cross section for Highway 3, Behchoko-Yellowknife, Northwest Territories, showing boundary conditions, meshing and thermistors location.**

### 4.5.2 Soil Properties

The thermal conductivity and volumetric heat capacity of the silty clay in frozen and unfrozen states were selected from Table 4.1. The material consists of silty clay with low thermal conductivity as shown in Table 4.6. The model was analyzed as a Full Thermal model. The in-situ volumetric water content was obtained from relations in Andersland and Ladanyi (2004).The low thermal conductivities in the frozen and unfrozen states are associated to the unfrozen water content that can be as much as 50% at about -3°C for silty clay (GEO-

SLOPE International Ltd, 2008). The final calibrated values of the thermal properties using TEMP/W are shown in Table 4.6.

**Table. 4.6. TEMP/W thermal material properties (Highway 3, Behchoko-Yellowknife)**

| Material | Thermal Conductivity (W/m.K) | | Vol. Heat Capacity (kJ/m³/°C) | | In-situ VWC (m³/m³) |
|---|---|---|---|---|---|
| | $k_f$ | $k_u$ | $C_f$ | $C_u$ | |
| Silty Clay | 0.694 | 0.313 | 2000 | 2500 | 0.4 |

### 4.5.3 Boundary Conditions

Climate data from Environment Canada website at the Yellowknife's station located at 62°27'47'' N/ 114°26'25'' W were taken for the first surface condition. A sine function boundary condition was stablished as a second surface boundary condition. The N-factors were obtained from ranges in Andersland and Ladanyi (2004) as shown in Table 4.7. A constant thermal boundary condition of 0°C was set at the bottom of the modelling to represent the annual average temperature, based on the thermistor readings at the location.

**Table. 4.7. TEMP/W thermal modifiers factors (Highway 3, Behchoko-Yellowknife).**

| Material | Freezing, $n_f$ | Thawing, $n_t$ |
|---|---|---|
| Surface | 0.25 | 0.73 |

## 4.6 Murtèl-Corvatsch Rock Glacier, Engadin Region, Switzerland

### 4.6.1 Geometry

The height of the model extends to a depth of 62 m where the thermistors string are shown in Figure 4.4. Longer lateral extensions were used in the model. However, it was observed that this has no effect on the simulated values compared to what has been used in the current modelling. The mesh size was 0.5 m by 0.5 m.

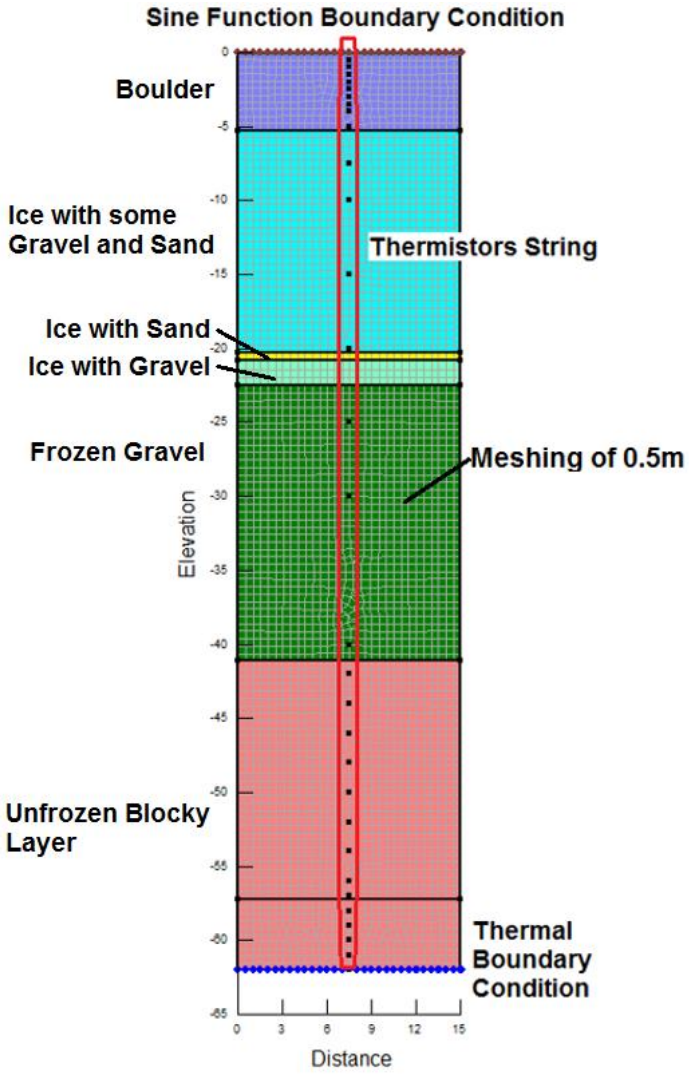


**Figures 4.4. Geothermal model cross section from project Murtèl-Corvatsch Rock Glacier, Engadin Region, Switzerland, showing boundary conditions, meshing and thermistors location.**

### 4.6.2 Soil Properties

The model consists of four main layers as follows: boulders in the top layer, ice with some silt and sand, frozen gravel and unfrozen blocky layer. The model was analyzed as a Full Thermal model. The thermal conductivity and volumetric heat capacity of the materials in frozen and unfrozen states were selected from Table 4.1. The high thermal conductivity in the top layer is associated to the large boulders content. The value of the in-situ volumetric water content was obtained from relations in Andersland and Ladanyi (2004). The final calibrated values of the thermal properties using TEMP/W are shown in Table 4.8.

**Table. 4.8. TEMP/W thermal material properties (Murtèl-Corvatsch Rock Glacier).**

| Material | Thermal Conductivity (kJ/days/m/°C) | | Vol. Heat Capacity (kJ/m³/°C) | | In-situ VWC (m³/m³) |
|---|---|---|---|---|---|
| | $k_f$ | $k_u$ | $C_f$ | $C_u$ | |
| Boulders, Top Layer | 5.208 | 2.894 | 1100 | 2000 | 0.05 |
| Ice with some Gravel and Sand | 2.002 | 0.579 | 1800 | 4200 | 0.9 |
| Frozen Gravel | 4.282 | 2.546 | 1560 | 2200 | 0.08 |
| Unfrozen Blocky Layer | 3.762 | 2.662 | 1600 | 2100 | 0.2 |

### 4.6.3 Boundary Conditions

The average air temperature was obtained from the Federal Office of Meteorology and Climatology (MeteoSwiss website) at the Piz Corvatsch station at 46°25'N / 9°49'E. A sine function boundary condition was applied on the surface with N-factors obtained from Andersland and Ladanyi (2004) as shown in Table 4.9.

**Table. 4.9. TEMP/W thermal modifiers factors (Murtèl-Corvatsch Rock Glacier).**

| Material | Freezing, $n_f$ | Thawing, $n_t$ |
|---|---|---|
| Surface | 0.9 | 2.0 |

The remoteness of the research site represented a challenge for the analysis of this mountain permafrost. Several climate parameters from the Piz Corvatsch meteorological station were not available for the period of analysis. Due to the absence of these parameters necessary to apply a climate boundary condition, a climate model was not used. Instead, only the sine model was used in the analysis.

A constant thermal boundary condition of 0.32°C was stablished at the bottom of the modelling to represent the annual average temperature based on measured data.

## 4.7 Chilean Andes Rock Glacier, Chile

### 4.7.1 Geometry

The model has a height of 18.8m with a mesh size of 0.5 m by 0.5 m. Any variation of the lateral measurement has no effect on the simulated data (Figure 4.5).

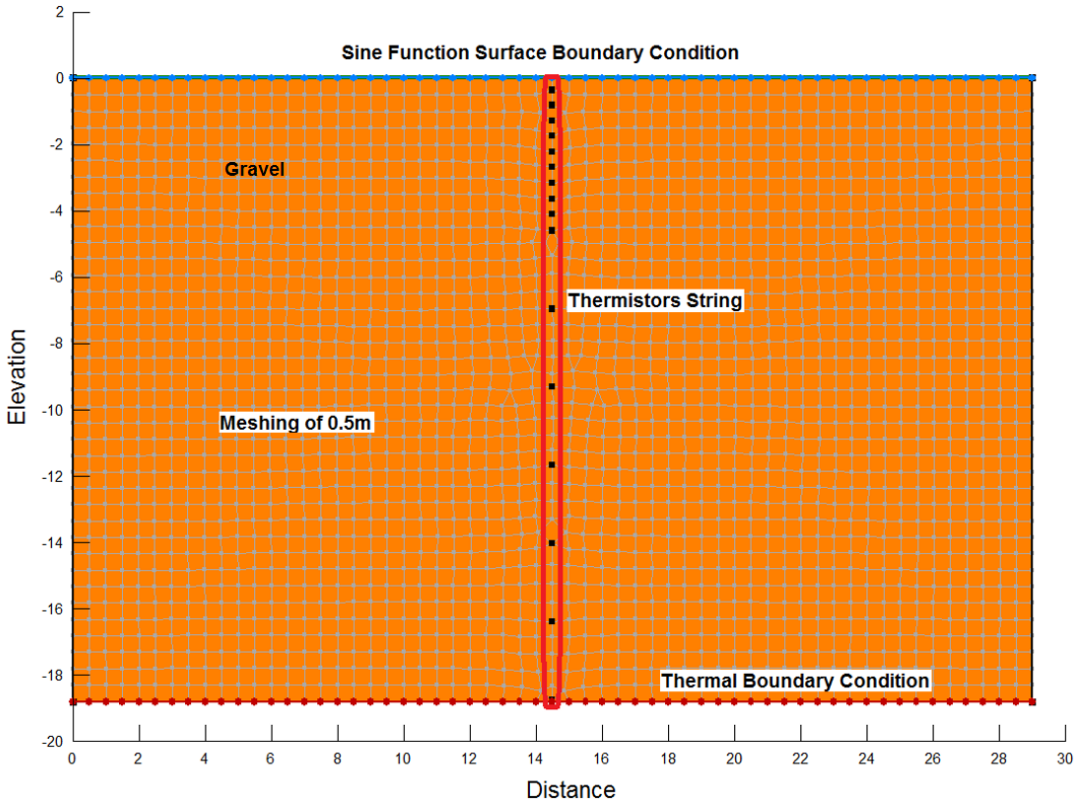


**Figure 4.5. Geothermal model cross section at the Chilean Andes Rock Glacier, Chile, showing boundary conditions, meshing and thermistors location.**

### 4.7.2 Soil Properties

Based on Monnier and Kinnard (2013) and Arenson et al. (2010), the material property is assumed as gravel. The model was analyzed as Full Thermal model with thermal conductivity and volumetric heat capacity in frozen and unfrozen states selected from Table 4.1. The in-situ volumetric water content was obtained from relations in Andersland and Ladanyi (2004). The final calibrated values of the thermal properties using TEMP/W are shown in Table 4.10.

**Table. 4.10. TEMP/W thermal material properties (Chilean Andes Rock Glacier).**

| Material | Thermal Conductivity (W/m.K) | | Vol. Heat Capacity (kJ/m³/°C) | | In-situ VWC (m³/m³) |
|---|---|---|---|---|---|
| | $k_f$ | $k_u$ | $C_f$ | $C_u$ | |
| Gravel | 4.630 | 1.736 | 1300 | 2300 | 0.03 |

### 4.7.3 Boundary Conditions

Climate data are not available at the site. A sine function of near-surface ground site temperature is used as a surface boundary condition. Then, the freezing and thawing N-factors used for the model are equal to one (Table 4.11).

A constant thermal boundary condition of -1.52°C was stablished at the bottom of the modelling to represent the measured annual average temperature.

**Table. 4.11. TEMP/W thermal modifiers factors (Chilean Andes Rock Glacier).**

| Material | Freezing, $n_f$ | Thawing, $n_t$ |
|---|---|---|
| Surface | 1.0 | 1.0 |

### 4.8 Alternate Procedure Based on Data of Temperature with Time

Rózański and Sobotka (2013) and Kurz et al. (2017) compared the thermal conductivity of clayey soils and silts from the ASTM D5334-14 standard approach to empirically estimated values. The needle probe test (ASTM D5334-14) shows that the thermal conductivity $k$ can be calculated using the quasi-steady state portion of the temperature vs. time function using the equations as follows:

$Equation\ 4.8$ $$k = \frac{q}{4\pi S},$$

$Equation\ 4.9$ $$S = \frac{T_2 - T_1}{lnt_2 - lnt_1},$$

Where $q$ is the heat input rate (W/m) obtained from equation 4.1, $S$ represents the slope of the change in temperature $T$ with time $t$. This slope $S$ is comparable to the slope of the simulated variations with time in and below the active layer of the research sites. The slope of temperature variation in the active layer defines the unfrozen thermal conductivity. The slope of temperature variation below the active layer defines the frozen thermal conductivity.

# CHAPTER 5: Results

## 5.1 Provincial Road PR391, Thompson, Manitoba

### 5.1.1 Performance Criteria

As stated in chapter 4, $R^2$ and RMSE were used as performance criteria between measured and simulated temperatures with depth. It is observed that the climate and sine function models show similar model performance using $R^2$. The RMSE between the measured data and the sine function model show values closer to 0 when compared to the climate model. Overall, the $R^2$ values obtained by the author of this thesis (January 2015 to July 2016) are higher than Flynn (2015) (January 2013 to July 2014). Similarly, the RMSE shows lower values in the period investigated in this study. Figures 5.1 to 5.4 show examples of linear regression analysis results for $R^2$ and RMSE. Deviation of residuals close to the line of best fit (1:1 Line) indicate a low difference between measured and simulated temperatures. Simulated temperatures that follow the trend of measured data about the linear fit (red line) show high $R^2$.

At the toe of the embankment (Figure 5.1), Flynn (2015) shows $R^2$ between 0.69 to 0.95 and RMSE between 0.89°C to 2.26°C (2013 - 2014). The author of this thesis (2015 – 2016) shows values between 1.0E-04 to 0.18 for $R^2$ and 0.25°C to 1.17°C for RMSE. The difference between measured and simulated temperatures by means of RMSE was lower in the period 2015 – 2016 when compared to 2013 – 2014.

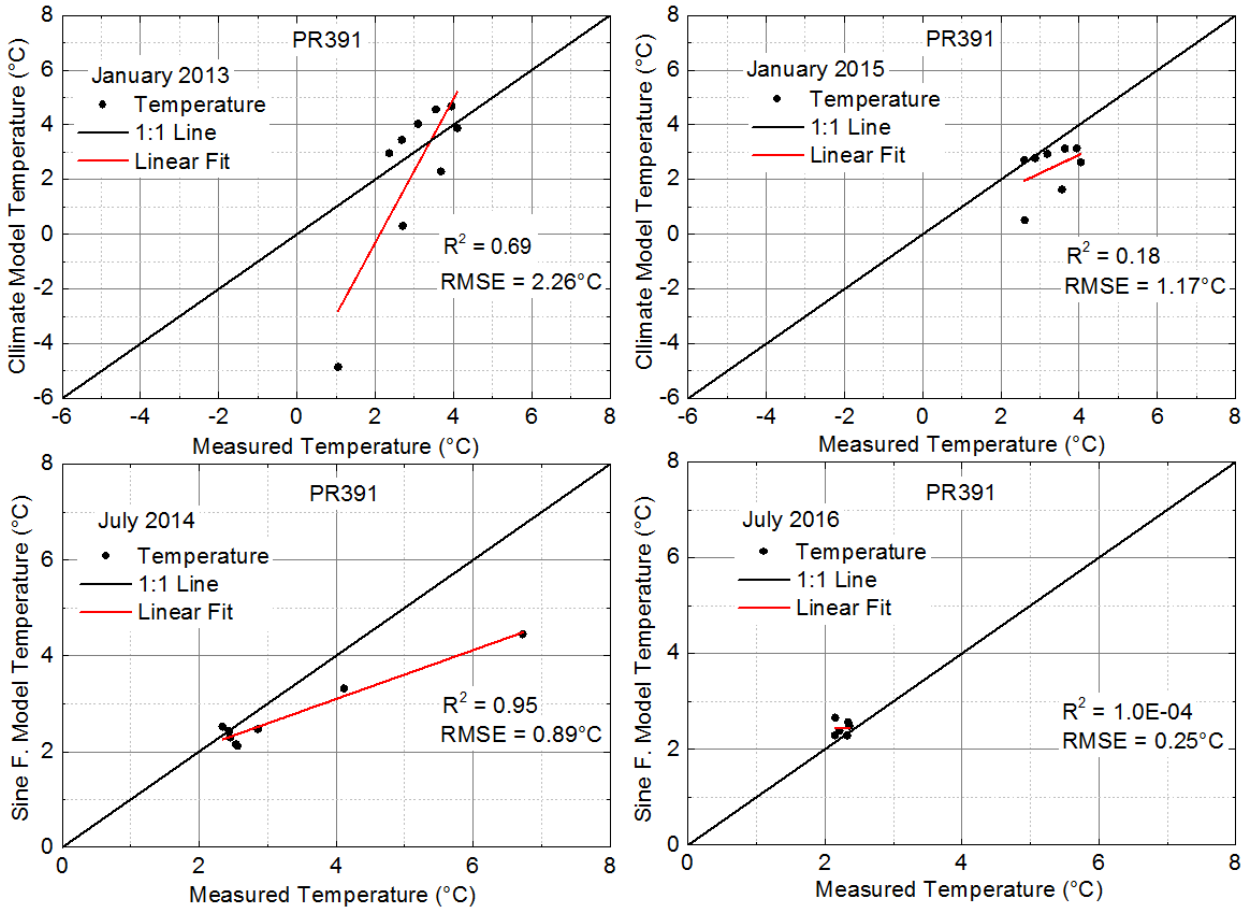


**Figure 5.1. Model performance results of measured and simulated temperatures at the toe of the embankment.**

At the mid-slope of the embankment (Figure 5.2), Flynn (2015) shows $R^2$ between 3.0E-06 to 0.92 and RMSE between 0.68°C to 1.95°C (2013 - 2014). The author of this thesis (2015 – 2016) show values between 1.0E-04 to 0.89 for $R^2$ and 0.98°C to 1.08°C for RMSE.

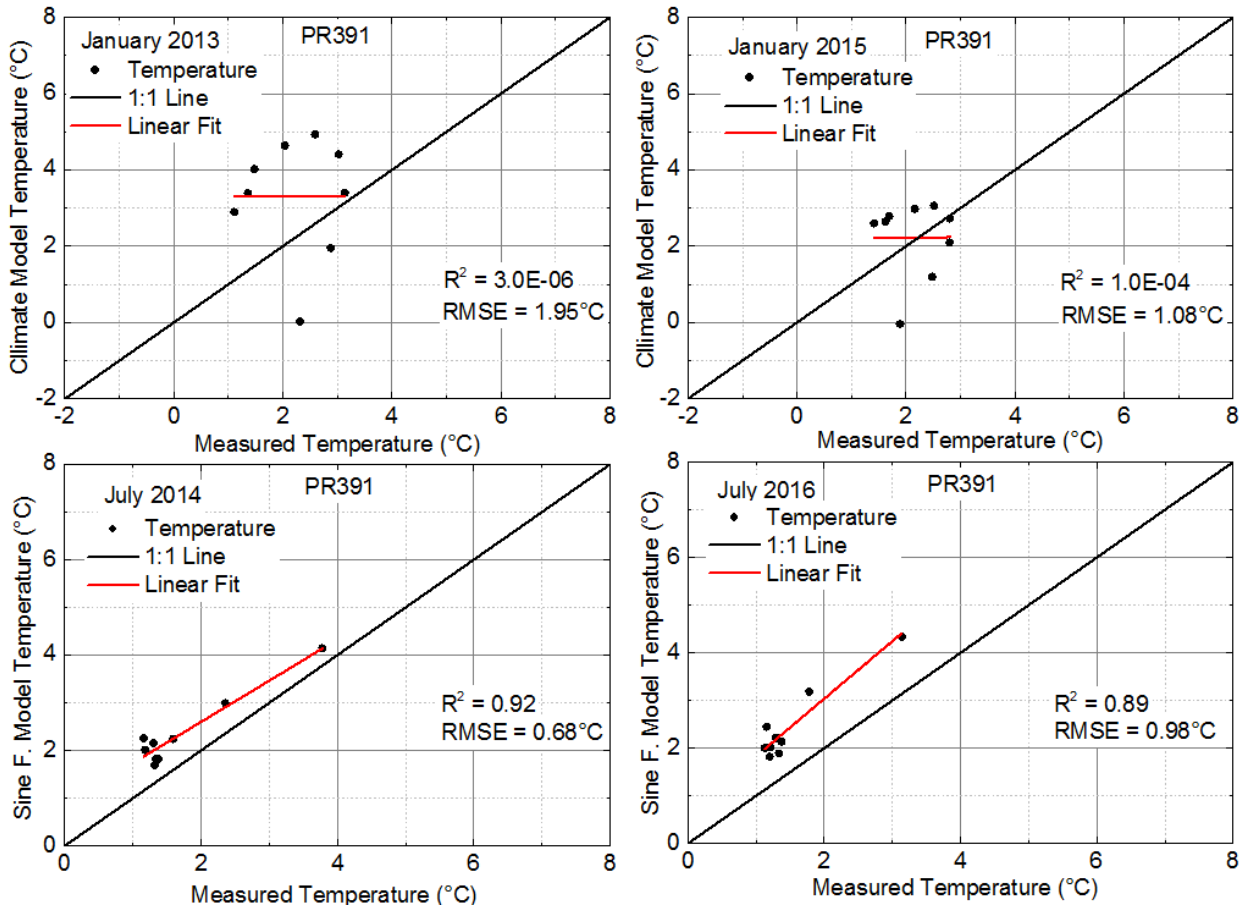


**Figure 5.2. Model performance results of measured and simulated temperatures at the mid-slope of the embankment.**

At the shoulder of the embankment (Figure 5.3), Flynn (2015) shows a calibration between 0.08 to 0.42 for $R^2$ and 1.57°C to 3.64°C for RMSE between the measured and simulated temperatures (2013 – 2014). The author of this thesis (2015 – 2016) show values between 0.05 to 0.10 for $R^2$ and 1.32°C to 2.10°C for RMSE. The difference between measured and simulated temperatures by means of RMSE was lower in the period 2015 – 2016 when compared to 2013 – 2014.

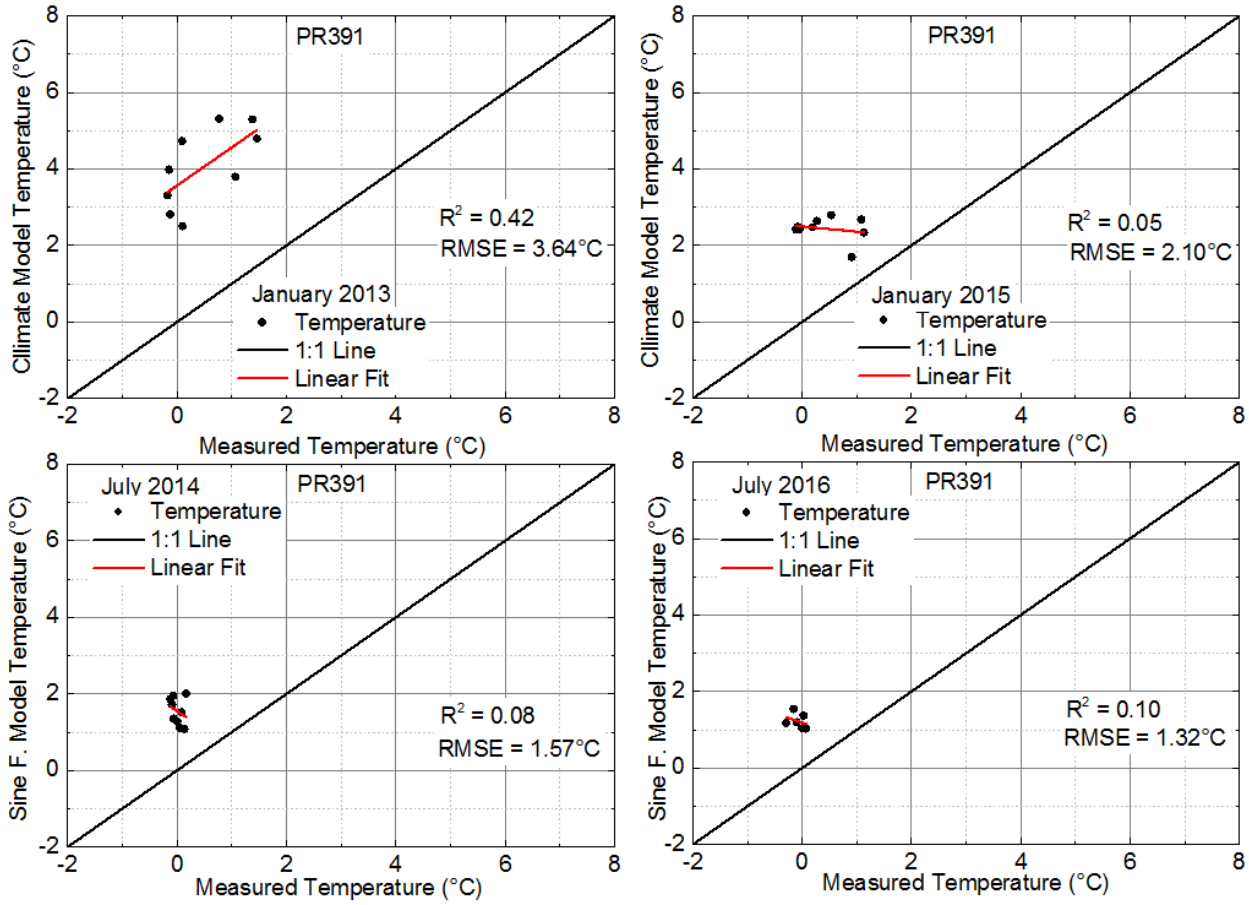


**Figure 5.3. Model performance results of measured and simulated temperatures at the shoulder of the embankment.**

At the centreline of the embankment (Figure 5.4), Flynn (2015) shows a calibration between 0.03 to 0.14 for $R^2$ and 1.49°C to 4.39°C for RMSE between the measured and simulated temperatures (2013 – 2014). The author of this thesis (2015 – 2016) show values between 0.02 to 0.10 for $R^2$ and 1.32°C to 2.42°C for RMSE. The difference between measured and simulated temperatures by means of RMSE was lower in the period 2015 – 2016 when compared to 2013 – 2014.

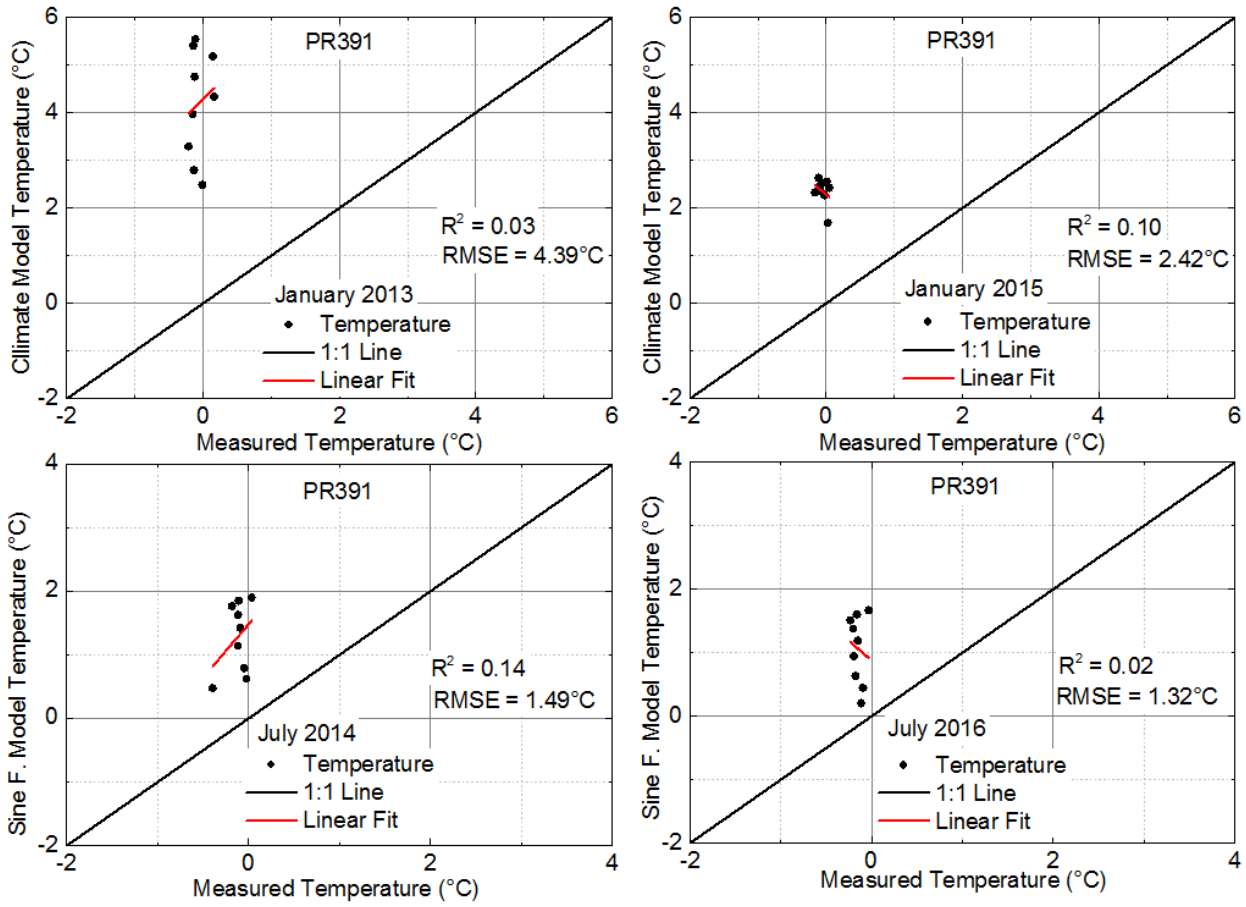


**Figure 5.4. Model performance results of measured and simulated temperatures at the centreline of the embankment.**

### 5.1.2 Sensitivity Analysis

The thermal conductivity and volumetric heat capacity in frozen and unfrozen states were evaluated further during the sensitivity analysis. Overall, the volumetric heat capacity (C) is more sensitive than the thermal conductivity (K).

Analysis results at 4 m below the toe of the embankment show higher temperature variations with volumetric heat capacity (Figure 5.6) than with thermal conductivity (Figure 5.5). The sensitivity analysis shows that the thermal

conductivity affected the temperature variations with time by +0.5%/-0.6%, +1.1%/-1.1% and +5.0%/-4.8% if K varies by ± 5%, ± 10% and ± 50%, respectively. The sensitivity analysis showed that the volumetric heat capacity affected the temperature variations with time by -0.9%/+0.9%, -1.7%/+1.9% and -7.5%/+11% if C varies by ± 5%, ± 10% and ± 50%, respectively.

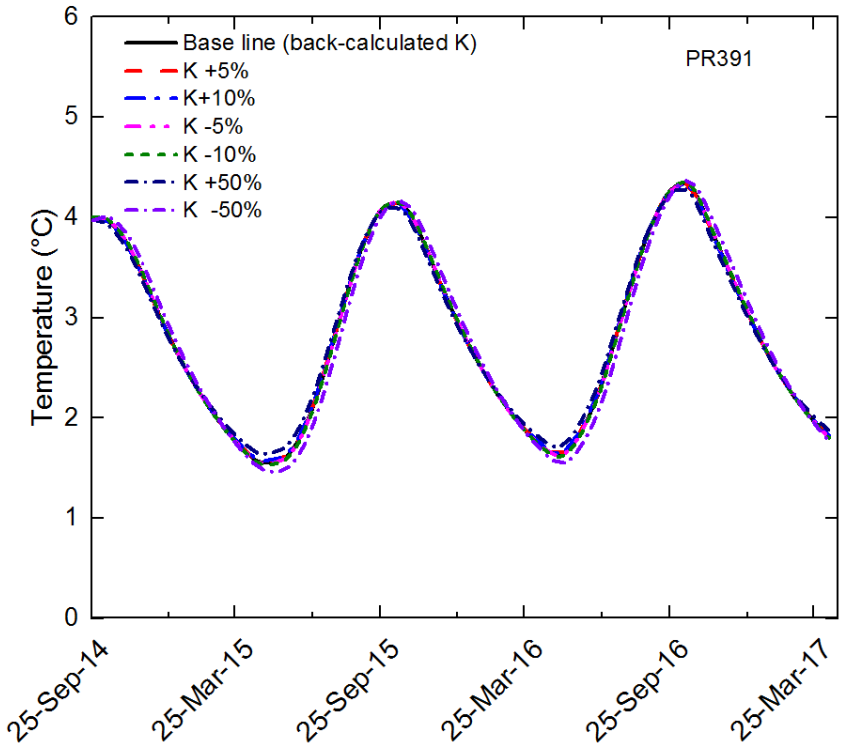


**Figure 5.5. Sensitivity of thermal conductivity at 4 m below the toe of the embankment.**

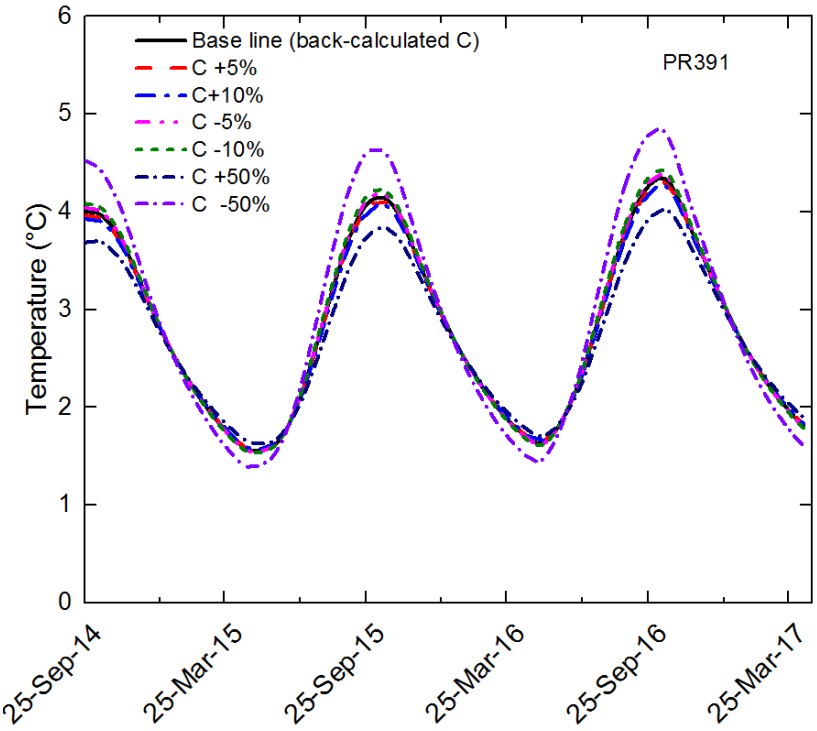


**Figure 5.6. Sensitivity of volumetric heat capacity at 4 m below the toe of the embankment.**

Analysis results at 3 m below the surface at the shoulder of the embankment shows higher temperature variations with volumetric heat capacity (Figure 5.8) than with thermal conductivity (Figure 5.7). The sensitivity analysis shows that the thermal conductivity affected the temperature variations with time by +1.9% /-2.1%, +3.7%/-4.2% and +14%/-25% if K varies by ± 5%, ± 10% and ± 50%, respectively. The sensitivity analysis shows that the volumetric heat capacity affected the temperature variations with time by -2.3%/+2.5%, -4.7%/+4.9% and -20%/+21% if C varies by ± 5%, ± 10% and ± 50%, respectively.

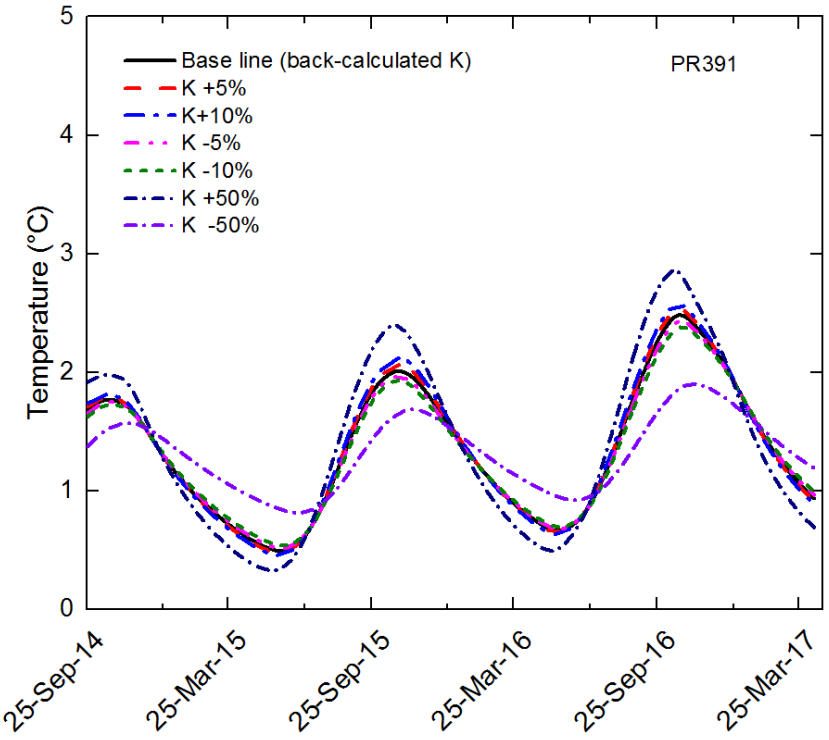


**Figure 5.7. Sensitivity of thermal conductivity at 3 m below the shoulder of the embankment.**

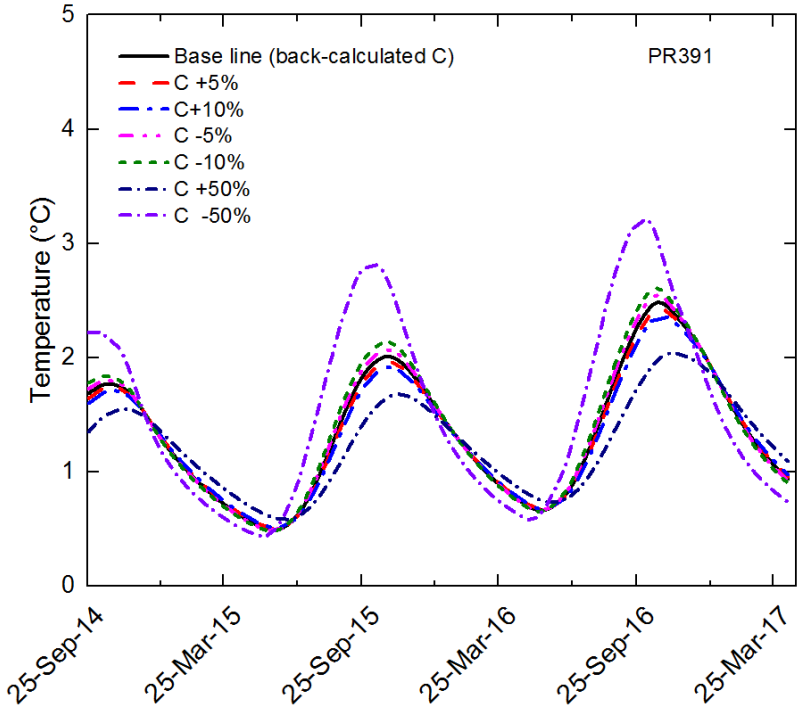


**Figure 5.8. Sensitivity of volumetric heat capacity at 3 m below the shoulder of the embankment.**

### 5.1.3 Thermal Regime

Figures 5.9 through 5.16 show measured and simulated temperatures with depth and temperature variations with time at the toe, mid-slope, shoulder and centreline of the embankment between September 2012 and April 2017, respectively. Collected measured data and simulated values between October 2014 and April 2017 (red color functions) analyzed by this thesis are compared with the period of September 2012 to September 2014 (black color functions) analyzed in Flynn (2015). As mentioned in Chapter 3, missing data at the toe (Figure 5.9) and shoulder of the embankment (Figures 5.13 and 5.14) in 2016 are the result of communication interruption with the data acquisition system. The depth of zero annual amplitude of the simulated values of all the profiles is found at around 9 m below the surface, which is consistent with the measured data.

Figures 5.9 and 5.10 show temperatures with depth and temperature variations with time below the toe of the embankment, respectively. Figure 5.9 shows small differences between the measured data and the TEMP/W models when compared to Flynn (2015). Figure 5.10 shows the annual variations at 4 m and 8 m below the toe of the embankment. Measured and simulated temperatures are relatively close between 2012 and 2017. Figures 5.11 and 5.12 show temperatures with depth and temperature variations with time at the mid-slope of the embankment, respectively. Measured and simulated data are relatively close. There seems to be a slight warming trend at 4 m and 8 m of depth (Figure 5.12).

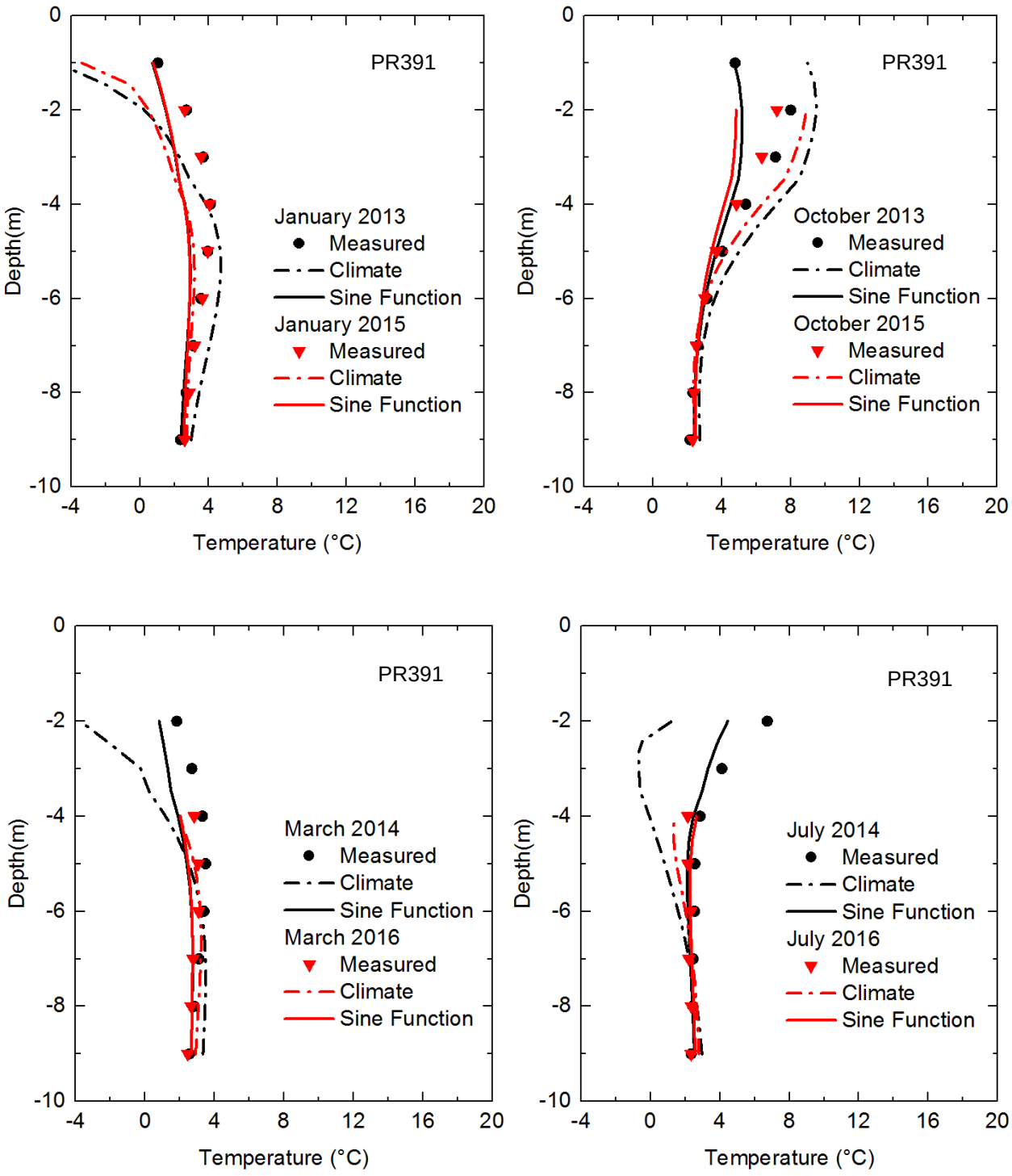


**Figure 5.9. Measured and simulated temperatures with depth at the toe of the embankment.**

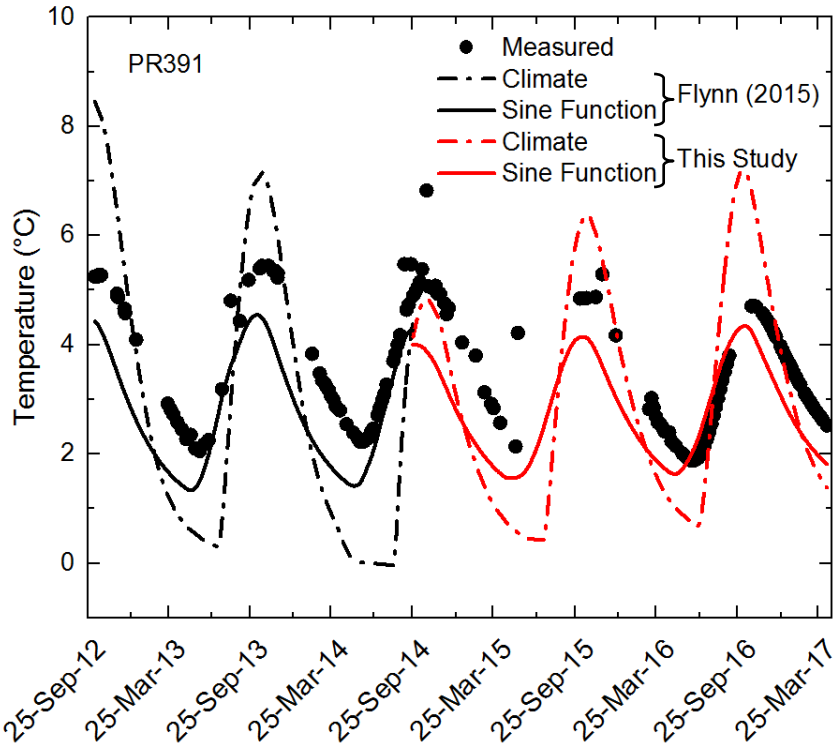


**(a)**

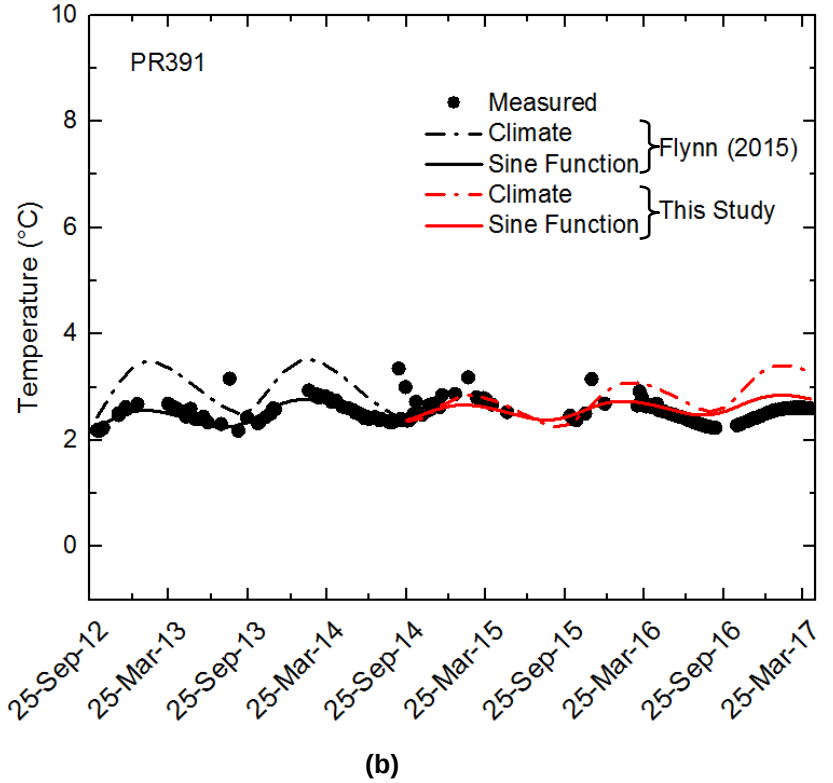


**(b)**

**Figure 5.10. Measured and simulated temperature vs. time relationships at a depth of (a) 4 m and (b) 8 m at the toe of the embankment.**

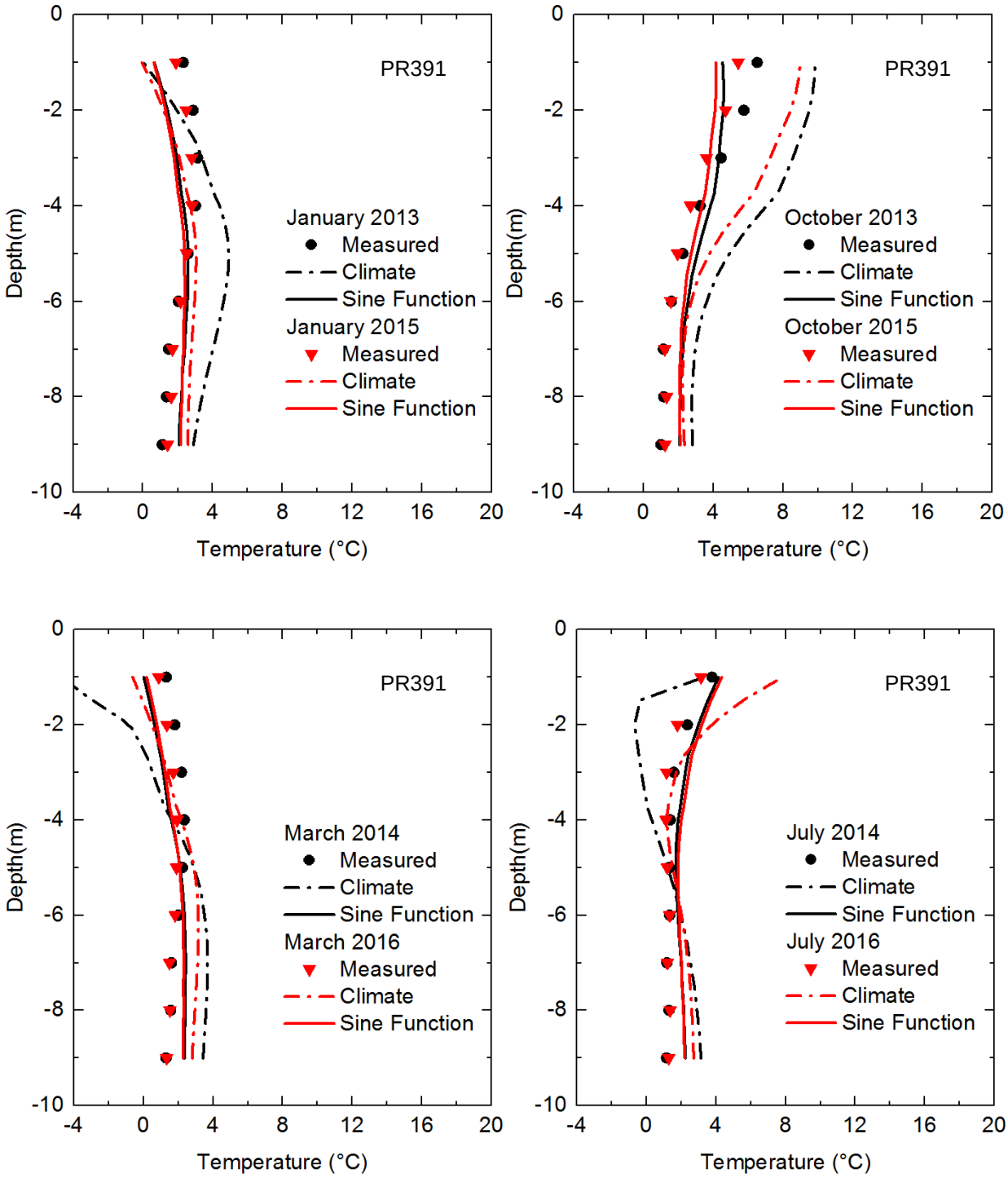


**Figure 5.11. Measured and simulated temperatures with depth at the mid-slope of the embankment.**

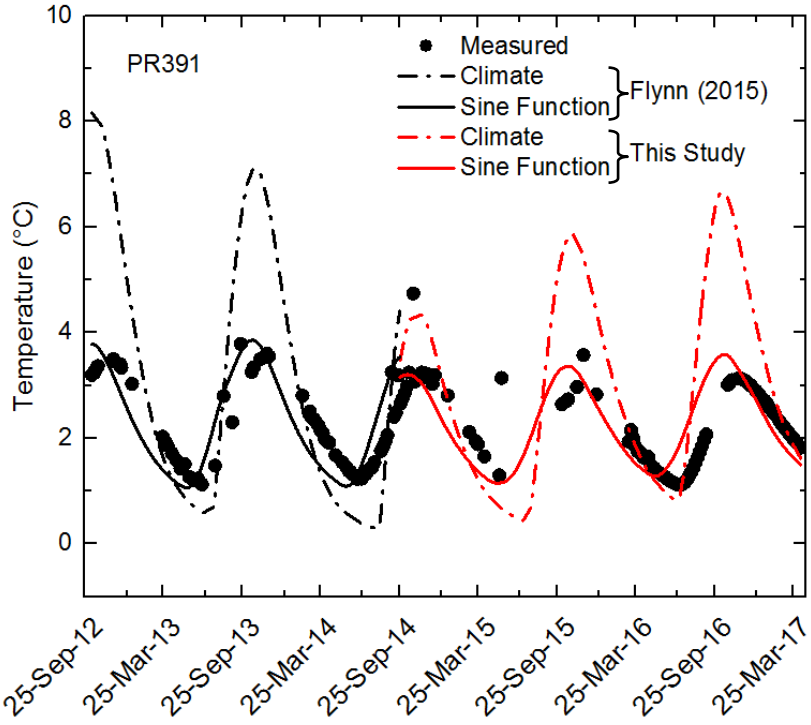


**(a)**

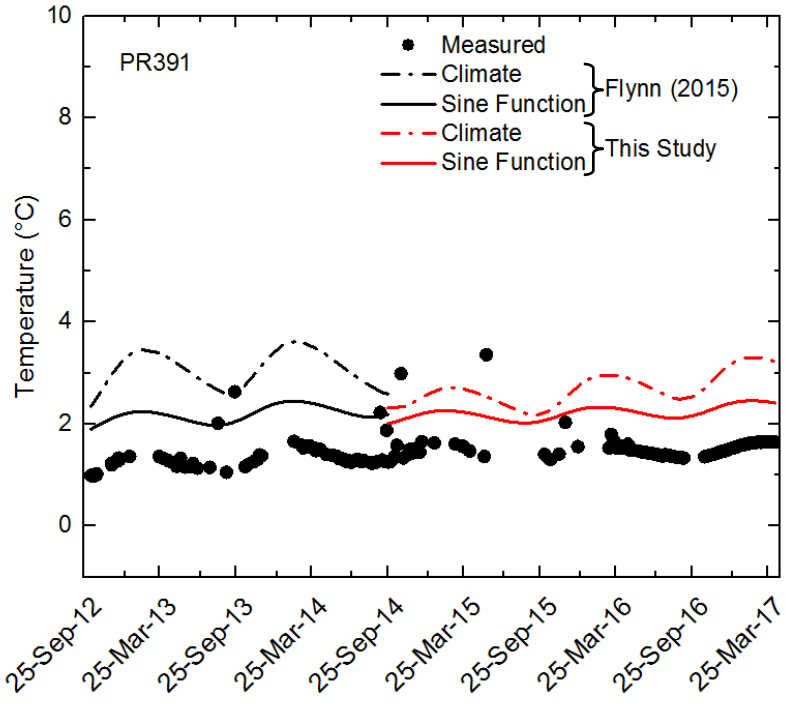


**(b)**

**Figure 5.12. Measured and simulated temperature vs. time relationships at a depth of (a) 4 m and (b) 8 m at the mid-slope of the embankment.**

Figures 5.13 to 5.14 show temperatures with depth and temperature variations with time below the shoulder of the embankment, respectively. Figure 5.13 shows relatively close values between the measured data and the sine model. Figure 5.14 shows that the climate and the sine models over predicted the annual variations at 9 m below the shoulder of the embankment. The warming trends between July 2014 and April 2016 below the shoulder and centreline of the embankment were not properly simulated in the model.

Figures 5.15 and 5.16 show temperatures with depth and temperature variations with time below the centreline of the embankment, respectively. Figure 5.15 shows that both models over predicted freezing temperatures.

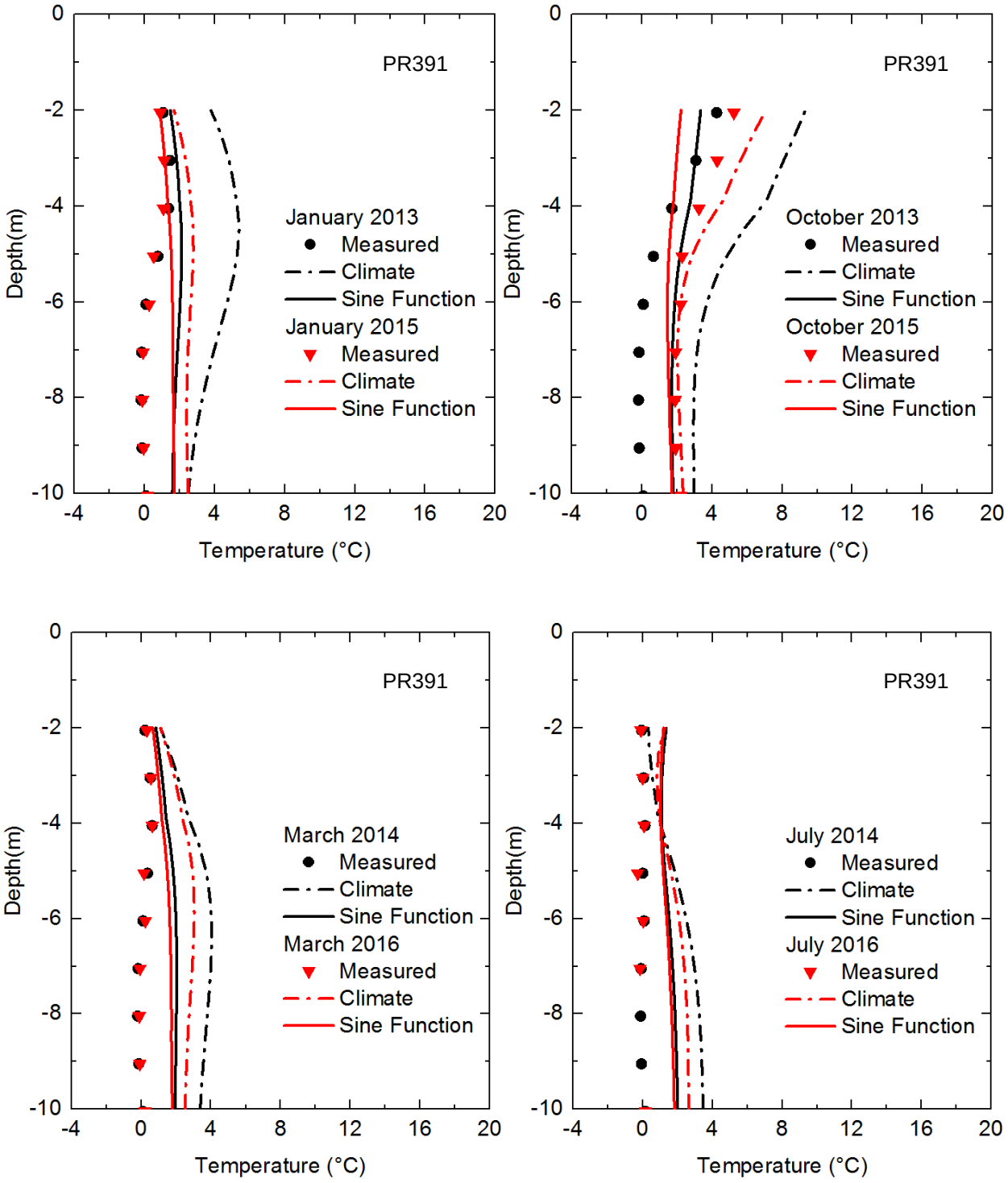


**Figure 5.13. Measured and simulated temperatures with depth at the shoulder of the embankment.**

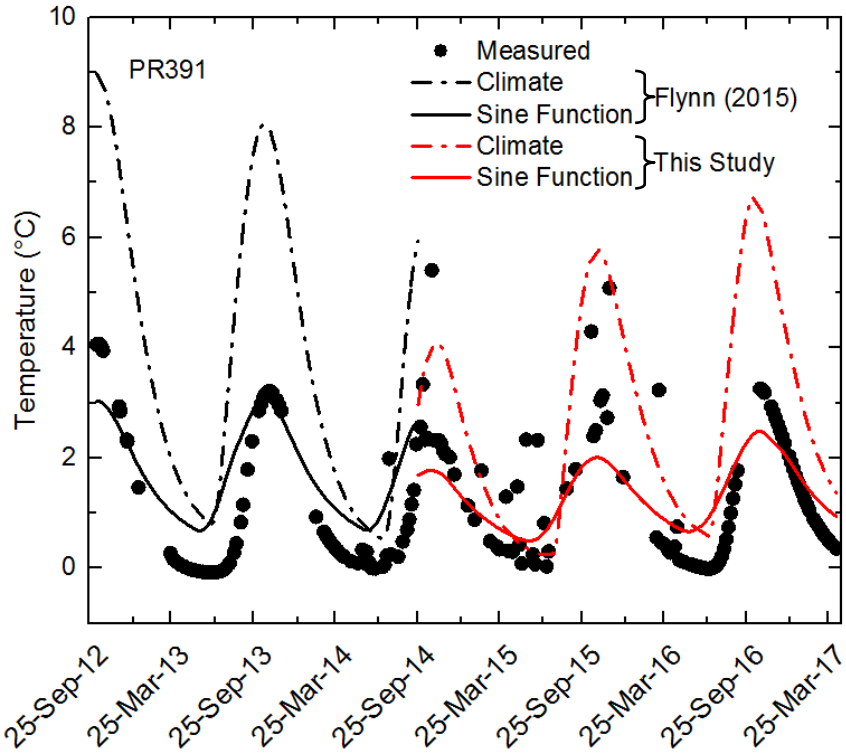


**(a)**

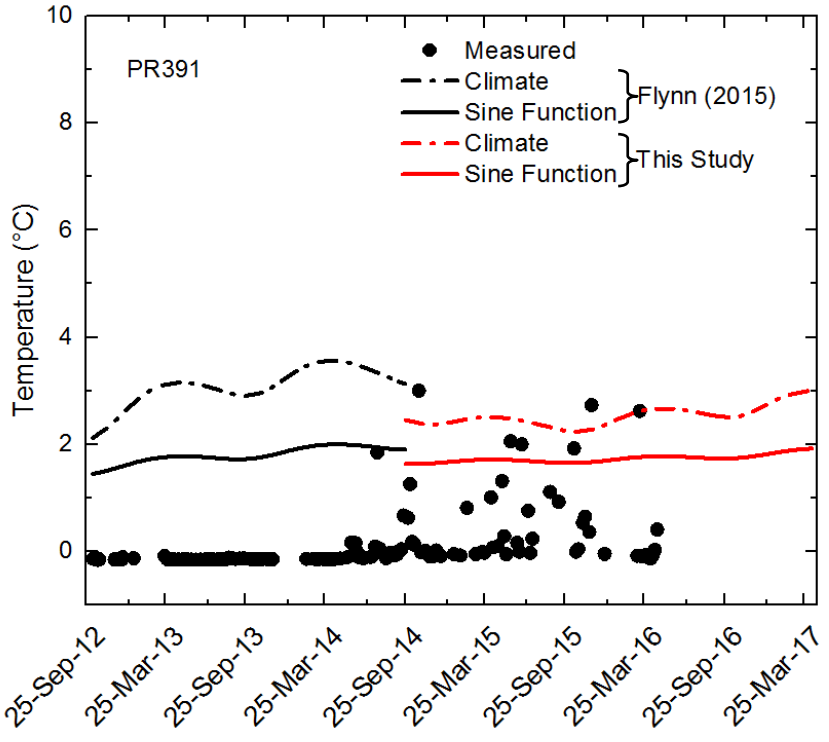


**(b)**

**Figure 5.14. Measured and simulated temperature vs. time relationships at a depth of (a) 3 m and (b) 9 m at the shoulder of the embankment.**

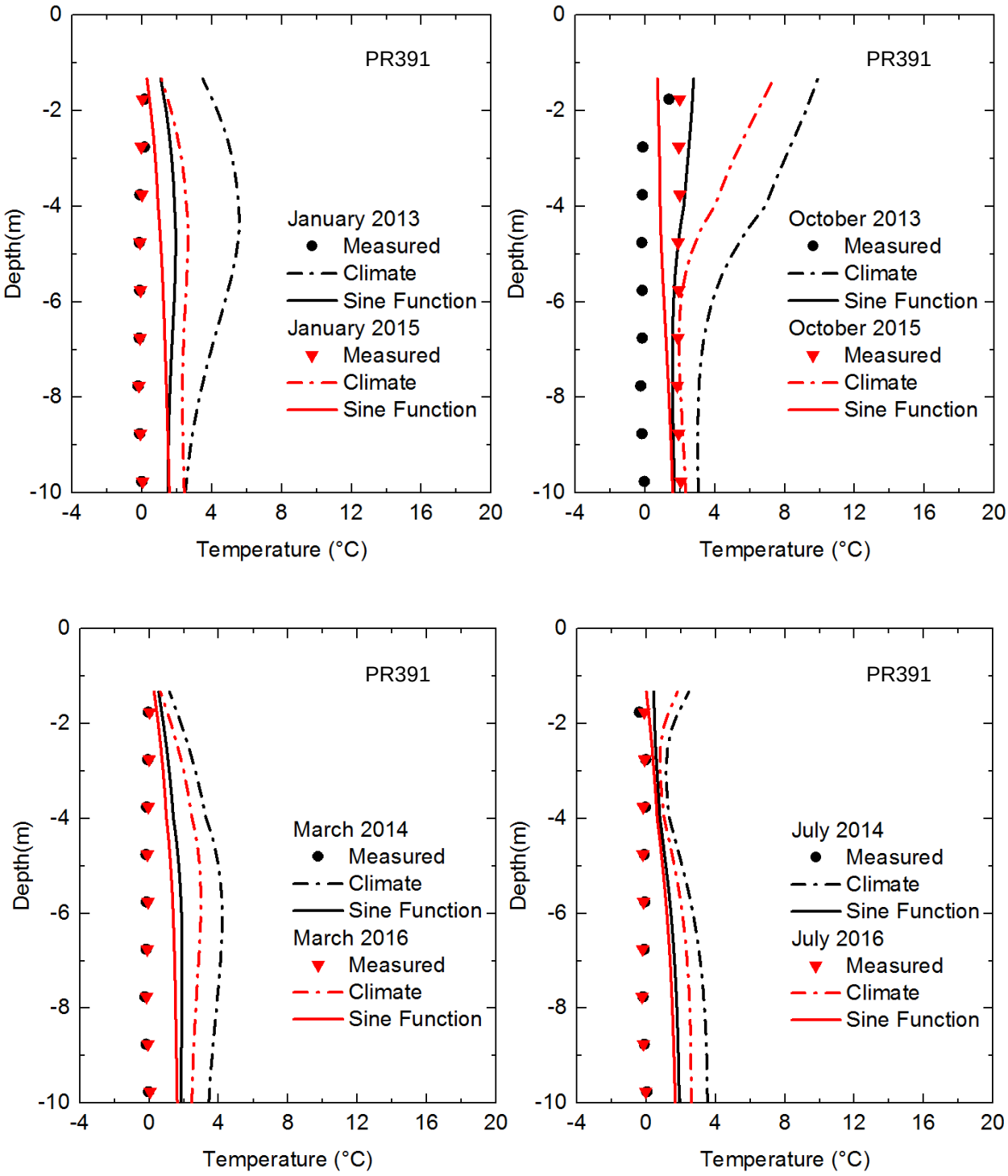


**Figure 5.15. Measured and simulated temperatures with depth at the centreline of the embankment.**

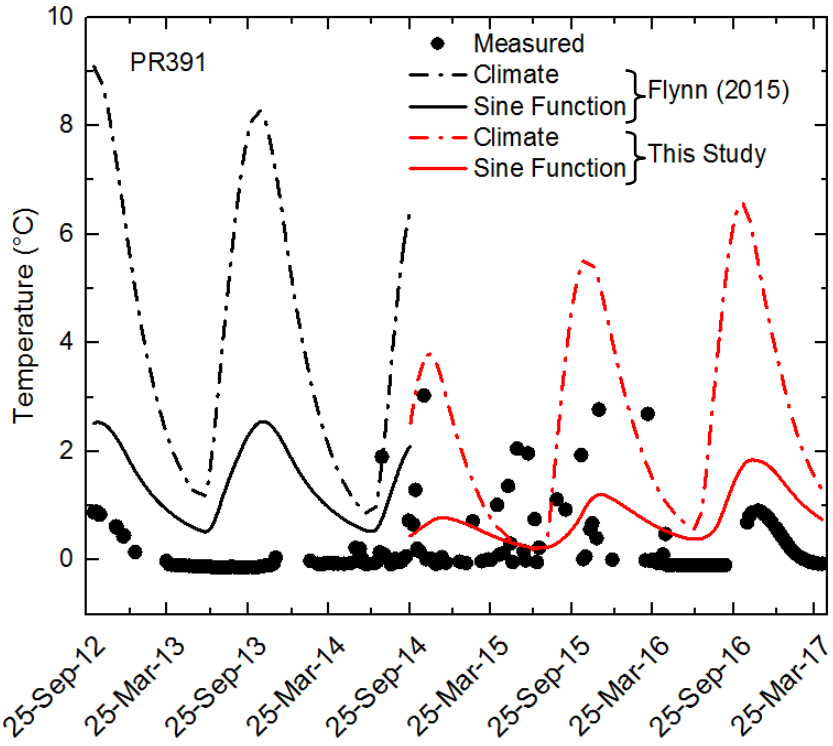


**(a)**

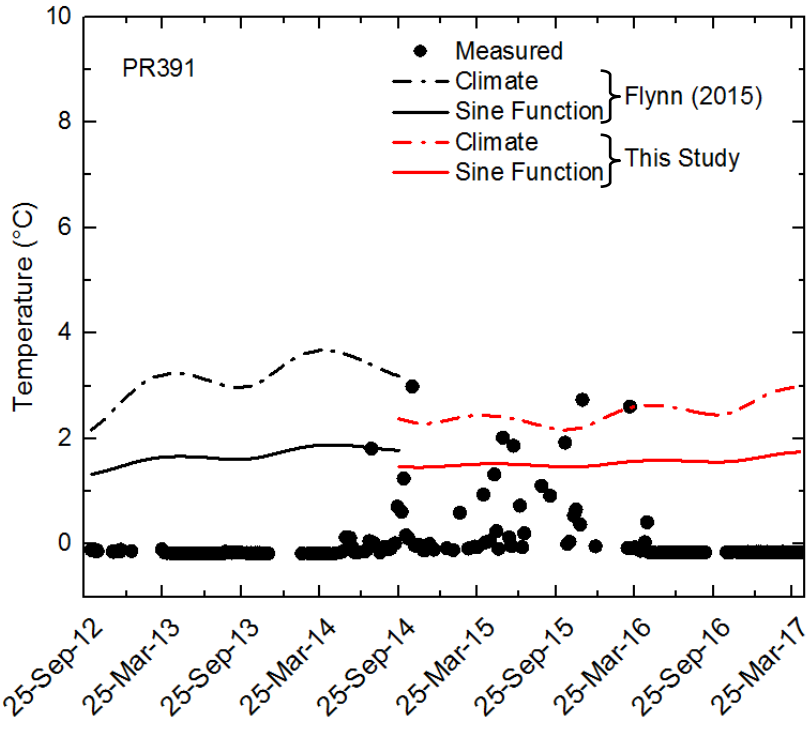


**(b)**

**Figure 5.16. Measured and simulated temperature vs. time relationships at a depth of (a) 3 m and (b) 9 m at the centreline of the embankment.**

## 5.2 Inuvik-Tuktoyaktuk Highway, Northwest Territories

### 5.2.1 Performance Criteria

Overall, the climate and sine function models indicate good prediction using $R^2$ with values close to 1. The RMSE indicate the lowest deviation at the centreline of the embankment with values close to 0. Figures 5.17 to 5.20 show linear regression analysis results for $R^2$ and RMSE at the top, base, centreline and toe of the embankment.

At the top of the embankment, climate model shows $R^2$ values between 0.57 to 0.95 and RMSE values between 0.43°C to 1.96°C. Sine function model shows $R^2$ values between 0.54 to 0.83 and RMSE values between 1.97°C to 2.64°C at the top of the embankment (Figure 5.17).

A the base of the embankment, climate model shows $R^2$ values between 0.75 to 0.93 and RMSE values between 1.61°C to 2.06°C. Sine function model shows $R^2$ values between 0.88 to 0.89 and RMSE values between 1.19°C to 2.98°C (Figure 5.18)

At the centreline of the embankment below the foundation surface, climate model shows $R^2$ values between 0.11 to 0.99 and RMSE values between 0.79°C to 1.46°C at the centreline of the embankment. Sine function model shows $R^2$ values between 0.13 to 0.99 and RMSE values between 1.40°C to 1.48°C (Figure 5.19).

Climate model shows $R^2$ values of 0.99 and RMSE values between 0.62°C to 2.88°C at the toe of the embankment. Sine function model shows $R^2$ values of

0.99 and RMSE values between 1.48°C to 4.03°C at the toe of the embankment (Figure 5.20)

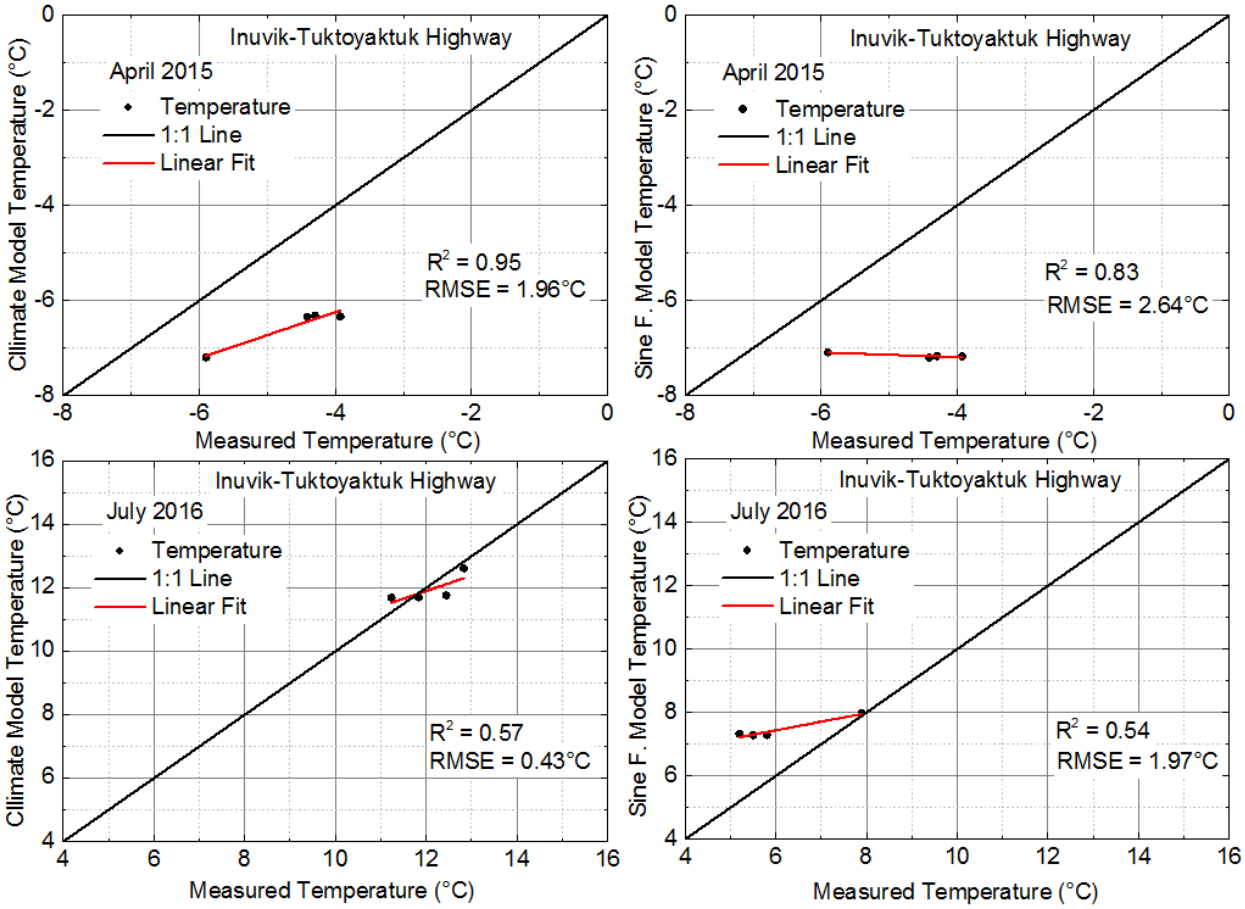


**Figure 5.17. Model performance results of measured and simulated temperatures at the top of the embankment.**

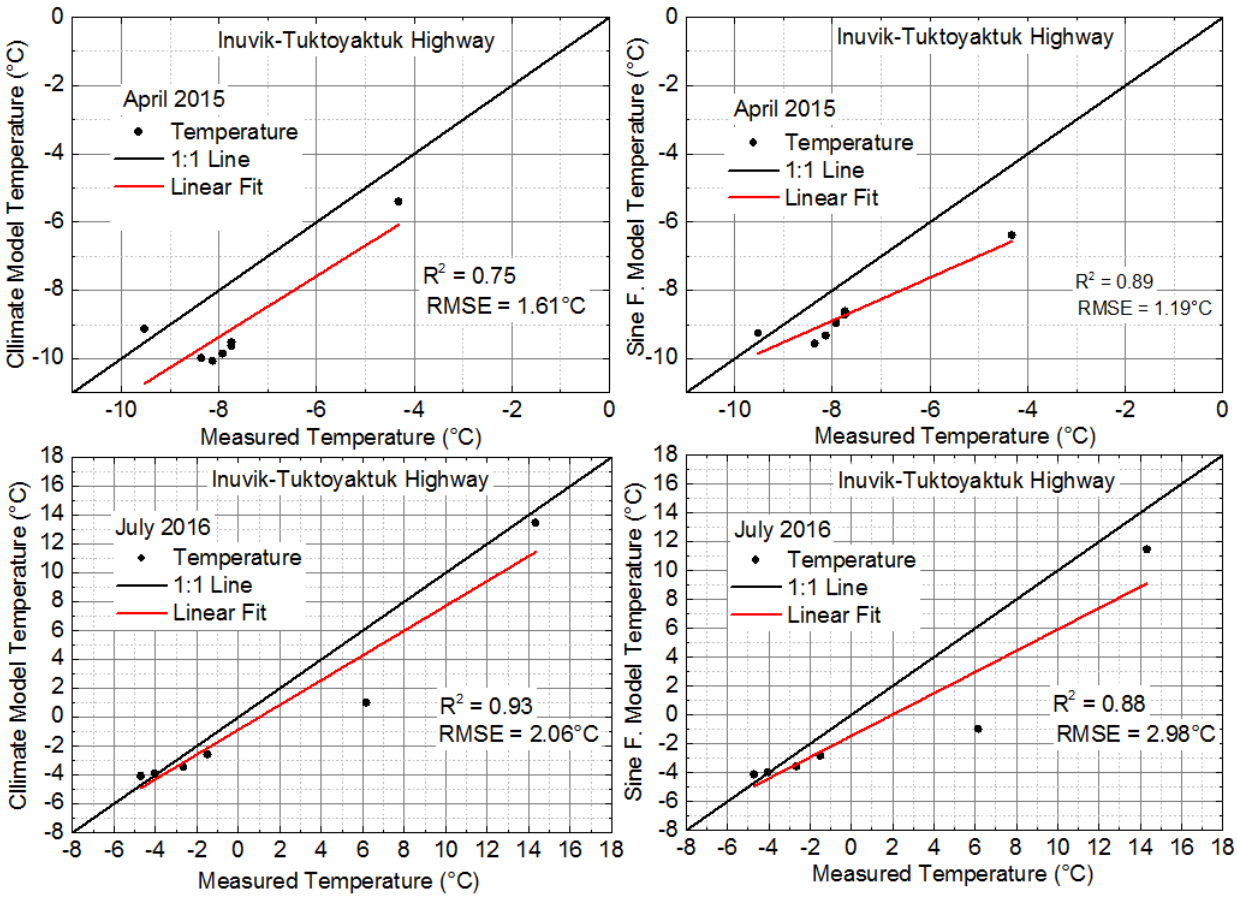


**Figure 5.18. Model performance results of measured and simulated temperatures at the base of the embankment.**

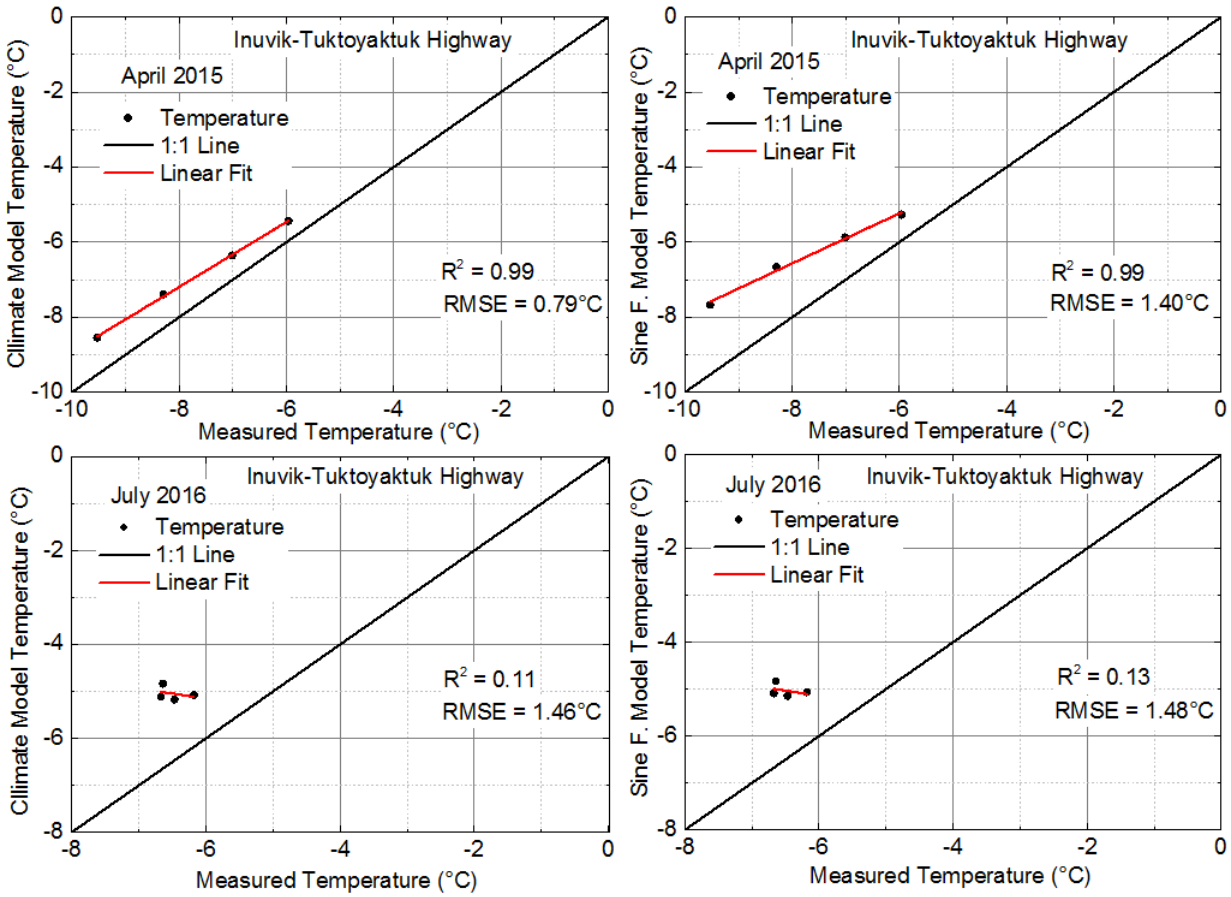


**Figure 5.19. Model performance results of measured and simulated temperatures at the centreline of the embankment below the foundation surface.**

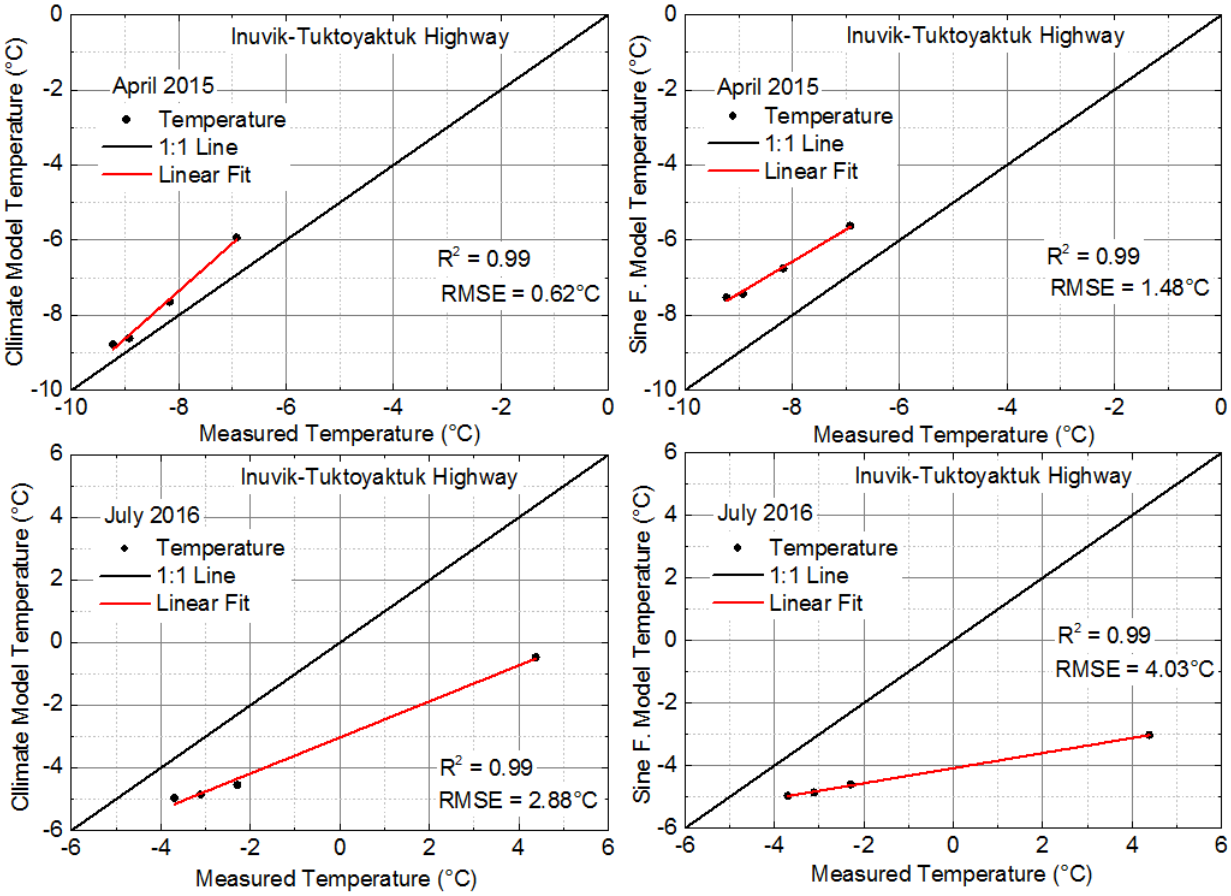


**Figure 5.20. Model performance results of measured and simulated temperatures at the toe of the embankment below the foundation surface.**

### 5.2.2 Sensitivity Analysis

The thermal conductivity and volumetric heat capacity in frozen and unfrozen states were evaluated further during the sensitivity analysis. Overall, the thermal conductivity (K) is more sensitive than the volumetric heat capacity (C).

Analysis results at 0.5 m below the top of the embankment show higher temperature variations with thermal conductivity (Figure 5.21) than with volumetric heat capacity (Figure 5.22). The sensitivity analysis shows that the thermal conductivity affected the temperature variations with time by +1.2%/ -0.9%, +2.5%/-1.9% and +14%/-27% if K varies by ± 5%, ± 10% and ± 50%, respectively. The sensitivity analysis shows that the volumetric heat capacity affected the temperature variations with time by -0.6%/+0.8%, -1.3%/+1.5% and -7.0%/+10% if C varies by ± 5%, ± 10% and ± 50%, respectively.

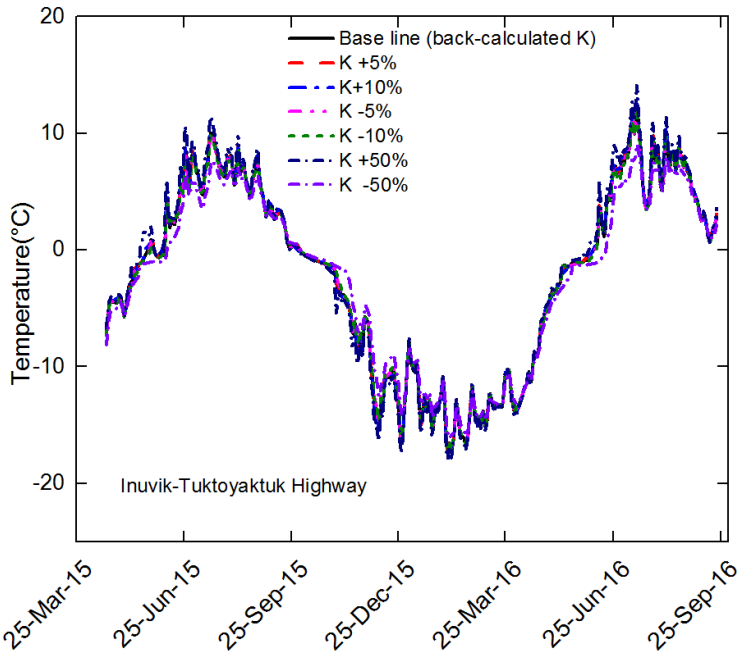


**Figure 5.21. Sensitivity of thermal conductivity at 0.5 m below the top of the embankment.**

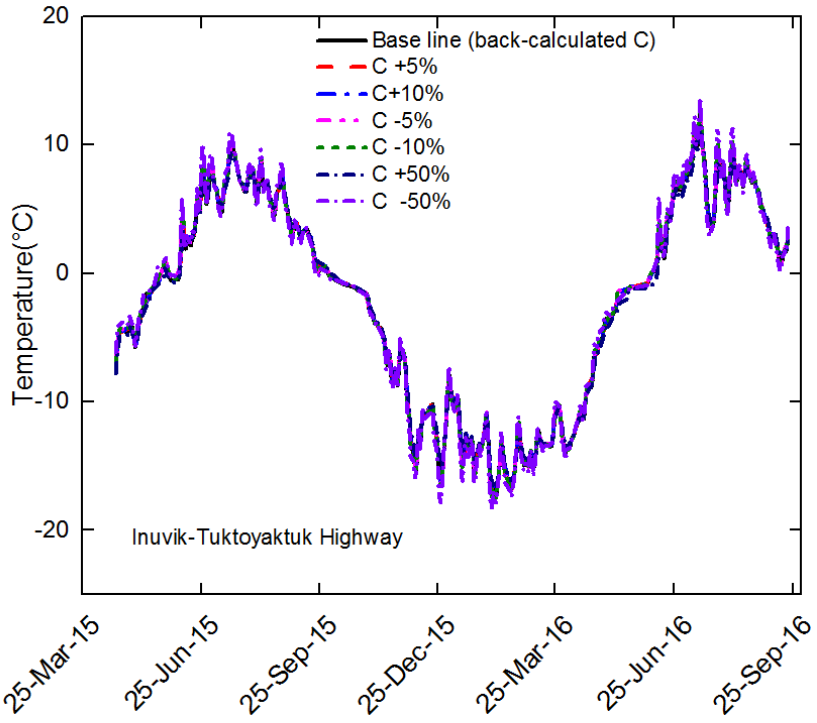


**Figure 5.22. Sensitivity of volumetric heat capacity at 0.5 m below the top of the embankment.**

Analysis results at 0.5 m below the surface at the toe of the embankment show higher temperature variations with thermal conductivity (Figure 5.23) than with volumetric heat capacity (Figure 5.24). The sensitivity analysis shows that the thermal conductivity affected the temperature variations with time by +28%/ -37%, +52%/-89% and +229%/-969% if K varies by ± 5%, ± 10% and ± 50%, respectively. The sensitivity analysis shows that the volumetric heat capacity affected the temperature variations with time by -4.7%/+4.9%, -10.5%/+9.1% and -62%/+25% if C varies by ± 5%, ± 10% and ± 50%, respectively.

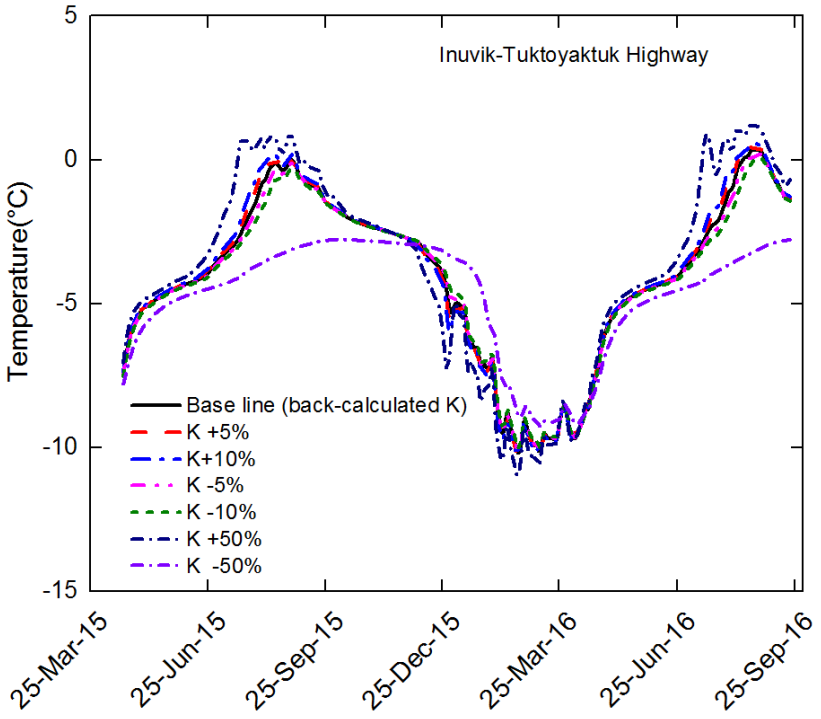


**Figure 5.23. Sensitivity of thermal conductivity at 0.5 m below the toe of the embankment.**

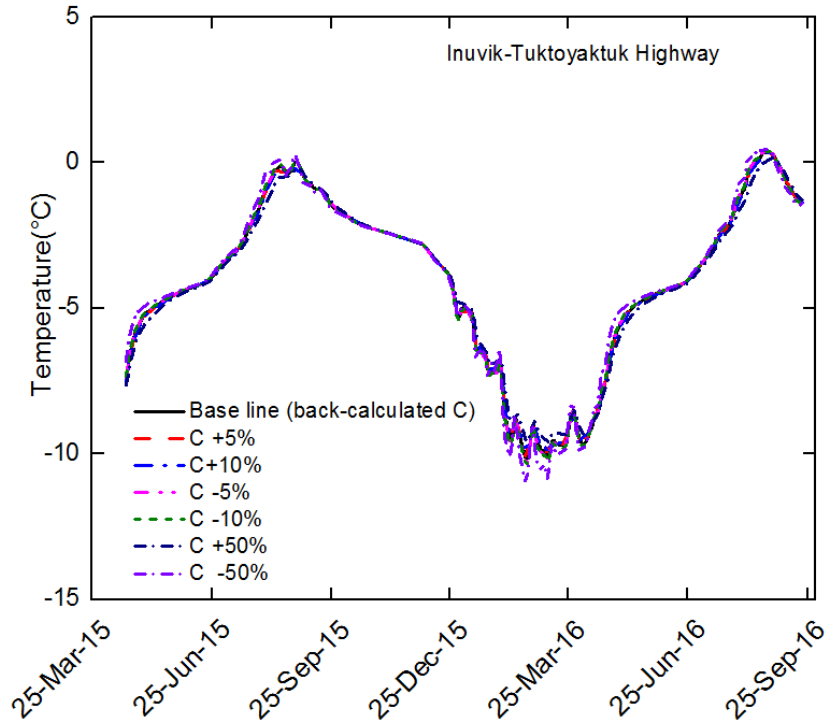


**Figure 5.24. Sensitivity of volumetric heat capacity at 0.5 m below the toe of the embankment.**

### 5.2.3 Thermal Regime

Measured data from the embankment and the foundation are simulated by TEMP/W between April 2015 and August 2016. Figures 5.25 and 5.26 show horizontal measured and simulated data at the top and the base of embankment, respectively. Figure 5.25 shows relatively close values between the measured and simulated temperatures. However, the climate model measurements in April 2015 over predicted the measured data. Figure 5.26 shows close values between the measured and simulated data.

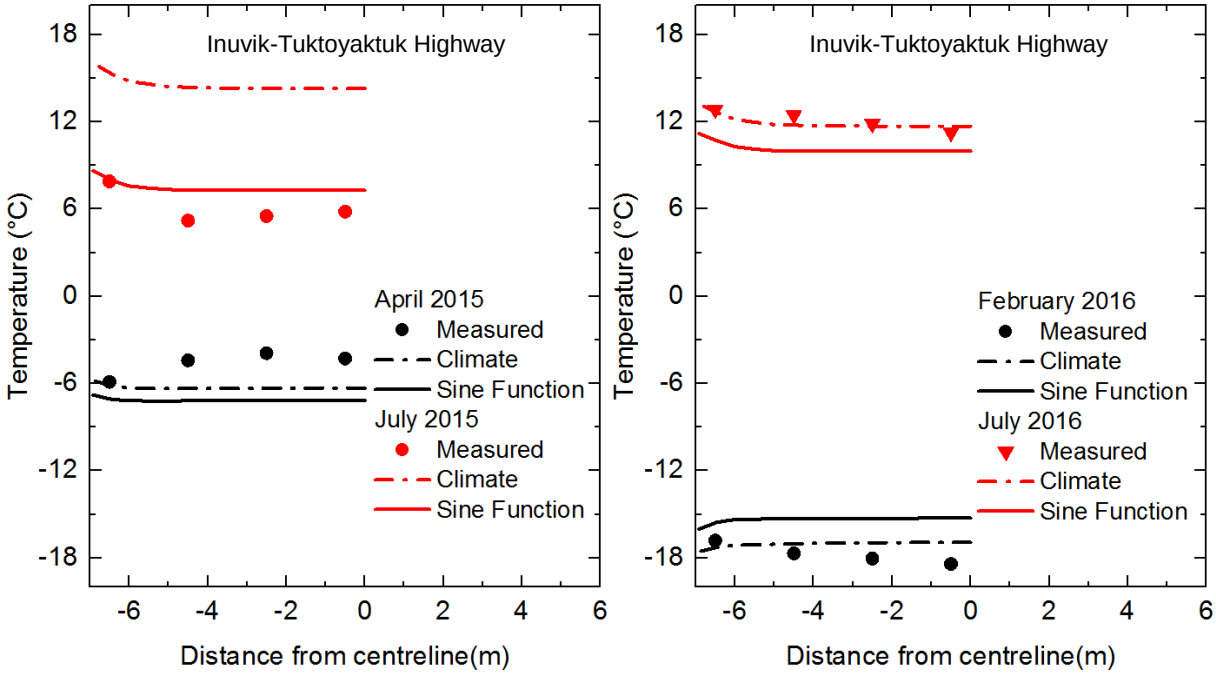


**Figure 5.25. Measured and simulated horizontal temperature changes at the top of the embankment at a depth of 0.5 m.**

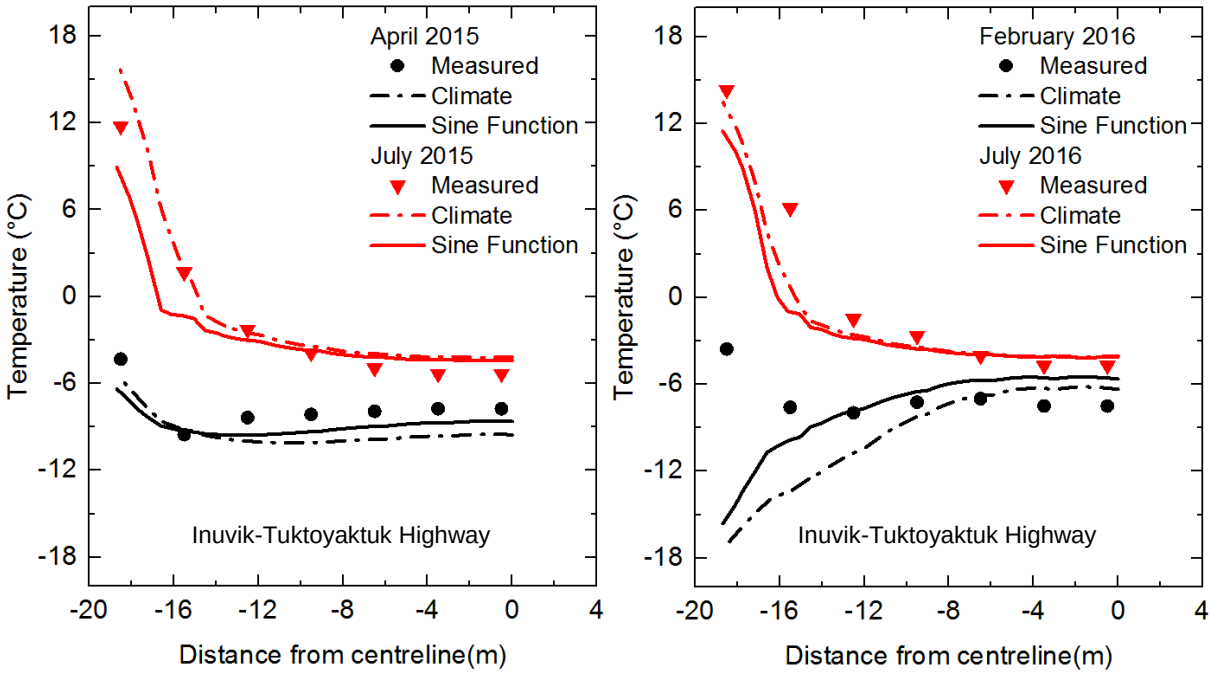


**Figure 5.26. Measured and simulated horizontal temperature changes at the base of the embankment at 0.6 m from the foundation surface.**

Figure 5.27 shows temperatures with depth at the centreline of the embankment below the foundation surface. Measured data and the models show close values with slight variations in summer season. Figure 5.28 shows the temperature with depth at the toe of the embankment below the foundation surface. Measured and simulated data show relatively close temperatures in 2015. In 2016, simulated values under predicted the measured data showing more disagreement near the surface. Figure 5.28 shows that the depth of zero annual amplitude is located more than 3.5 m below the foundation surface. Measured and simulated thickness of the active layer show similar temperatures at around 0.5 to 1 m below the surface.

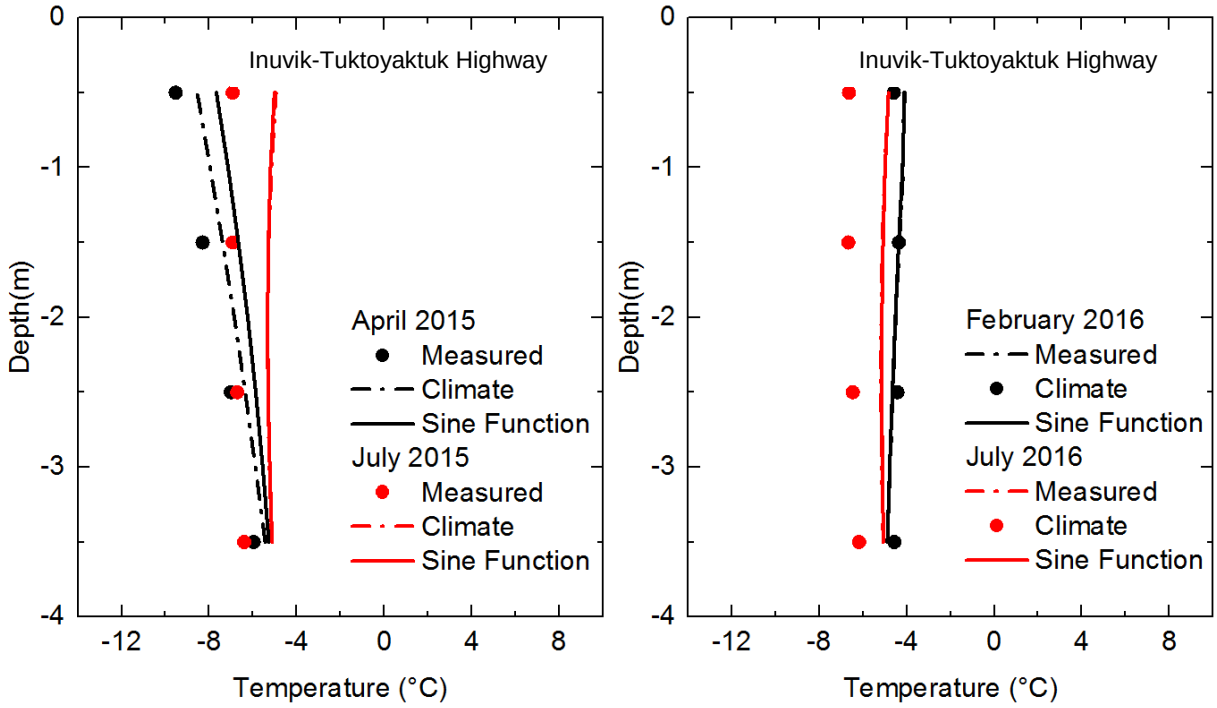


**Figure 5.27. Measured and simulated temperatures with depth at the centreline of the embankment below the foundation surface.**

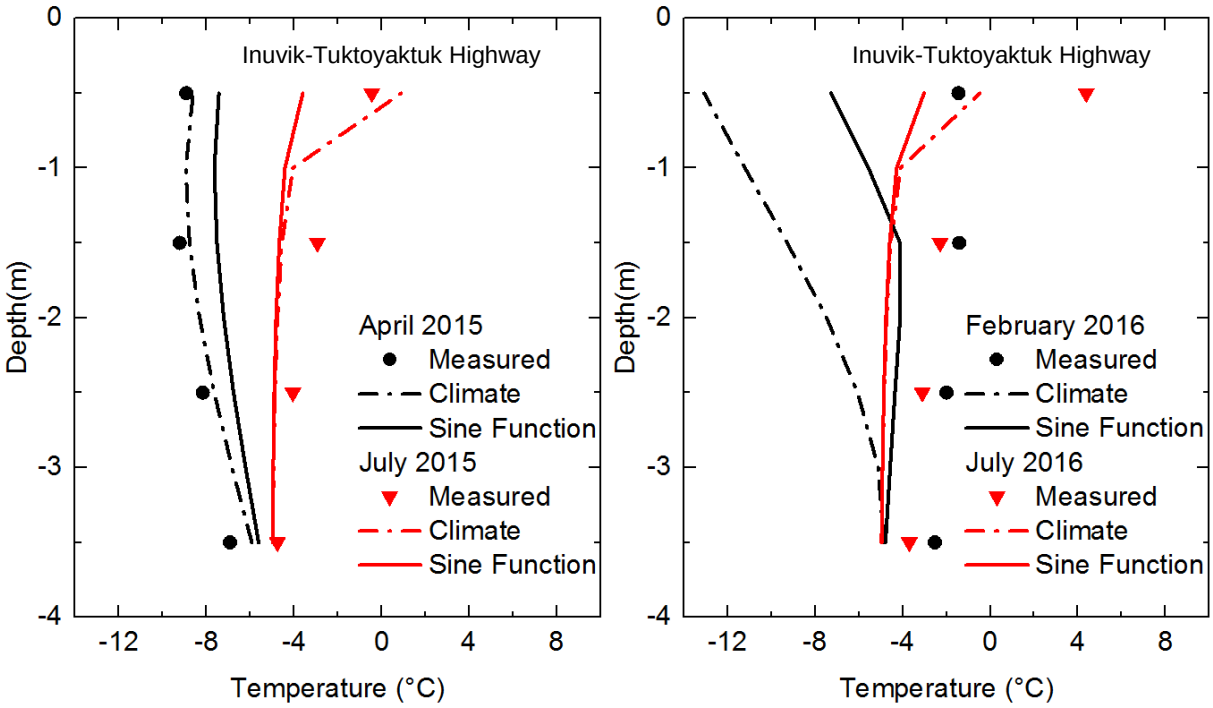


**Figure 5.28. Measured and simulated temperatures with depth at the toe of the embankment below the foundation surface.**

Figures 5.29 to 5.30 show temperature variations in and below the active layer of the embankment respectively. Temperatures are relatively close between the measured data and the TEMP/W models in and below the active layer. Figures 5.31 and 5.32 show the temperature variations in and below the active layer at the toe of the embankment, respectively. In the active layer (Figure 5.31), the models predicted reasonably well the measured data after the winter in 2015. Below the active layer (Figure 5.32), the models slightly under predicted the temperature variations after June 2015. They simulated constant values at -5°C with slight cooling in winter.

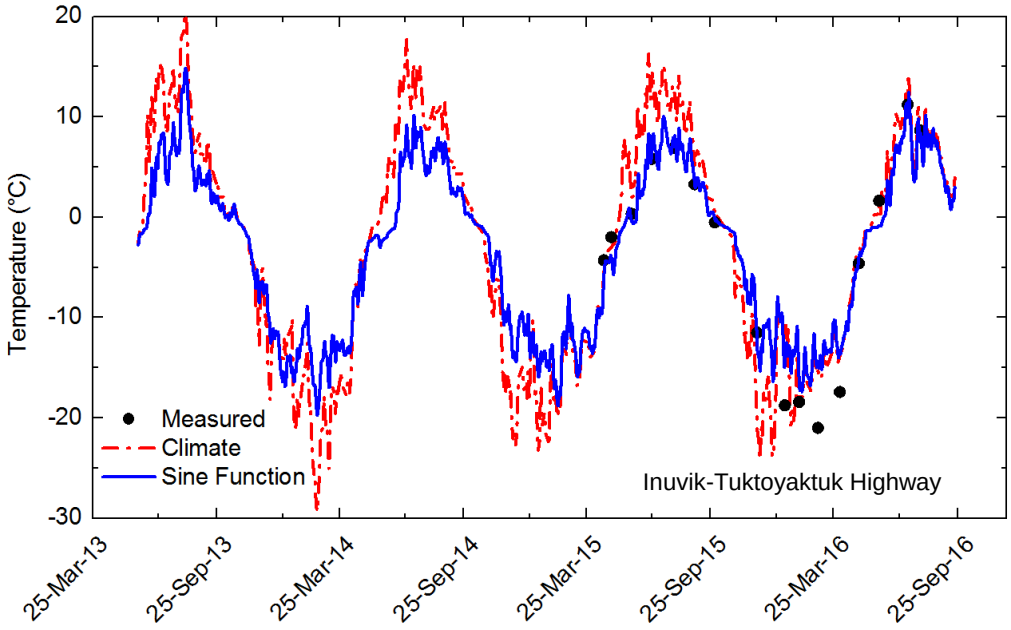


**Figure 5.29. Measured and simulated temperature vs. time relationships in the active layer at a depth of 0.5 m at the centreline of the embankment.**

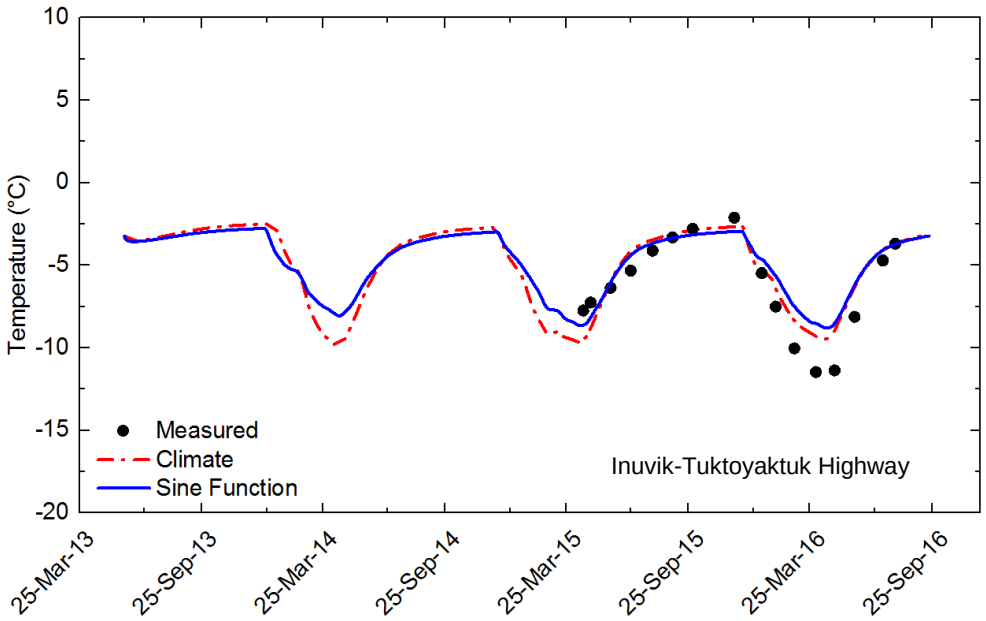


**Figure 5.30. Measured and simulated temperature vs. time relationships below the active layer at a depth of 4.5 m at the centreline of the embankment.**

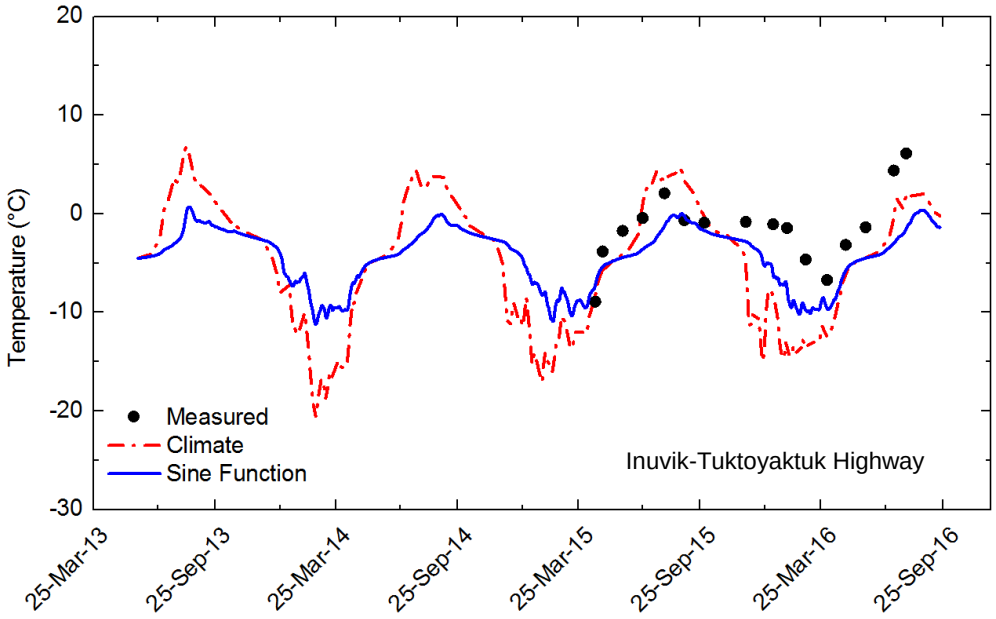


**Figure 5.31. Measured and simulated temperature vs. time relationships in the active layer at a depth of 0.5 m at the toe of the embankment.**

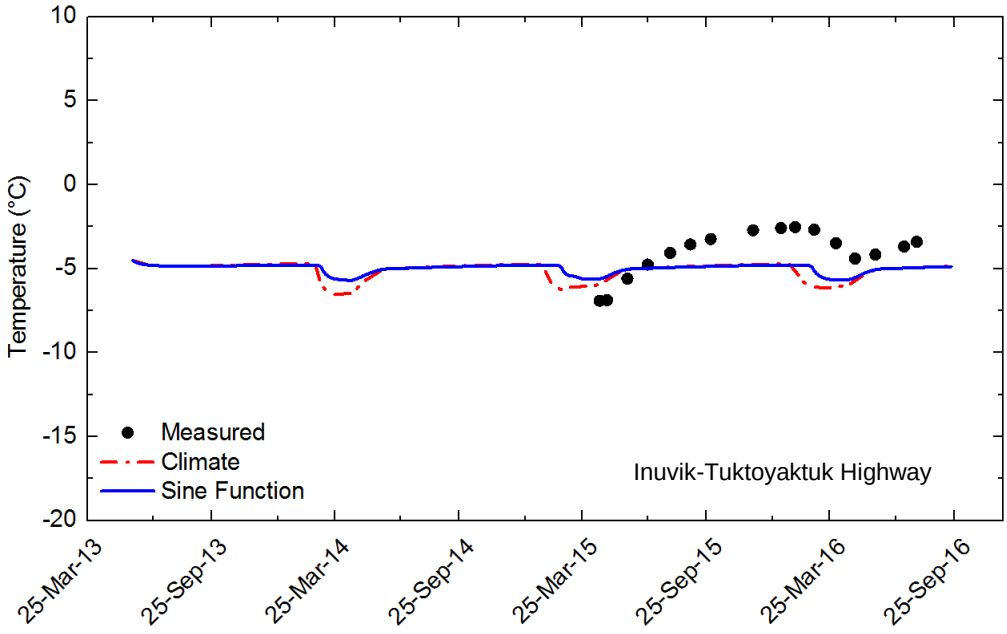


**Figure 5.32. Measured and simulated temperature vs. time relationships below the active layer at a depth of 3.5 m at the toe of the embankment.**

## 5.3 Highway 3, Behchoko-Yellowknife, Northwest Territories

### 5.3.1 Performance Criteria

Overall, the sine function model indicate good prediction using $R^2$ with values close to 1. RMSE indicates lower deviation in winter with the climate model and in summer with the sine function model.

Climate model shows $R^2$ values between 0.19 to 0.97 and RMSE values between 0.87°C to 3.88°C. Sine function model shows $R^2$ values between 0.80 to 0.81 and RMSE values between 0.88°C to 2.40°C (Figure 5.33)

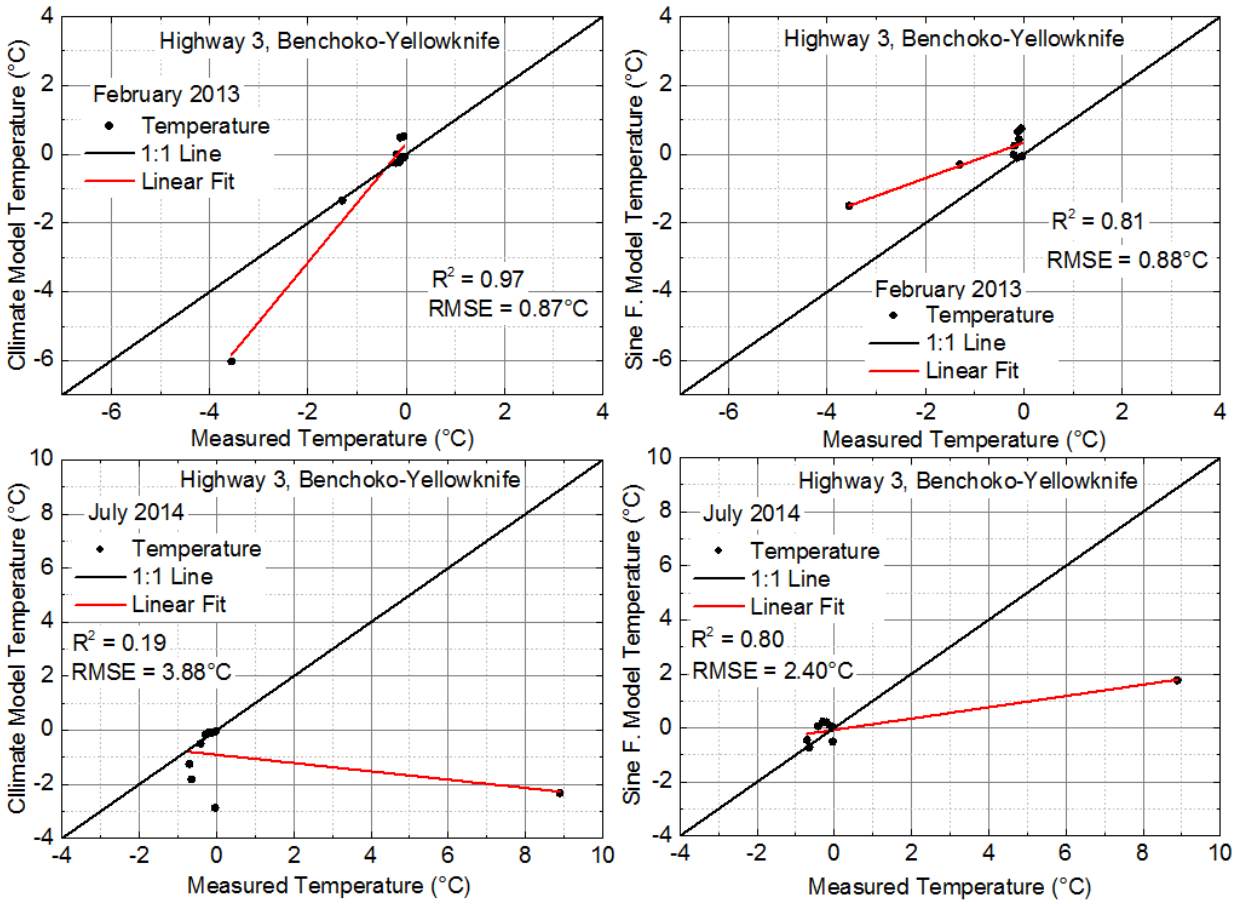


**Figure 5.33 Model performance results of measured and simulated temperatures.**

### 5.3.2 Sensitivity Analysis

The thermal conductivity and volumetric heat capacity in frozen and unfrozen states were evaluated further during the sensitivity analysis. Overall, the thermal conductivity (K) is more sensitive than the volumetric heat capacity (C).

Analysis results at 1.0 m below the surface showed slightly higher temperature variations with thermal conductivity (Figure 5.34) than with volumetric heat capacity (Figure 5.35). The sensitivity analysis shows that the thermal conductivity affected the temperature variations with time by +3.5%/

-4.3%, +7.4%/-8.4% and +27%/-54% if K varies by ± 5%, ± 10% and ± 50%, respectively. The sensitivity analysis showed that the volumetric heat capacity affected the temperature variations with time by -2.7%/+2.9%, -5.7%/+5.6% and -25%/+31% if C varies by ± 5%, ± 10% and ± 50%, respectively.

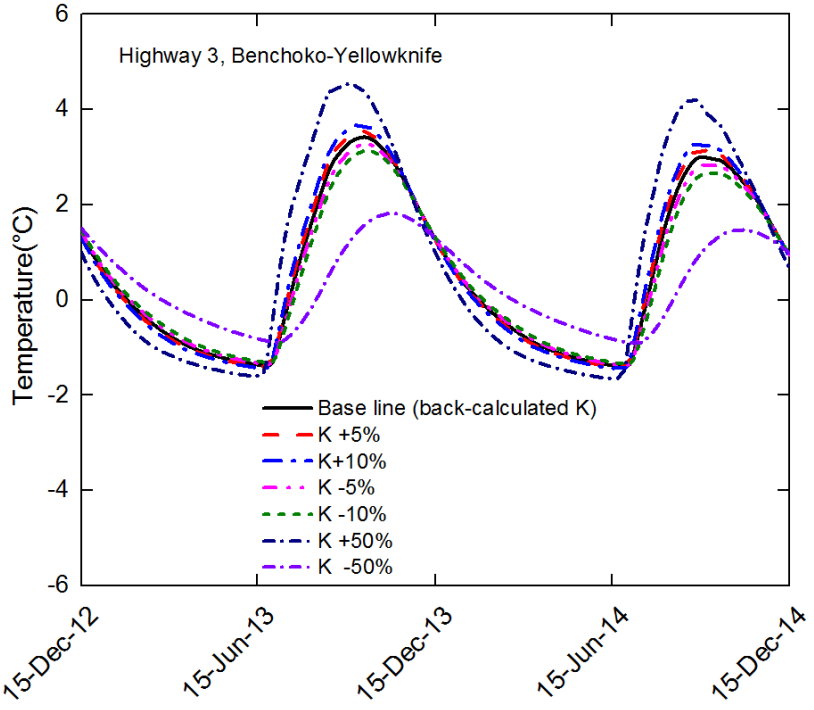


**Figure 5.34. Sensitivity of thermal conductivity at 1 m below the surface.**

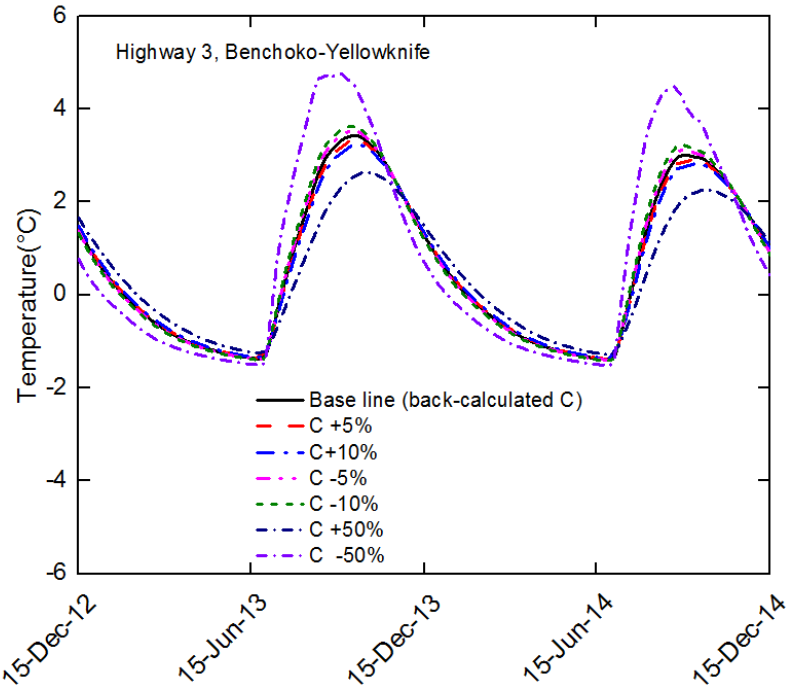


**Figure 5.35. Sensitivity of volumetric heat capacity at 1 m below the surface.**

### 5.3.3 Thermal Regime

The climate and sine models simulated measured data between December 2012 and December 2014. Figures 5.36 and 5.37 represent the temperature with depth in the winter (February) and the summer (July) between 2013 and 2014, respectively. Measured and simulated data show relatively close temperatures. As stated in the afore-mentioned section, the climate model shows better simulation in winter, whereas the sine model shows better simulation in summer. The temperature with depth shows a warm permafrost at around -1°C. The measured and simulated temperatures show an active layer of around 3 m of depth. The depth of zero annual amplitude is simulated at about 6 to 7 m below the surface.

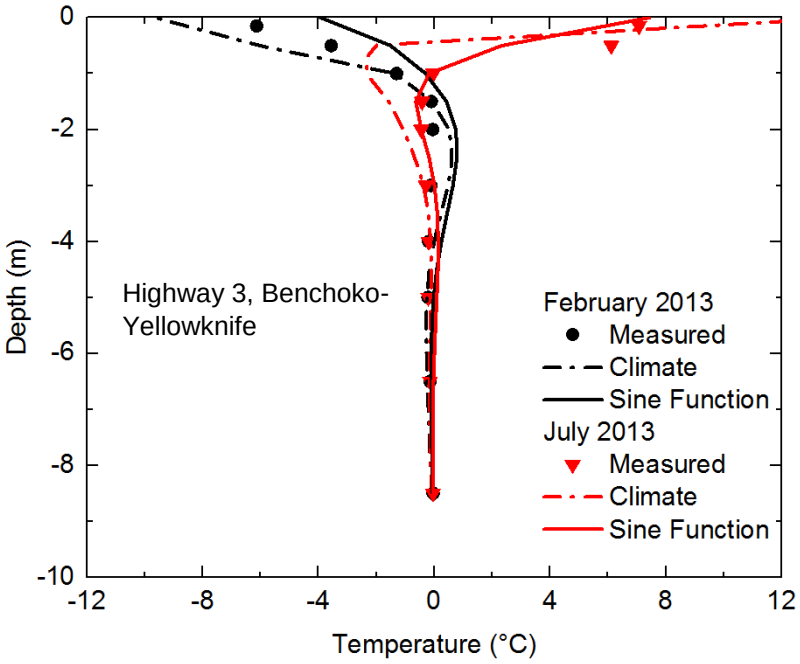


**Figure 5.36. Measured and simulated temperatures with depth.**

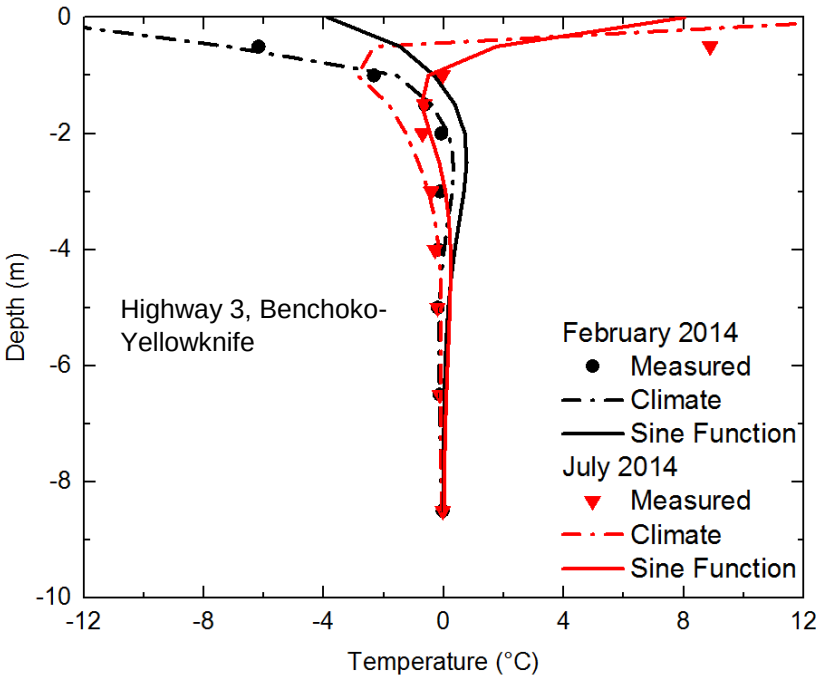


**Figure 5.37. Measured and simulated temperatures with depth.**

Figures 5.38 and 5.39 show the temperature variations in and below the active layer, respectively. In the active layer (Figure 5.38), the models slightly over predicted thawing temperatures. The sine model shows temperatures closer to measured data in summer, whereas the climate model shows closer temperatures in winter.

Simulated temperatures show close values to measured data below the active layer. (Figure 5.39). The sine model slightly over predicted the temperatures and was not able to capture the observed seasonal variations.

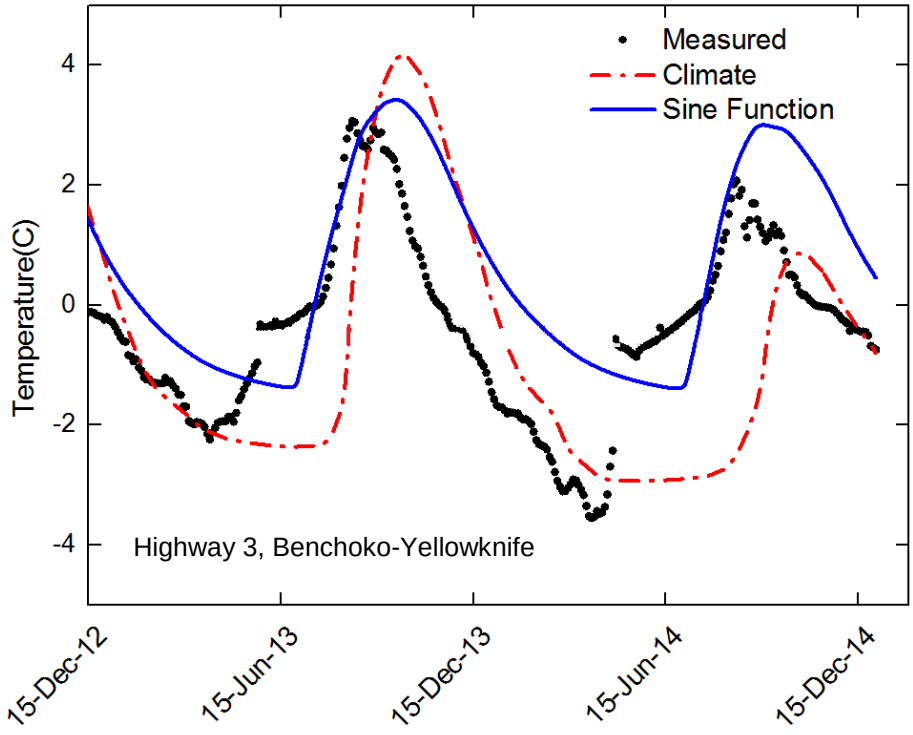


**Figure 5.38. Measured and simulated temperature vs. time relationships in the active layer at a depth of 1 m below the surface.**

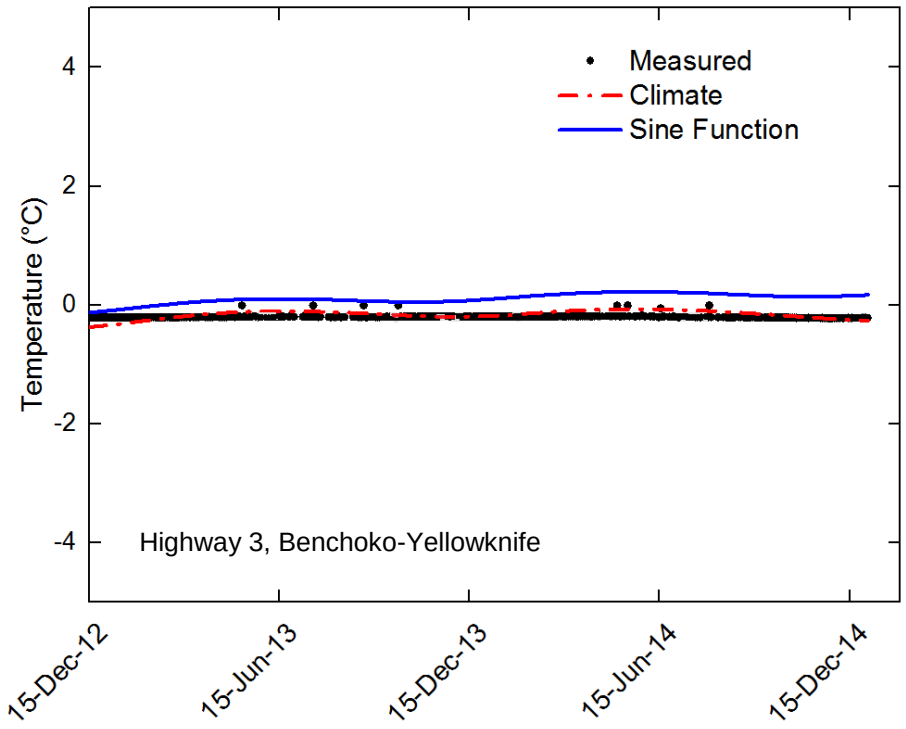


**Figure 5.39. Measured and simulated temperature vs. time relationships below the active layer at a depth of 5 m below the surface.**

## 5.4 Murtèl-Corvatsch Rock Glacier, Engadin Region, Switzerland

### 5.4.1 Performance Criteria

Overall, the sine function model indicates better prediction ($R^2$) in winter when compared to summer. Furthermore, RMSE indicates lower values in winter compared to summer. The sine function model shows $R^2$ values between 0.02 to 0.86 and RMSE values between 1.08°C to 2.82°C (Figure 5.40)

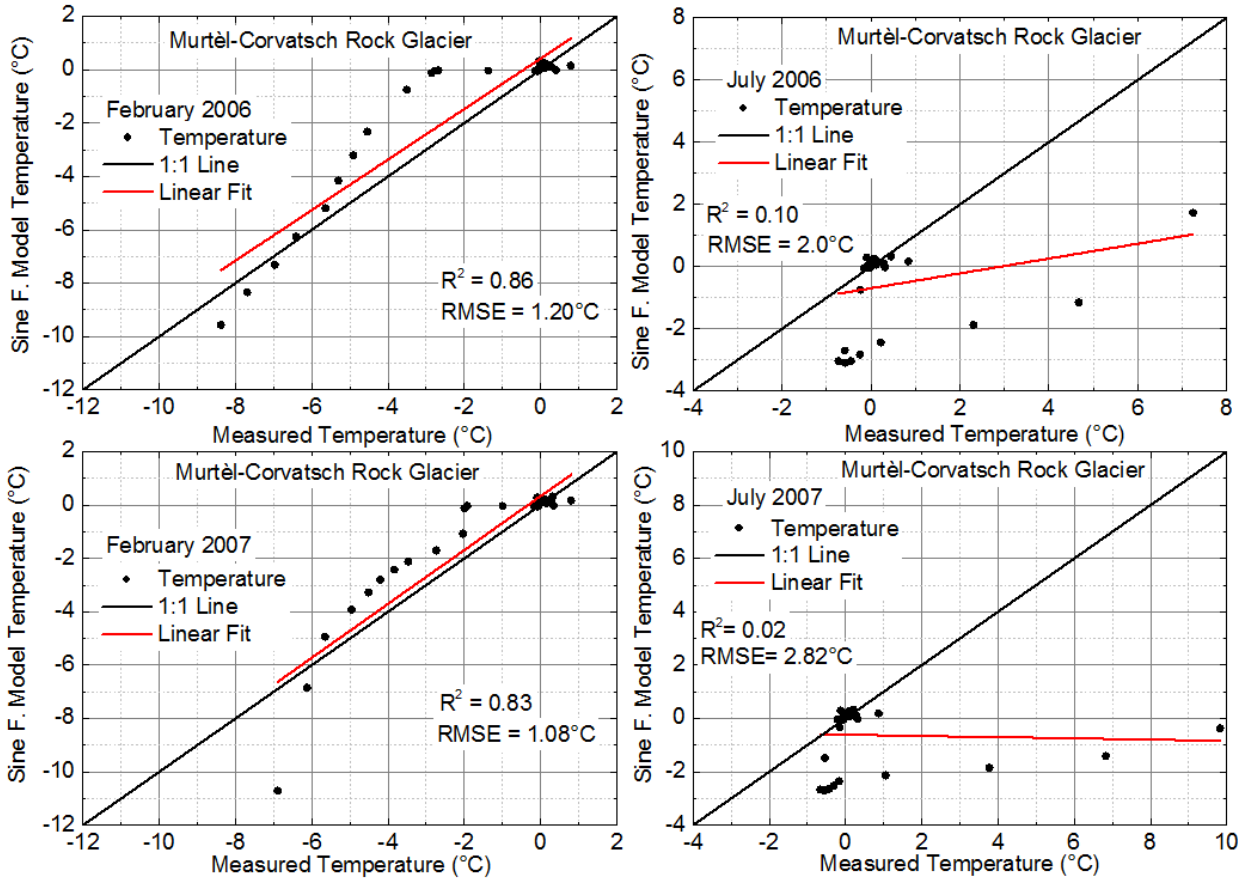


**Figure 5.40. Model performance results of measured and simulated temperatures.**

### 5.4.2 Sensitivity Analysis

The thermal conductivity and volumetric heat capacity in frozen and unfrozen states were evaluated further during the sensitivity analysis. Overall, the thermal conductivity (K) is more sensitive than the volumetric heat capacity (C).

Analysis results at 0.5 m below the surface showed slightly higher temperature variations with thermal conductivity (Figure 5.41) than with volumetric heat capacity (Figure 5.42). The sensitivity analysis showed that the thermal conductivity affected the temperature variations with time by +2.2%/

-1.2%, +10%/-3.2% and +23%/-39% if K varies by ± 5%, ± 10% and ± 50%, respectively. The sensitivity analysis showed that the volumetric heat capacity affected the temperature variations with time by -0.7%/+0.1%, -1.8%/+4.5% and -12%/+18% if C varies by ± 5%, ± 10% and ± 50%, respectively.

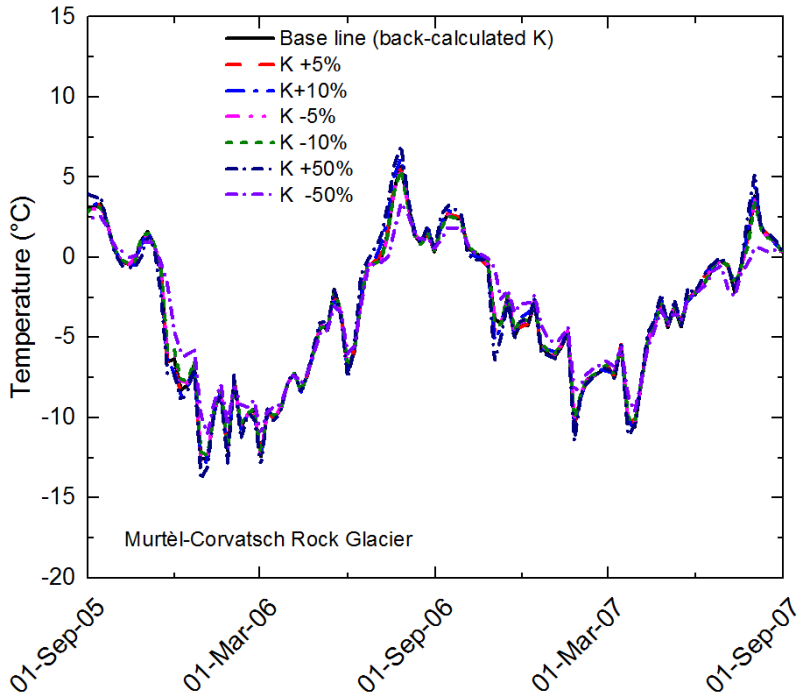


**Figure 5.41. Sensitivity of thermal conductivity at 0.5 m below the surface.**

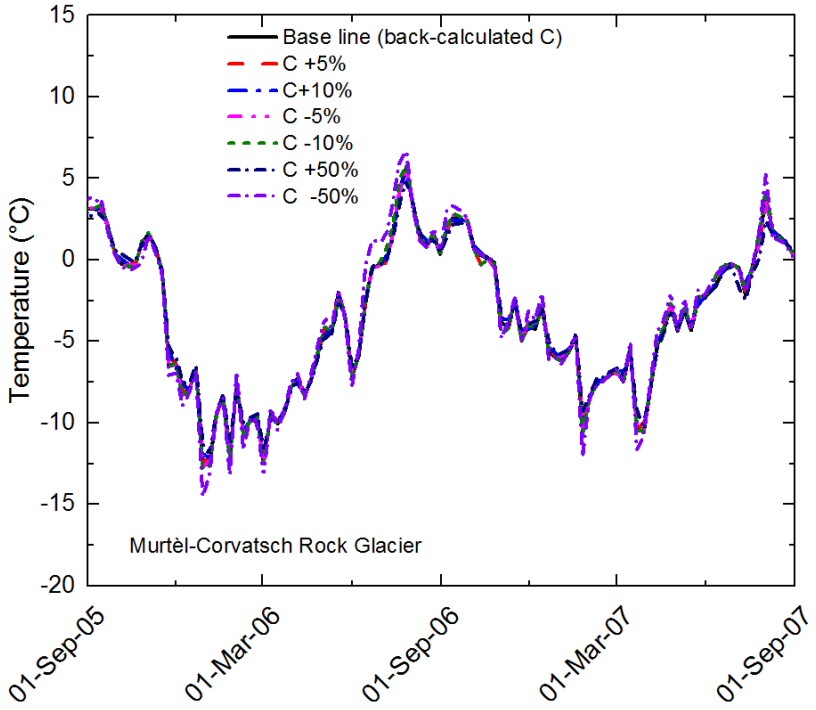


**Figure 5.42. Sensitivity of volumetric heat capacity at 0.5 m below the surface.**

### 5.4.3 Thermal Regime

Figures 5.43 and 5.44 represent measured and simulated temperatures with depth in 2006 and 2007, respectively. The sine model under predicted temperatures below the active layer at 2.5 m depth in July and over predicted temperatures in February in the ice-rich layer.

Both measured and simulated data indicated the location of the depth of zero annual amplitude at about 20 to 25 m below the surface. Below this depth, the model shows an average temperature of 0°C that increases starting at around 45 m depth. The model shows an active layer thickness of around 0.5 m, while the measured data shows a thickness of 2 m.

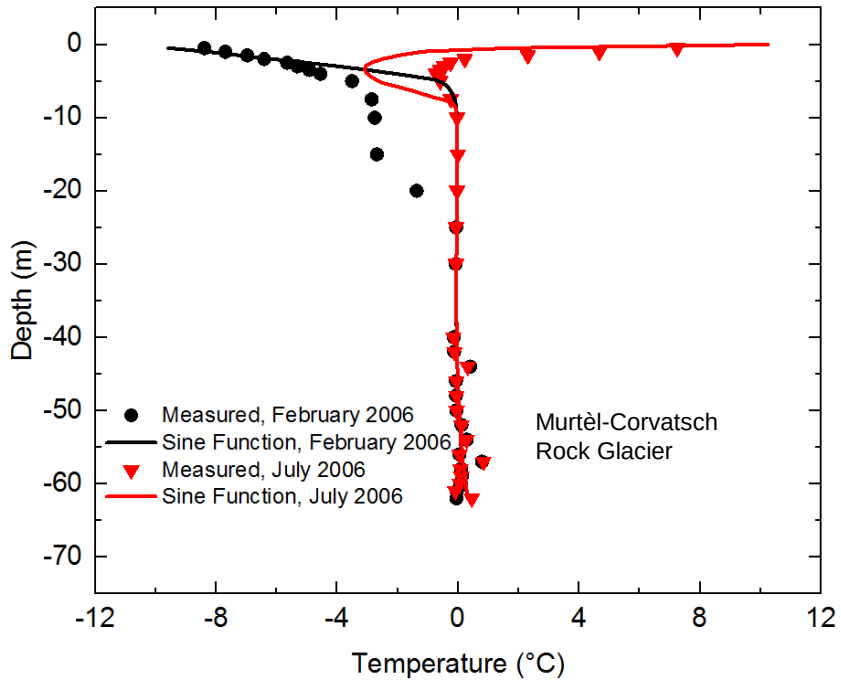


**Figure 5.43. Measured and simulated temperatures with depth.**

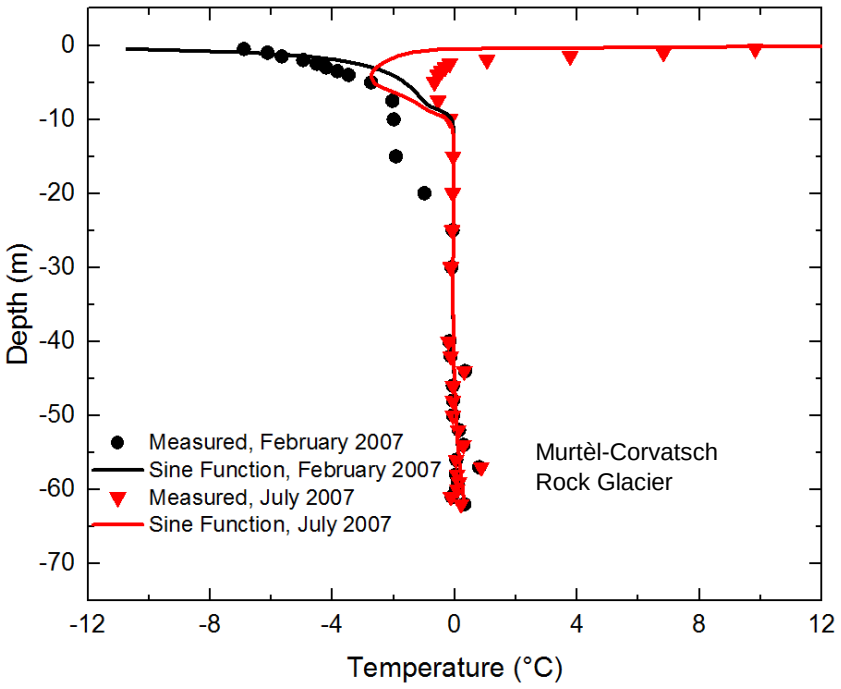


**Figure 5.44. Measured and simulated temperatures with depth.**

Figures 5.45 and 5.46 show the variations with time of measured and simulated temperatures in and below the active layer, respectively. Figure 5.45 shows a sine model that under predicted the highest and lowest values represented in winter and summer, respectively.

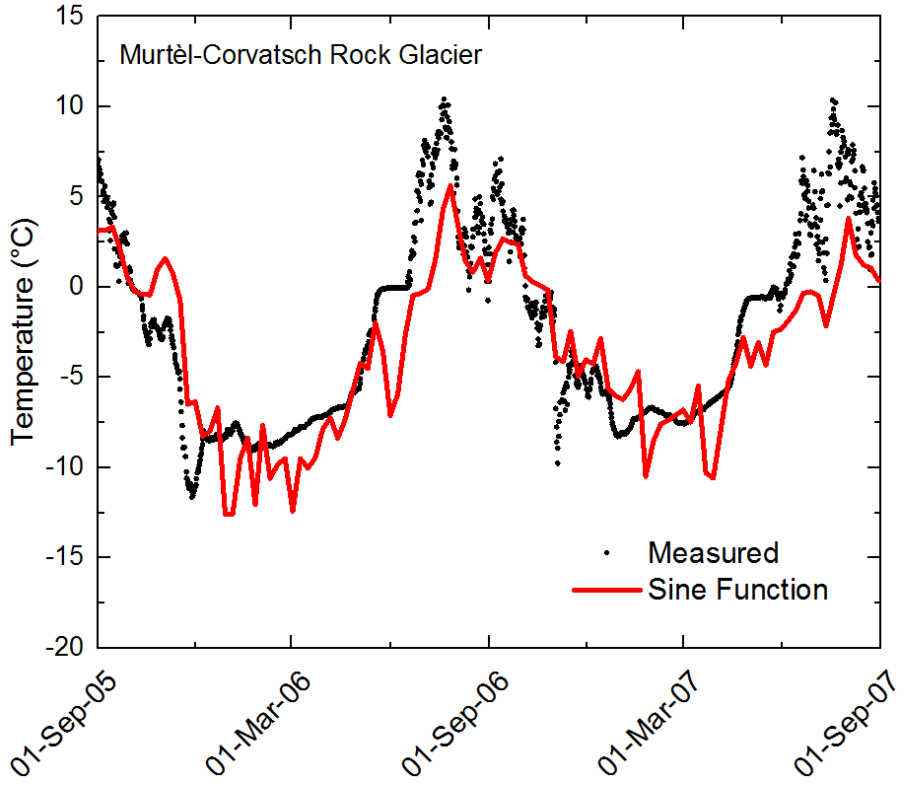


**Figure 5.45. Measured and simulated temperature vs. time relationships in the active layer at a depth of 0.5 m below the surface.**

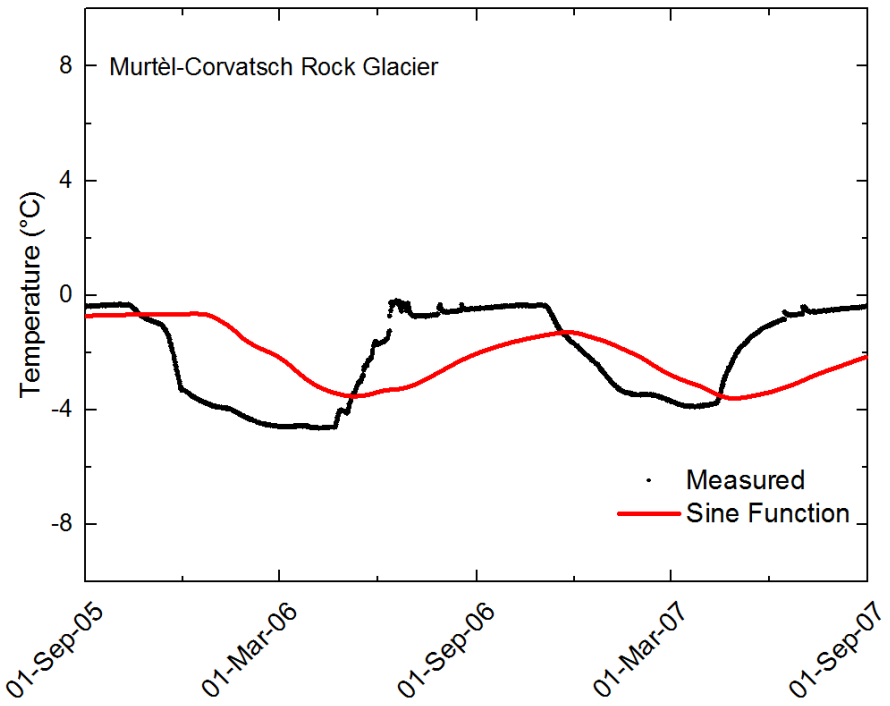


**Figure 5.46. Measured and simulated temperature vs. time relationships below the active layer at a depth of 4 m below the surface.**

## 5.5 Chilean Andes Rock Glacier, Chile

### 5.5.1 Performance Criteria

The sine function model indicates better prediction ($R^2$) in summer when compared to winter. Overall, RMSE show values close to 0. Sine function model shows $R^2$ values between 0.50 to 0.98 and RMSE values between 0.30°C to 1.31°C (Figure 5.47).

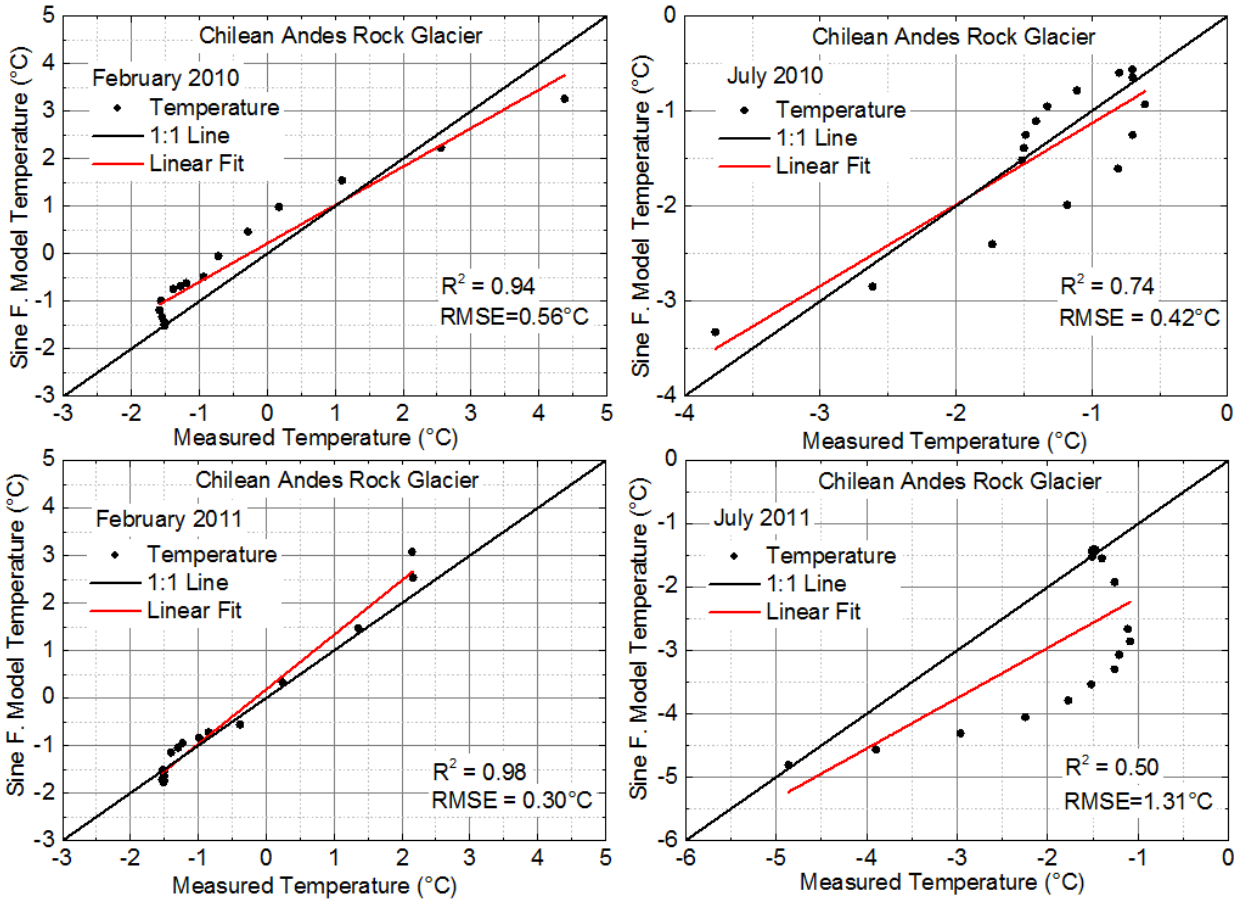


**Figure 5.47. Model performance of measured and simulated temperatures.**

### 5.5.2 Sensitivity Analysis

The thermal conductivity and volumetric heat capacity in frozen and unfrozen states were evaluated further during the sensitivity analysis. Overall, the thermal conductivity (K) is more sensitive than the volumetric heat capacity (C).

Analysis results at 1 m below the surface show slightly higher temperature variations with thermal conductivity (Figure 5.48) than with volumetric heat capacity (Figure 5.49). The sensitivity analysis shows that the thermal conductivity affected the temperature variations with time by +3.6%/-4.1%,

+6.6%/-8.6% and +24%/-53% if K varies by ± 5%, ± 10% and ± 50%, respectively. The sensitivity analysis showed that the volumetric heat capacity affected the temperature variations with time by -2.2%/+2.3%, -4.5%/+4.5% and -20%/+15% if C varies by ± 5%, ± 10% and ± 50%, respectively.

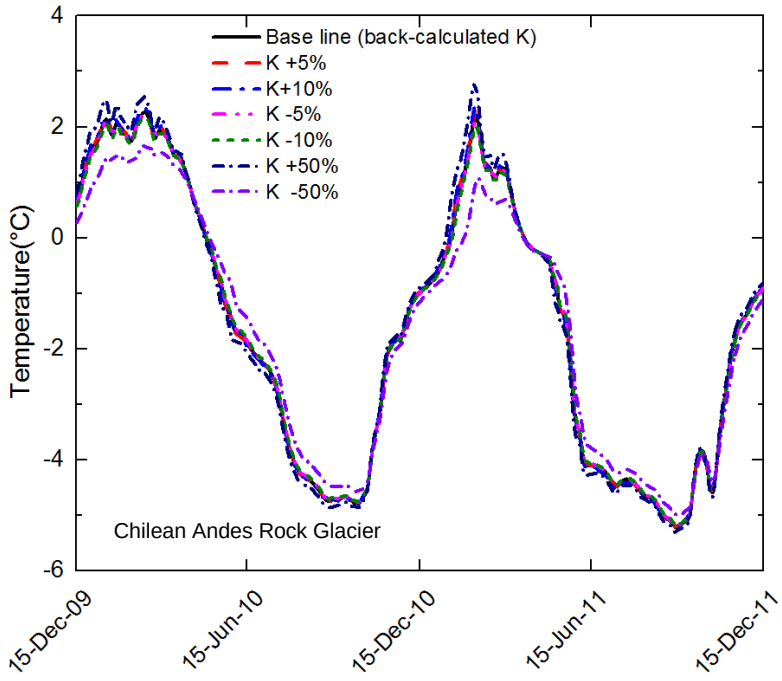


**Figure 5.48. Sensitivity of thermal conductivity at 1 m below the surface.**

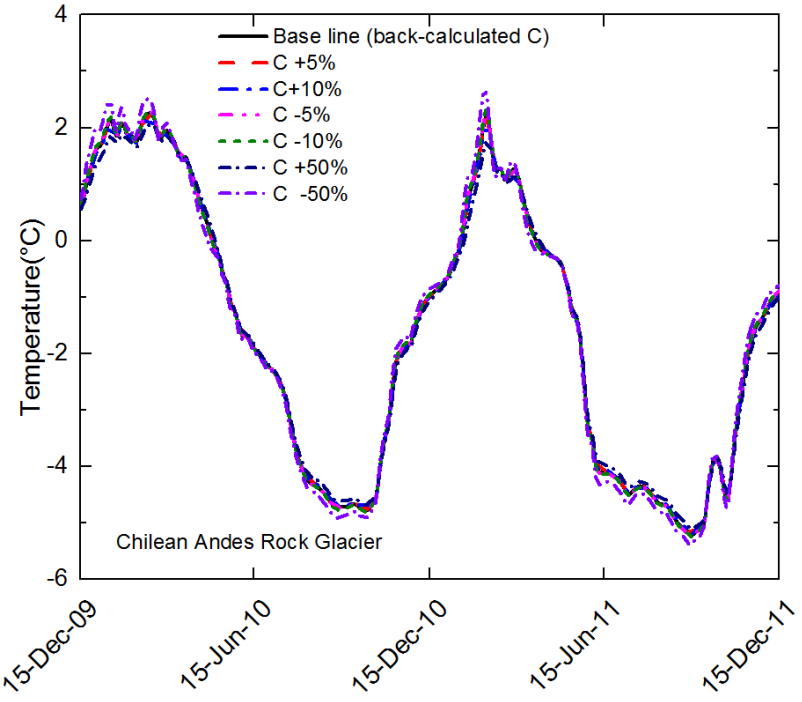


**Figure 5.49. Sensitivity of volumetric heat capacity at 1 m below the surface.**

### 5.5.3 Thermal Regime

Figures 5.50 and 5.51 show the measured and simulated temperature with depth obtained in the winter (February) and the summer (July) of 2010 and 2011, respectively. The sine model values are relatively close to the measured data. The model simulated well the thickness of the active layer at around 2 m below the surface, which is similar to the thickness of the measured data. The model simulates the depth of zero annual amplitude at around 14 to 16 m below the surface, which is close to the 12 m of depth of the measured data.

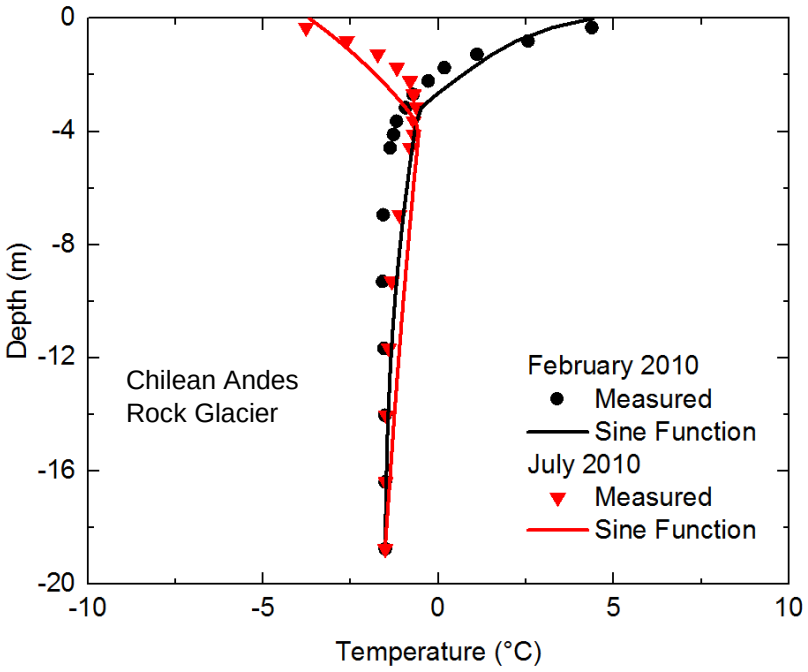


**Figure 5.50. Measured and simulated temperatures with depth.**

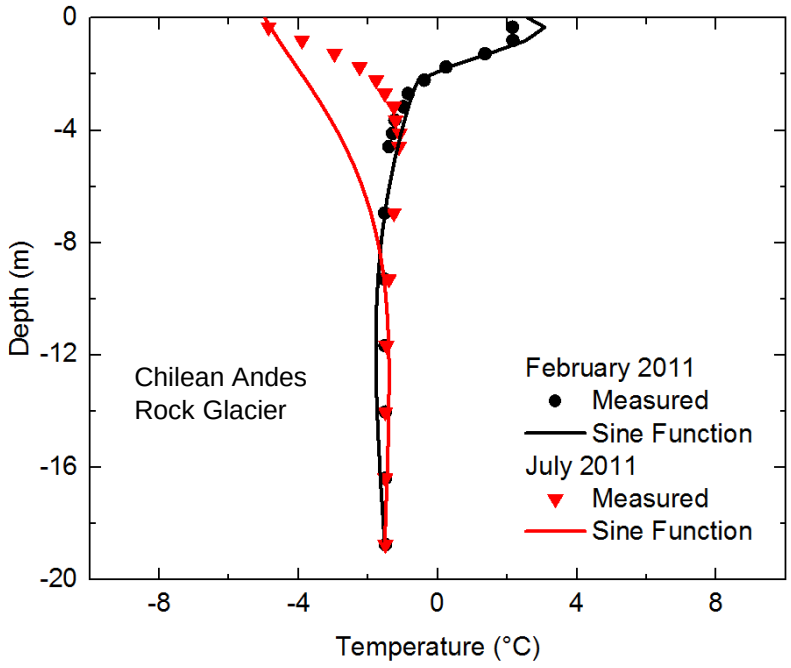


**Figure 5.51. Measured and simulated temperatures with depth.**

Figure 5.52 and 5.53 show variations with time of measured and simulated temperatures in and below the active layer, respectively. Measured and

simulated temperatures are close in the active layer at 1 m below the surface (Figure 5.52). Below the active layer, the model under predicted temperatures at 4 m below the surface (Figure 5.53).

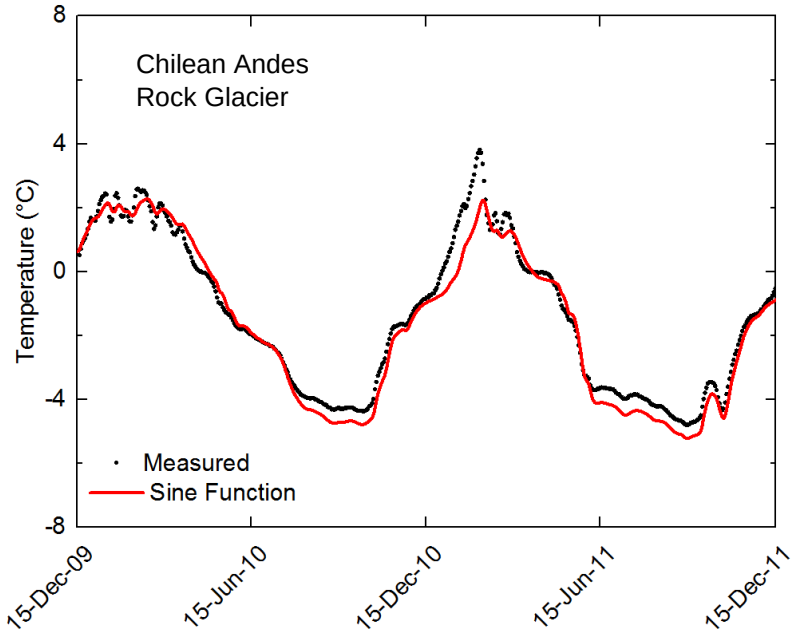


**Figure 5.52. Measured and simulated temperature vs. time relationships in the active layer at a depth of 1 m below the surface.**

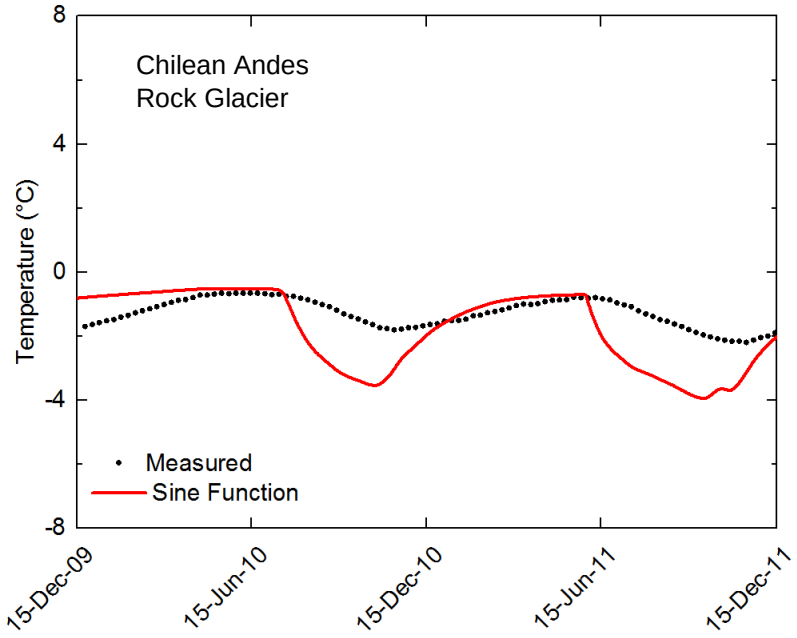


**Figure 5.53. Measured and simulated temperature vs. time relationships below the active layer at a depth of 4 m below the surface.**

### 5.6 Alternate Procedure Based on Data of Temperature with Time

Table 5.1 shows estimated thermal conductivities (W/m.K) by using equation 4.8. Approximated values of the slope *S* were obtained from equation 4.9 using the variation of temperature with time in and below the active layer of the climate and sine function models. The estimated thermal conductivities are comparable to the calibrated values shown in Chapter 4.

**Table 5.1. Thermal conductivities based on the climate and sine function models at the sites.**

| Site | Soil | Slope of the Temperature vs. Time Variation $S$ in Active | | Thermal Conductivity (W/m.K) $k_u$ | | Slope of the Temperature vs. Time Variation $S$ below | | Thermal Conductivity (W/m.K) $k_f$ | |
|---|---|---|---|---|---|---|---|---|---|
| | | Climate | Sine Function | Climate | Sine Function | Climate | Sine Function | Climate | Sine Function |
| PR391 | Silty Clay[a] | 0.021 | 0.012 | 1.146 | 1.148 | - | - | - | - |
| | Saturated Gravel[b] | 0.138 | 0.024 | 2.337 | 2.327 | - | - | - | - |
| Inuvik-Tuktoyaktuk | Silty Sand | 0.440 | 0.340 | 2.936 | 2.901 | 0.077 | 0.048 | 4.057 | 4.010 |
| | Clay | 0.215 | 0.140 | 1.446 | 1.447 | 0.021 | 0.019 | 2.349 | 2.360 |
| Behchoko-Yellowknife | Silty Clay | 0.265 | 0.215 | 0.364 | 0.322 | 0.011 | 0.014 | 0.694 | 0.713 |
| Murtèl-Corvatsch | Top Layer, Gravel | - | 0.320 | - | 2.915 | - | 0.045 | - | 5.212 |
| Chilean Andes | Gravel | - | 0.173 | - | 1.704 | - | 0.025 | - | 4.671 |

[a]Measured at the toe of the embankment at 8 m below the surface. [b]Measured at the shoulder of the embankment at 3 m below the surface.

# CHAPTER 6: Discussions

## 6.1 Introduction

The thermal properties of soils can be estimated by using finite element methods under specific conditions (Helwany, 2007). TEMP/W has been used to simulate in-situ temperatures by assuming external conditions and calibrating the thermal conductivity and volumetric heat capacity of soils.

The ranges of thermal properties of soils at the research sites were obtained from various studies (Flynn, 2015; Andersland and Ladanyi, 2004; Arenson et al., 2015; GEO-SLOPE International Ltd.,2008; Eppelbaum et al., 2014; and Robertson, 1988).

During the calibration process, it was necessary to use high thermal conductivities to achieve high temperature variations in coarse-grained soils. Then, it was noticed that these variations required low volumetric heat capacities. On the other hand, fine-grained soils required low thermal conductivities and high volumetric heat capacities to achieve low variations of temperature in the same period. Furthermore, it was noticed that the frozen thermal conductivities should be higher than the unfrozen thermal conductivities for coarse and fined grained soils. However, the volumetric heat capacities in frozen state should be lower than the volumetric heat capacities in unfrozen state for coarse and fine-grained soils. Finally, the thermal properties were calibrated until the best fit of the measured and simulated temperature

variations with depth and time was achieved. Sensitivity analysis was carried out to determine which thermal properties show more importance for calibration.

## 6.2 Provincial Road PR391, Thompson, Manitoba

### 6.2.1 Performance Criteria

Overall, better performance is shown at the mid-slope and toe of the embankment (Figure 5.1 to Figure 5.2). For RMSE, better performance is shown with the sine function model. There is more disagreement between the models and the measured data at the shoulder and centreline of the embankment (Figure 5.3 to Figure 5.4). The geothermal model could not predict the freezing temperatures in the saturated gravel and the zone of the afore-mentioned frost bulb. More latent heat or energy has to be released in the model to better simulate the variation of temperatures in this zone.

### 6.2.2 Sensitivity Analysis

For silty clay (toe of embankment) and saturated gravel (shoulder of embankment), the volumetric heat capacity shows more sensitivity than the thermal conductivity. Overall, thermal properties in saturated gravel found to be more sensitive than thermal properties in silty clay. Silty clay showed low sensitivity as the temperature variations are affected by only +5.0%/-4.8% when K varies by ± 50% and -7.5%/+11% when C varies by ±50 % (Figure 5.5).

### 6.2.3 Thermal Regime

Overall, the sine function model was more accurate at simulating variations of ground temperature than the climate model. This is due to the fact that the

climate model does not include the type of ground surface. The region near and inside the frost bulb (Figures 5.14 and 5.16) showed trends of warming and freezing measured data that are over predicted by the models. Flynn (2015) states the discrepancy between the measured data and the geothermal models in the permafrost region (below shoulder and centreline of the embankment) is related to the unfrozen water content function that was unable to predict the rate at which the water in the soil could freeze at 0 °C. The geothermal model needs to remove more energy to freeze the ground after the thawing phase.

In general, measured and simulated data predicted further thawing of the degrading permafrost. Measurements below the shoulder (Figure 5.14) and the centreline (Figure 5.16) of the embankment show slight warming temperatures probably coming from beneath the toe region that experienced a slight increase (Figure 5.10).

## 6.3 Inuvik-Tuktoyaktuk Highway, Northwest Territories

### 6.3.1 Performance Criteria

Overall, $R^2$ values indicate good agreement between the measured data and the climate and sine function models (Figure 5.17 to Figure 5.20). RMSE shows the lowest values in the base at the centreline of the embankment that indicates good fit of measured and simulated values (Figure 5.19). Due to limited measured data per thermistors string (four at the top and toe of embankment and seven at the base of embankment), high variations in RMSE values were found.

### 6.3.2 Sensitivity Analysis

Thermal conductivity (K) indicated to be more sensitive than volumetric heat capacity (C). Thermal properties of clay at the foundation of the embankment were found to be more sensitive than thermal properties of silty sand at the embankment. For instance, temperature variations are affected by +229%/ -969% if K varies by ±50% (Figure 5.23). This means that the thermal conductivity of clay has more uncertainty in the model calibration.

### 6.3.3 Thermal Regime

Thermal regimes at the top, base, centreline and toe of the embankment are shown between Figure 5.25 and Figure 5.32. In general, both climate and sine function models show relatively close temperatures to the measured data. Simulated temperatures are under predicted near and at the toe of the embankment in February 2016 (Figures 5.26 and 5.28). This is due to accumulation of snow as seen in De Guzman et al. (2015). The models need to capture the insulation effect of the snow cover in this area.

## 6.4 Highway 3, Behchoko-Yellowknife, Northwest Territories

### 6.4.1 Performance Criteria

For $R^2$, the sine function model shows better prediction of values in summer compared to the climate model that performs better in winter. For RMSE, the models indicate lower values in winter. The climate model under predicted the rate of cooling below the active layer in summer (Figure 5.33).

### 6.4.2 Sensitivity Analysis

Thermal conductivity (K) is more sensitive than volumetric heat capacity (C). As shown in Figure 5.34, when K varies by ± 10 % the change in temperature variation is relatively low (+7.4%/-8.4%). This is an indication of low uncertainty about this thermal property.

### 6.4.3 Thermal Regime

Overall, climate and sine function models show values close to measured temperatures (Figure 5.36 to Figure 5.39). The sine model showed temperatures closer to measured data in summer, whereas the climate model showed closer temperatures in winter. This is due to the fact that sine function model takes into account the type of surface of the ground, which is clear is summer and closer to assumed terrain conditions. Uncertainties in the sine function model are increased in winter when the snow thickness may vary and surface temperature are not properly estimated.

The low amplitude of temperature variation in and below the active layer represents a soil that can retain a high content of unfrozen water in winter, reflecting a low thermal conductivity in the frozen and the unfrozen states (Figures 5.38 and 5.39).

## 6.5 Murtèl-Corvatsch Rock Glacier, Engadin Region, Switzerland

### 6.5.1 Performance Criteria

$R^2$ and RMSE showed better performance in winter than in summer (Figure 5.40). The model was not properly calibrated in the area near and inside the ice

rich layer (Figure 4.4) where temperatures are under predicted in summer and over predicted in winter. The model needs to improve the rate at which the latent heat is released or absorbed below the active layer.

### 6.5.2 Sensitivity Analysis

Thermal conductivity (K) is more sensitive than volumetric heat capacity (C). The analysis was carried out in the top layer only (large boulders) due to the lower soil layers show low temperature variations at 0°C.

### 6.5.3 Thermal Regime

The sine model under predicted temperatures below the active layer at 2.5 m depth in July and over predicted temperatures in February in the ice-rich layer. This is due to the fact that the model did not capture short variations of temperature produced near and inside this layer (Figures 5.43 and 5.44)

Figure 5.45 shows a model that follows the same trend of the variations with time. The time lag shown in Figure 5.46 is associated to the rate at which the latent heat is released or absorbed below the active layer.

## 6.6 Chilean Andes Rock Glacier, Chile

### 6.6.1 Performance Criteria

Overall, $R^2$ and RMSE criteria showed good agreement between measured and simulated temperatures. $R^2$ performs better in summer. RMSE shows values close to 0 with the exception of July 2011, where more deviation respect to the measured data is seen (Figure 5.47).

### 6.6.2 Sensitivity Analysis

Overall, the thermal conductivity (K) is more sensitive than the volumetric heat capacity (C). The model shows a K with low sensitivity. Temperatures vary by only +6.6%/-8.6% when K changes by ± 10% (Figure 5.48).

### 6.6.3 Thermal Regime

Overall, the sine function model showed relatively close values to the measured data as seen in Figures 5.50 and 5.51. Below the active layer the sine function model under predicted temperature variations (Figure 5.53). The model did not capture the low rate of cooling during winter. The simulation can be improved by reducing the rate at which the unfrozen volumetric water content freezes, which is 95% frozen for gravel at -0.8°C (GEO-SLOPE International Ltd, 2008).

## 6.7 Summary of Discussions

$R^2$ shows similar performance for climate and sine function models. However, RMSE shows better calibration for the sine function model when compared to the climate model. This is due to the sine function model is taking into account the type of surface and the mean air temperature. The range of N-factors are selected depending on the assumed terrain conditions. Then, the calibration of the sine function model can be better adjusted to the closer measured data. On the other hand, the climate model uses climate parameters only. The climate model does not define specific terrain temperatures that affect the heat transfer in the lower layers of the ground. Furthermore, the climate

parameters are approximated as they are taken from meteorological stations located several kilometers apart from the research sites

Limited data over climate and terrain characteristics affect the precision of the calibration. Mountain permafrost was the most affected due to absence of close meteorological stations and data over actual surface conditions. A precise estimation of the unfrozen water content in Inuvik-Tuktoyaktuk Highway and Highway 3, Behchoko-Yellowknife affected the proper simulation of the rate of freezing and thawing in the active layer. Furthermore, the calibration performance is affected by the rate at which the latent heat is released and absorbed in the permafrost layer as shown in PR391 (Figure 5.13 to Figure 5.16), Murtèl-Corvatsch and Chilean Andes rock glaciers (Figures 5.46 and Figure 5.53).

In general, the thermal conductivity is more sensitive than the volumetric heat capacity. Major changes in temperature variations are noticed at ±50% of change of the thermal parameters. Thermal properties of fine-grained soils were found to be more sensitive than thermal properties of coarse-grained soils. Fine-grained soils, like clay, can retain up to 50% of unfrozen water content at temperatures lower than -3°C. Thus, the thermal conductivity of clay is more sensitive to temperature variations when retained water is not completely frozen.

The sensitivity analysis shows that when the thermal conductivity is increased, the variation of temperature tends to increase its amplitude. On the other hand, when the volumetric heat capacity is increased, the variation of

temperature tends to decrease its amplitude. This is why materials with high thermal conductivity, like rocks, usually show low volumetric heat capacity.

*Lowland permafrost*

Three sites are located in lowland areas: Provincial Road PR391, Inuvik-Tuktoyaktuk Highway, Northwest Territories and Highway 3, Behchoko-Yellowknife, Northwest Territories. Thermal properties from the literature and calibration are shown between Table 6.1 to Table 6. 3.

PR391 shows silty clay and clayey silt with calibrated thermal conductivities within the middle and high limit of the range of the literature. Similarly, saturated gravel and dry gravel show calibrated thermal conductivities within the middle and high limit of the range of the literature. Silty clay and clayey silt show calibrated volumetric heat capacities within the middle and high limit of the range. For saturated gravel, the unfrozen calibrated volumetric heat capacity slightly surpassed the high limit of its range due water saturation. Dry gravel shows a calibrated volumetric heat capacity within the middle and the low limit of the range due to low volumetric water content as compared to saturated gravel (Table 6.1).

Thermal properties indicate low difference between Flynn (2015) and the author of this thesis. For silty clay, the difference between Flynn (2015) and the calibrated unfrozen and frozen thermal conductivities are 7% for both. The difference between unfrozen and frozen volumetric heat capacities are 3% and 4%, respectively. In saturated gravel, the difference between initial and calibrated unfrozen and frozen thermal conductivities are 16% and 5%, respectively. The

difference between initial and calibrated unfrozen and frozen volumetric heat capacities are 4% and 5%, respectively.

**Table 6.1. Thermal properties from calibration and literature at Provincial Road 391, Thompson, Manitoba.**

| Site | Soil | Thermal Conductivity (W/m.K) | | Vol. Heat Capacity (kJ/m³/°C) | |
|---|---|---|---|---|---|
| | | $k_u$ | $k_f$ | $C_u$ | $C_f$ |
| | | **Range of Parameters from Literature** | | | |
| Provincial Road 391 | Clay | 0.1 - 1.8 | 0.1 - 2.2 | 1000 - 3100 | 560 - 3120 |
| | Silt | 0.1 - 1.8 | 0.1 - 2.2 | 1160 - 3030 | 560 - 3120 |
| | Gravel | 0.25 - 3 | 0.5 - 4 | 1500 - 2340 | 560 - 3120 |
| | | **Calibrated Parameters** | | | |
| | Silty Clay | 1.157 | 1.736 | 2850 | 2050 |
| | Clayey Silt w/Organics | 1.273 | 1.968 | 2700 | 1950 |
| | Saturated gravel | 2.315 | 3.588 | 2400 | 1850 |
| | Dry Gravel | 1.273 | 2.431 | 1650 | 1500 |

At Inuvik-Tuktoyaktuk Highway silty sand and clay show calibrated thermal conductivities within the high limit of their ranges. Clay over predicted the limit of the range of the frozen thermal conductivity by 5%. Calibrated values for silty sand show high thermal conductivities in the frozen and unfrozen states when they are compared to clay. Silty sand and clay show calibrated volumetric heat capacities within the middle and high limit of their ranges (Table 6.2). Clay shows calibrated volumetric heat capacities relatively high due to substantial moisture content encountered at the site (De Guzman et al. 2017).

**Table 6.2. Thermal properties from calibration and literature at Inuvik-Tuktoyaktuk Highway, Northwest Territories.**

| Site | Soil | Thermal Conductivity (W/m.K) | | Vol. Heat Capacity (kJ/m³/°C) | |
|---|---|---|---|---|---|
| | | $k_u$ | $k_f$ | $C_u$ | $C_f$ |
| | | **Range of Parameters from Literature** | | | |
| Inuvik-Tuktoyaktuk Highway | Sand | 0.25 - 3 | 0.5 - 4 | 1310 - 2780 | 560 - 3120 |
| | Clay | 0.1 - 1.8 | 0.1 - 2.2 | 1000 - 3100 | 560 - 3120 |
| | | **Calibrated Parameters** | | | |
| | Silty Sand | 2.894 | 4.005 | 2430 | 1950 |
| | Clay | 1.424 | 2.315 | 2800 | 2000 |

Behchoko-Yellowknife shows calibrated thermal conductivities near the lowest range of the literature. The calibrated low thermal conductivities in and below the active layer are associated to the retained unfrozen water content. As mentioned in section 4.5.2, around 50% of water can stay unfrozen at about -3 °C for silty clay. Measured ground temperatures at this location may range from -0.01°C to -0.2°C below the active layer. Volumetric heat capacities are within the middle and high limit of the range (Table 6.3).

**Table 6.3. Thermal properties from calibration and literature at Highway 3, Behchoko-Yellowknife, Northwest Territories.**

| Site | Soil | Thermal Conductivity (W/m.K) | | Vol. Heat Capacity (kJ/m³/°C) | |
|---|---|---|---|---|---|
| | | $k_u$ | $k_f$ | $C_u$ | $C_f$ |
| | | **Range of Parameters from Literature** | | | |
| Highway 3, Behchoko-Yellowknife | Silty Clay | 0.1 - 1.8 | 0.1 - 2.2 | 1000 - 3100 | 560 - 3120 |
| | | **Calibrated Parameters** | | | |
| | Silty Clay | 0.313 | 0.694 | 2500 | 2000 |

*Mountain permafrost*

Murtèl-Corvatsch Rock Glacier, Engadin Region, Switzerland and Chilean Andes Rock Glacier, Chile are examples of mountain permafrost. Thermal properties from the literature and calibration are shown between Table 6.4 to Table 6.5.

Murtèl-Corvatsch top layer and Chilean Andes show thermal conductivities within the middle and high range of the literature. These two locations show a frozen thermal conductivity higher than the limit of the range for gravel (4 W/m.K). Generally, rock fragments or debris are part of the structure in mountain permafrost. According to table 4.1, rocks can show up 6.3 W/m.K of frozen thermal conductivity. These values can vary depending on the content of quartz or other mineral of high thermal conduction in the rock. The frozen thermal conductivity in Chilean Andes is slightly above the range from the literature. The assumed material represents a coarsed-grained soil that could include higher dry density or quartz content.

**Table 6.4. Thermal properties from calibration and literature at Murtèl-Corvatsch rock glacier, Engadin Region, Switzerland.**

| Site | Soil | Thermal Conductivity (W/m.K) | | Vol. Heat Capacity (kJ/m³/°C) | |
|---|---|---|---|---|---|
| | | $k_u$ | $k_f$ | $C_u$ | $C_f$ |
| | | Range of Parameters from Literature | | | |
| Murtèl-Corvatsch, Rock Glacier | Boulder | 1.2 - 5.9 | 1.5 - 6.3 | 1500 - 2340 | 560 - 3120 |
| | Ice | 0.56 - 0.58 | 2.1 - 2.76 | 4192.2 - 4217.7 | 1567 - 1887.3 |
| | Gravel | 0.25 - 3 | 0.5 - 4 | 1500 - 2340 | 560 - 3120 |
| | | Calibrated Parameters | | | |
| | Boulders, Top Layer | 2.894 | 5.208 | 2000 | 1100 |
| | Ice with some Gravel and Sand | 0.579 | 2.002 | 4200 | 1800 |
| | Frozen Gravel | 2.546 | 4.282 | 2200 | 1560 |
| | Unfrozen Blocky Layer | 2.662 | 3.762 | 2100 | 1600 |

**Table 6.5. Thermal properties from calibration and literature at Chilean Andes rock glacier.**

| Site | Soil | Thermal Conductivity (W/m.K) | | Vol. Heat Capacity (kJ/m³/°C) | |
|---|---|---|---|---|---|
| | | $k_u$ | $k_f$ | $C_u$ | $C_f$ |
| | | Range of Parameters from Literature | | | |
| Chilean Andes, Rock Glacier | Gravel | 0.25 - 3 | 0.5 - 4 | 1500 - 2340 | 560 - 3120 |
| | | Calibrated Parameters | | | |
| | Gravel | 1.736 | 4.630 | 2300 | 1300 |

Murtèl-Corvatsch top layer and Chilean andes rock glaciers show volumetric heat capacities within the middle and low limit of the range. This is associated to the estimated low volumetric water content, which varies between 0.03 - 0.05. As the heat capacity depends on the water content, rock and gravel will show low frozen volumetric heat capacities at freezing temperatures.

The physical principles controlling permafrost phenomena in mountainous regions are the same as in lowland areas. However, the mountain topography and the high redistribution of sediments and snow in mountain permafrost enrich the variety of phenomena as compared to permafrost in lowland areas (Gruber et al. 2015).

This study showed that sites with coarse-grained soils showed higher thermal conductivities than sites mainly having fine-grained soils. Fine-grained soils increase their thermal conductivity under decreasing freezing temperatures as shown in Inuvik-Tuktoyaktuk Highway and stated by Farouki (1981). Frozen thermal conductivities in mountainous areas showed higher values when compared to lowland areas. However, sites in areas of mountain permafrost showed lower frozen volumetric heat capacities when compared to sites in lowland areas.

### 6.8 Alternate Procedure Based on Data of Temperature with Time

The slope *S* of the temperature variations with time was estimated to analytically determine the thermal conductivity. Approximate values of the slope *S* were obtained from equation 4.9 using the variation of temperature with time in and below the active layer of the climate and sine function models. Sites located in colder areas and containing higher presence of coarse-grained soils, showed relatively higher slopes compared to areas of degrading or warm permafrost. In general, frozen thermal conductivities are defined by lower slopes. This is due to the fact that less variation in temperature is reported below the active layer.

PR391 only shows thermal conductivities in unfrozen state because TEMP/W models were not able to predict freezing conditions. As mentioned in section 6.2.3, the PR391 models need to remove more energy to show freezing temperatures in the ground after the thawing phase. The soil temperatures in Inuvik-Tuktoyaktuk (Figure 5.29) and Murtèl-Corvatsch (Figure 5.45) showed higher variation in temperature with time in the active layers compared to other sites. The climate model of Benchoko-Yellowknife shows the lowest slope below the active layer, which is comparable to the low variation in temperature with time shown in Figure 5.39. As mentioned in sections 4.6.3 and 4.7.3, only the sine function model was used in Murtèl-Corvatsch and Chilean Andes sites. They show low slopes in the frozen state, which are in accordance with the high thermal conductivity.

# CHAPTER 7: Summary, Conclusions and Recommendations

## 7.1 Summary

The purpose of this study was to evaluate the thermal properties of soils at five selected sites of ground temperature monitoring. Measured data were collected from five research sites: 1) Provincial Road PR391, Thompson, Manitoba, Canada; 2) Inuvik-Tuktoyaktuk Highway, Northwest Territories, Canada; 3) Highway 3, Behchoko-Yellowknife, Northwest Territories, Canada; 4) Murtèl-Corvatsch Rock Glacier, Engadin Region, Switzerland; and 5) Chilean Andes Rock Glacier, Chile. The collections of temperature were carried out through thermistors strings installed at different depths and locations.

The project background and the thermal properties for Provincial Road PR391 were collected by Batenipour (2012), Kurz (2014) and Flynn (2015). Measured data was obtained between September 2012 and April 2017. Measured data from Inuvik-Tuktoyaktuk Highway were obtained by De Guzman et al. (2015) and De Guzman et al. (2017). Ground temperatures from Highway 3, Behchoko-Yellowknife were obtained by Stirling et al. (2015). Murtèl-Corvatsch and Chilean Andes Rock Glaciers were the only cases of mountain permafrost. Measured temperatures from Murtèl-Corvatsch were obtained by Arenson (2002) and Harris et al. (2009).

The sites were modeled with a finite element software for geothermal analysis (TEMP/W) to calibrate the thermal conductivity and volumetric heat capacity. The thermal properties were further evaluated using a sensitivity analysis. This analysis showed that thermal conductivity is more sensitive to the

model than volumetric heat capacity. Furthermore, thermal properties of fine-grained soils resulted to be more sensitive than thermal properties of coarse-grained soils.

The geothermal models developed to simulate the temperature variations with depth and time in and below the active layer showed good agreement with the measured data.

The thesis discusses the differences between the thermal properties in lowland and mountain permafrost. In this study an alternate method is presented that take into account the slope *S* of temperature variations with time to determine the thermal conductivity in frozen and unfrozen states.

## 7.2 Conclusions

1) Soils with high thermal conductivity, containing coarse-grained soils and low unfrozen volumetric water content showed higher temperature variations in the permafrost layer than fine-grained soils.

2) Warming discontinuous permafrost like Highway 3, Behchoko-Yellowknife showed low thermal conductivities. This site is susceptible to further thaw settlement as a reason of the high unfrozen water content.

3) Most calibrated thermal properties are found within the range of values in the literature. Sites in areas of mountain permafrost showed higher frozen thermal conductivities and lower frozen volumetric heat capacities when compared to sites in lowland areas.

4) The variation of temperature with time, slope *S,* used to determine the thermal conductivity of soils (ASTM D5334-14) is similar to the slope of the variation of temperature with time obtained from the observed data. The slope provided by the geothermal models was used to estimate the thermal conductivities of soils in the frozen and unfrozen states.

### 7.3 Recommendations

1) More research has to be done to expand the confidence of the geothermal modeling in permafrost under different conditions and types of soils. Further data can be obtained in PERMOS website for additional analysis of the mountain permafrost.

2) Due to remoteness and limited data, thermal properties in mountain permafrost are more difficult to evaluate. It is useful to incorporate the environmental conditions at the site in the geothermal model such as vegetation, ground elevations, existence of bodies of water, etc. This can be done using a geographic information system (GIS).

3) A software can be developed to evaluate the thermal properties as an automated process. This computer programme may use an algorithm that recognizes the changes in ground temperature and type of soil to determine the thermal properties.

# References

Alfaro, M.C., Ciro, G.A., Thiessen, K.J., and Ng, T. 2009. “A Case Study of Degrading Permafrost Beneath a Road Embankment.” *Journal of Cold Regions Engineering* 23(3): 93–112.

Andersland, O., and Ladanyi, B. 2004. *Frozen Ground Engineering*. John Wiley and Sons.

Angillieri, M. 2009. A Preliminary Inventory of Rock Glaciers at 308S Latitude, Cordillera Frontal of San Juan, Argentina. *Quaternary International.* 195(1–2): 151–157.

Arenson, L., and M. Jakob. 2010. A New GIS Based Mountain Permafrost Distribution Model. *63rd Canadian Geotechnical Conference & 6th Canadian Permafrost Conference*: 452–58. http://pubs.aina.ucalgary.ca/cpc/CPC6-452.pdf.

Arenson, L., Colgan, W., and Marshall, H. P.. 2015. *Physical, Thermal, Mechanical Properties of Snow, Ice and Permfrost*. Snow and Ice-Related Hazards, Risks, and Disasters. Elsevier Inc.

Arenson, L. 2002. Unstable Alpine Permafrost: A Potentially Important Natural Hazard-Variations of Geotechnical Behaviour with Time and Temperature. *PhD Thesis*, Swiss Federal Institute of Technology, Zurich.

Arenson, L., Pastore, S., Trombotto, D., Bolling, S., Quiroz, M., and Ochoa, X. 2010. Characteristics of Two Rock Glaciers in the Dry Argentinean Andes

Based on Initial Surface Investigations. In *Geo2010*, 1501–1508.

Arenson, L. , and Jakob, M. 2010. Short Communication:The Significance of Rock Glaciers in the Dry Andes - A Discussion of Azócar and Brenning (2010) and Brenning and Azócar (2010). *Permafrost and Periglacial Processes* 21(3): 282–285.

ASTM C177. 2013. Standard Test Method for Steady-State Heat Flux Measurements and Thermal Transmission Properties by Means of the Guarded-Hot-Plate Apparatus. *Annual Book of ASTM Standards*: 1–23.

ASTM D5334. 2014. Standard Test Method for Determination of Thermal Conductivity of Soil and Soft Rock by Thermal Needle Probe Procedure 1. *Annual Book of ASTM Standards*: 1–6.

Azocar, G.F., and Brenning, A. 2010. Hydrological and Geomorphological Significance of Rock Glaciers in the Dry Andes, Chile (27–338S). *Permafrost Periglac. Process.* 21(1): 42–53.

Azocar, G. F., Brenning, A, and Bodin, X. 2016. Permafrost Distribution Modeling in the Semi-Arid Chilean Andes. *The Cryosphere* 11: 877-890.

Barsch, D. 1996. *Rockglaciers: Indicators for the Present and Former Geoecology in High Mountain Environments*. Springer Series in Physical Environment 16.

Batenipour, H. 2012. Understanding the Performance of Highway Embankments on Degraded Permafrost. *PhD Thesis*, University of Manitoba, Winnipeg.

Berthling, I. 2011. Beyond Confusion: Rock Glaciers as Cryoconditioned Landforms. *Geomorphology*, 131(3–4), 98–106 (doi: 10.1016/j.geomorph.2011.05.002)

BGC Engineering, Inc. 2011. *Highway 3-Climate Change Vulnerability Assessment-Final Report*.

Birch, F., and Clark, H. 1940. The Thermal Conductivity of Rocks and Its Dependence upon Temperature and Composition. *American Journal of Science*. 238: 529–558.

Brenning, A. 2005. Climatic and Geomorphological Controls of Rock Glaciers in the Andes of Central Chile: Combining Statistical Modelling and Field Mapping. *PhD thesis*, Humboldt-Universität zu Berlin.

Brenning, A. 2010. The significance of Rock Glaciers in the Dry Andes – Reply to L. Arenson and M. Jakob. *Permafrost Periglacial Process*., 21(3), 286–288 (doi: 10.1002/ppp.702)

Brown, J., Ferrians, Jr., O. J., Heginbottom, J. A., and Melinkov, E. S. 1997. Circum-Arctic Map of Permafrost and Ground Ice Conditions, 1: 10,000,000-Scale Map, US Geol. Surv.

Brown, R.J.E., and Kupsch, W.O. 1974. Permafrost Terminology. *National Research Council of Canada, Associate Committee Geotechnical Research* 111: 62.

Brown, R.J.E. 1966a. Influence of Vegetation on Permafrost. In *Proc. International Conference on Permafrost(1963), Lafayette, IN, U.S*, National Academy of Sciences, 20–25.

Brown, R.J.E. 1966b. Relation between Mean Annual Air and Ground Temperatures in the Permafrost Region in Canada. In Proc. International Conference.

Brown, R.J.E., Johnston, G.H., Mackay, J.R., Morgenstern, N. R., and Shilts, W.W. 1981. *Permafrost Distribution and Terrain Characteristics. Permafrost Engineerin Design and Construction*. John Wiley and Sons.

Brown, W.G. 1963. Graphical Determination of Temperature under Heated or Cooled Areas on the Ground Surface. Ottawa, Canada: Div. of Building Research, National Research Council, Canada.

Canadian Cryospheric Information Network Website, 2016

Chai, T., and Draxler, R. 2014. Root Mean Square Error (RMSE) or Mean Absolute Error (MAE)? – Arguments Against Avoiding RMSE in the Literature. *Geoscientific Model Development.* 7, 1247-1250.

De Guzman, E. M., Piamsalee, A., Alfaro, M., Arenson, L., Doré, G., and Hayley, D. 2015. Initial Monitoring of Instrumented Test Sections along the Inuvik-Tuktoyaktuk Highway. In *68e Conférence Canadienne de Géotechnique et 7e Conférence Canadienne Sur Le Pergélisol*.

De Guzman, E. M., Alfaro, M., Doré, G., and Arenson, L. 2017. Performance of Instrumented Sections along a Highway in the Canadian Artic.*19th International Conference on Soil Mechanicsan and Geotechnical Engineering*. Seoul, Korea.

Environment Canada, Historical Data. http://climate.weather.gc.ca/historical_data/search_historic_data_e.html. February 12, 2018.

Eppelbaum, L., Kutasov, I., and Pilchin, A. 2014. *Applied Geothermics.* Springer-Verlag Berlin Heidelberg.

Donahue, R. L., Miller, R. W., and Shickluna, J. C. 1977. *Soils: An Introduction to Soils and Plant Growth*. Prentice-Hall.

Farouki, O. T. 1981. *Thermal Propeties of Soils*. United States Army Corps of Engineers, Cold Regions Research and Engineering Laboratory.

Flynn, D. 2015. Field and Numerical Studies of an Instrumented Highway Embankment in Degrading Permafrost. *M.Sc. Thesis*, University of Manitoba, Winnipeg, Manitoba.

Flynn, D., Kurz, D., Alfaro, M., Graham, J., and Arenson, L. 2016. Forecasting Ground Temperatures under a Highway Embankment on Degrading Permafrost. *Journal of Cold Regions Engineering* 30(4).

Fujii, Y., and Higuchi, K. 1972. On the Permafrost at the Summit of Mt. Fuji. *Seppyo* 34: 173–86.

GEO-SLOPE International Ltd. 2008. *Thermal Modeling with TEMP / W 2007*.

Gruber, S. , and Haeberli, W. 2009. Mountain Permafrost. In *Permafrost Soils*, Springer-Verlag Berlin Heidelberg, 33–44. http://www.springerlink.com/index/10.1007/978-3-540-69371-0.

Gruber, S., Burn, C. R., Arenson, L., Geertsema, M., Harris, S., Smith, S. L., Bonnaventure, P., and Benkert, B. 2015. Permafrost in Mountainous Regions of Canada. In *68e Conférence Canadienne de Géotechnique et 7e Conférence*

*Canadienne Sur Le Pergélisol*.

Haeberli, W., Hallet, B., Arenson L., Elconin, R., Humlum, O., Kääb, A., Kaufmann, V., Ladanyi, B., D. Matsuoka, N., Springman, S., and Von der Mühll, D. 2006. Permafrost Creep and Rock Glacier Dynamics. *Permafrost Periglac Process* 17: 189–214.

Hanna, A.J., Forsyth, R.J. and Garvin, D. 1990. Thaw Settlement around a Building on Warm Ice-Rich Permfrost. *Collection Nordicana, proceedings of the Fifth Canadian Permafrost Conference*, No 54, 419-424.

Hansson, K., Šimůnek, Mizoguchi, M., Lundin, L.C., and van Genuchten, M.T. 2004. Water Flow and Heat Transport in Frozen Soil: Numerical Solution and Freeze–Thaw Applications. Vadose Zone Journal 3:693–704.

Harris, C., Von der Mühll, D., Isaksen, K., Haeberli, W., Sollid, J.L., King, L., Holmlund, P., and D. Dramis, F., Guglielmin, M., Palacios. 2003. Warming Permafrost in European Mountains. *Global and Planetary Change* 39: 215–225.

Harris, C., et al. 2009. Permafrost and Climate in Europe: Monitoring and Modelling Thermal, Geomorphological and Geotechnical Responses. *Earth-Science Reviews* 92(3-4): 117–71. http://dx.doi.org/10.1016/j.earscirev.2008.12.002.

Hausmann, H., Krainer, K., Brückl, E., Mostler, and W. 2007. Internal Structure and Ice Content of Reichenkar Rock Glacier (Stubai Alps, Austria) Assessed by Geophysical Investigations. *Permafrost and Periglacial Processes* 18: 351–367.

Helwany, S. 2007. *Applied Soil Mechanics with ABAQUS Applications*. John Wiley and Sons, Inc.

Hermansson, Å., Charlier, R. , Collin F., Erlingsson S., Laloui L., and Mate, S. 2008. *Water in Road Structures.* In Springer Science+Business Media B.V. 2009.

International Permafrost Association. 2008. *Manual for Monitoring and Reporting Permafrost Measurements.*

Holländer, H., Wang, Z., Assefa, K., and Woodbury, A. 2016. Improved Recharge Estimation from Portable, Low-Cost Weather Stations. *Groundwater.* 54(2): 243-254.

International Permafrost Association. 2016. http://ipa.arcticportal.org/.

Johnston, G.H., Ladanyi, B., Morgenstern, N.R., and Penner, E. 1981. Engineering Characteristics of Frozen and Thawing Soils. *Permafrost: Engineering Design and Construction*, John Wiley and Sons.

Jumikis, A. 1966. *Thermal Soil Mechanics*. Rutgers University Press.

Krainer, K., Mostler, W., and Spötl, C. 2007. Discharge from Active Rock Glaciers, Austrian Alps: A Stable Isotope Approach. *Austrian Journal of Earth Sciences* 100: 102–112.

Kurz, D, Alfaro, M, Bartley G, and Graham, J. 2012. Thermal conductivity of Clay and Peat Samples from Northern Manitoba. *65th Canadian Geotechnical Conference*, Winnipeg, MB.

Kurz, D. 2014. Understanding the Effects of Temperature on the Behaviour of Clay.

*PhD Thesis*, University of Manitoba, Winnipeg, Manitoba.

Matasci, C. 2012. Swiss Tourism in the Age of Climate Change - Vulnerability , Adaptive Capacity , and Barriers to Adaptation. *École Polytechnique Fédérale de Lausanne, Switzerland*.

Meteoswiss, Federal Ofiice of Meteorology and Climatology http://www.meteoswiss.admin.ch/home.html?tab=overview. February 12, 2018.

Monnier, S., Camerlynck, C., and Rejiba F. 2009. Ground-penetrating radar surveys on rock glaciers in the Vanoise Massif (Northern French Alps): methodological issues. Géomorphologie : Relief, Processus, Environnement 15(2): 129 -140.

Monnier, S., and Christophe K. 2013. Internal Structure and Composition of a Rock Glacier in the Andes (Upper Choapa Valley, Chile) Using Borehole Information and Ground-Penetrating Radar. *Annals of Glaciology* 54(64): 61–72.

Monnier, S., and Christophe K. 2015. Internal Structure and Composition of a Rock Glacier in the Dry Andes, Inferred from Ground-Penetrating Radar Data and Its Artefacts. *Permafrost and Periglacial Processes* 26(4): 335–346.

Noetzli, J., and Von der Mühll, D. 2010. *PERMOS 2010: Permafrost in Switzerland 2006/2007 and 2007/2008*.

Ochsner, T.E. 2008. Measuring Soil Temperature. In *Soil Science: Step-by-Step Field Analysis*, Soil Science Society of America, Inc., 235–251.

Riseborough, D., Shiklomanov, N., Etzelmüller, B., Gruber, S., and Marchenko, S.

2008. Recent Advances in Permafrost Modelling. *Permafrost and Periglacial Processes* 19(2): 137–156.

Robertson, E. 1988. *Thermal Properties of Rocks*. United States Department of the Interior Geological Survey.

Różański, A, and Sobótka, M. 2013. On the Interpretation of the Needle Probe Test Results: Thermal Conductivity Measurement of Clayey Soils. *Studia Geotechnica et Mechanica* 35(1): 195–207.

Rykiel, E.J. 1996. Testing Ecological Models: The Meaning of Validation. *Ecological Modelling* 90: 229–244.

Saltelli, A., Ratto, M., Andres, T., Campolongo, F., Cariboni, J., Gatelli, D., Saisana, M., and Tarantola, S. 2008. *Global Sensitivity Analysis: The Primer*. Chichester, UK: John Wiley & Sons.

Stearns, S.R. 1966. *Permafrost (Perennially Frozen Ground)*. I – A2, 72.

Stirling, J. L., Seto, J.T. C., and Arenson, L.U. 2015. NWT Highway 3 Test Sections near Yellowknife. In *68e Conférence Canadienne de Géotechnique et 7e Conférence Canadienne Sur Le Pergélisol*,.

Stötter, J. 1994. Veränderungen der Kryosphäre in Vergangenheit und Zukunft sowie Folgeerscheinungen.

Terzaghi, K. 1952. Permafrost. *Journal of the Boston Society of Civil Engineers* 39 (1): 1-50.

Trombotto, D., Buk, E., and Hernandez, J. 1999. Rock Glaciers in the Southern

Central Andes (Appr. 338 S.L.) Mendoza, Argentina: A Review. *Bamberger Geogr. Schrift. 19*: 145–173.

Von der Mühll, D., and Haeberli, W. 1990. Thermal Characteristics of the Permafrost with an Active Rock Glacier (Murtel/Corvatsch, Grisons, Swiss Alps). *Journal of Glaciology.* 36(123): 151 - 158.

William, P. J., and Smith, M. W. 1989. "The Frozen Earth: Fundamentals of Geocryology, Stu." Polar Res., 306 pp., Cambridge Univ. Press, New York.

# Appendix

The electronic files collected and created for the elaboration of the thesis were provided to Dr. Marolo Alfaro at the University of Manitoba as a USB flash drive. The files comprise the documentation as follows:

Chapter 3

- Copy of the measured data from the five research sites.
- Copy of the data obtained from the climate stations.

Chapter 4, 5, 6

- TEMP/W files containing the geothermal modelling of the five research sites.
- Origin 2015 files containing the graphs of the five research sites.
- Calibration analysis files
- Sensitivity analysis files